12-2022

Oscillation Analysis and its Mitigation Using Inverter-Based Resources in Large-Scale Power Grids

Khaled Alshuaibi
kalshuai@vols.utk.edu

To the Graduate Council:

I am submitting herewith a dissertation written by Khaled Alshuaibi entitled "Oscillation Analysis and its Mitigation Using Inverter-Based Resources in Large-Scale Power Grids." I have examined the final electronic copy of this dissertation for form and content and recommend that it be accepted in partial fulfillment of the requirements for the degree of Doctor of Philosophy, with a major in Electrical Engineering.

Yilu Liu, Major Professor

We have read this dissertation and recommend its acceptance:

Fangxing Li, David Icove, Lin Zhu, Wenpeng Yu

Accepted for the Council:

Dixie L. Thompson

Vice Provost and Dean of the Graduate School

(Original signatures are on file with official student records.)

To the Graduate Council:

I am submitting herewith a dissertation written by Khaled Mohammed Alshuaibi entitled "Oscillation Analysis and its Mitigation Using Inverter-Based Resources in Large-Scale Power Grids." I have examined the final paper copy of this dissertation for form and content and recommend that it be accepted in partial fulfillment of the requirements for the degree of Doctor of Philosophy, with a major in Electrical Engineering.

Dr. Yilu Liu, Major Professor

We have read this dissertation
and recommend its acceptance:

Dr. Fangxing Li

Dr. David Icove

Dr. Lin Zhu

Dr. Wenpeng Yu

Accepted for the Council:

Carolyn R. Hodges

Vice Provost and Dean of the Graduate School

To the Graduate Council:

I am submitting herewith a dissertation written by Khaled Mohammed Alshuaibi entitled "Oscillation Analysis and its Mitigation Using Inverter-Based Resources in Large-Scale Power Grids." I have examined the final electronic copy of this dissertation for form and content and recommend that it be accepted in partial fulfillment of the requirements for the degree of Doctor of Philosophy, with a major in Electrical Engineering.

Dr. Yilu Liu, Major Professor

We have read this dissertation
and recommend its acceptance:

Dr. Fangxing Li

Dr. David Icove

Dr. Lin Zhu

Dr. Wenpeng Yu

Accepted for the Council:

Carolyn R. Hodges

Vice Provost and Dean of the Graduate School

(Original signatures are on file with official student records.)

Oscillation Analysis and its Mitigation Using Inverter-Based Resources in Large-Scale Power Grids

A Dissertation Presented for the

Doctor of Philosophy

Degree

The University of Tennessee, Knoxville

Khaled Mohammed Alshuaibi

December 2022

This dissertation is dedicated to my parents.

Acknowledgements

First and foremost, all praise to Allah for giving me the courage, blessing, and strength to complete this dissertation.

My deepest gratitude goes to Dr. Yilu Liu for her unfailing support, patience, and continuous guidance through every stage of my Ph.D. study. I sincerely appreciate the time she spent providing me with feedback, suggestions, and ideas to enhance the quality of my research. I am grateful for this opportunity to work with such a mentor, and words cannot express my gratitude and appreciation.

I greatly appreciate Dr. Fangxing Li, Dr. David Icove, Dr. Lin Zhu, and Dr. Wenpeng Yu, for agreeing to serve on my Ph.D. committee. I am thankful for their time, effort, and valuable comments and suggestions on my dissertation.

I would like to express my sincere gratitude and appreciation to Dr. Lin Zhu and Dr. Yi Zhao for their time, help, and support. I greatly appreciate all their valuable comments and feedback on my research.

I would like to thank Dr. Shutang You, Dr. Ibrahim Altarjami, Dr. Meshal, Dr. Yuqing Dong, Chengwen Zhang, Hongyu Li, and all the Power IT lap group for their help and support during my Ph.D. journey. I am thankful for the professors and staff at the department of Electrical Engineering and Computer Science at the University of Tennessee Knoxville and for all those who provided me with help and support during this journey.

I would like to express my profound gratitude to my beloved parents, Mohammed and Mashael, for their countless sacrifices, continuous support, and unconditional love. I am also thankful for the encouragement and support from my brothers and sister, Turki, Ahmad, Haya, and Suliman.

Finally, I would like to thank King Saud University for providing me with the opportunity to pursue a Ph.D. degree. I am thankful for their financial support and trust.

Abstract

In today's interconnected power grids, forced oscillations and poorly damped low-frequency oscillations are major concerns that can damage equipment, limit power transfer capability, and deteriorate power system stability.

The first part of the dissertation focuses on the impact of a wide-area power oscillation damping (POD) controller via voltage source converter-based high voltage direct current (VSC-HVDC) in enhancing the power system stability and improving the damping of low-frequency oscillation. The POD controller's performance was investigated under a three-phase temporary line fault. The Great Britain (G.B.) power grid model validated the POD controller performance via active power modulation of VSC-HVDC through TSAT-RTDS hybrid simulation.

The developed POD controller is also implemented on a general-purpose hardware platform CompactRIO and tested on a hardware-in-the-loop (HIL) test setup with actual PMU devices and a communication network impairment simulator. A variety of real-world operating conditions is considered in the HIL tests, including measurement error/noise, occasional/consecutive data package losses, constant/random time delays, and multiple backups PMUs.

The second part of the dissertation proposes a two-dimensional scanning forced oscillation grid vulnerability analysis method to identify areas/zones and oscillation frequency in the system critical to forced oscillation. These critical areas/zones can be considered effective actuator locations to deploy forced oscillation damping controllers. Additionally, a POD controller through inverter-based resources (IBRs) is proposed to reduce the forced oscillation impact on the entire grid.

The proposed method is tested when the external perturbation is active power and compared with the reactive power perturbation result. The proposed method is validated through a case study on the 2000-bus synthetic Texas power system model. The simulation results demonstrate that the critical areas/zones of forced oscillation are related to the areas that highly participate in the natural oscillation. Furthermore, forced oscillation through active power disturbance can have a more severe impact than reactive power disturbance, especially at resonance. The proposed forced oscillation controller can mitigate the impact of the forced oscillation on the entire system when the actuator is close to the forced oscillation source. In addition, active power modulation of IBR can provide better damping performance than reactive power modulation.

Table of Contents

List of Tables

List of Figures

Chapter 1

Introduction

1.1 Background and Motivation

Environmental concerns and global warming caused by excessive fossil fuel consumption have encouraged the rapid development and implementation of renewable energy sources (RESs) such as wind and solar systems [1]. However, as RES penetration increases, the power system experiences stability issues due to the lack of system inertia that results from replacing the conventional synchronous generators with RESs. Moreover, there is always a mismatch between demand and generation due to the intermittent nature of RESs. As a result, the grid becomes vulnerable to frequency deviation [2, 3].

Furthermore, RESs' uncertainty can expose the power system to inter-area oscillations, transients, and voltage instability [4, 5]. Also, with the increasing load variability and high penetration of RESs of intermittent nature, such as wind generation [6, 7, 8], forced oscillation events could increase considerably.

Damping Low-frequency oscillation is a major factor in operating the large interconnected power system securely and economically. Power system stabilizers (PSSs) through synchronous generators are utilized to dampen low-frequency oscillation [9]. PSS output is added to the voltage reference of the automatic voltage regulator (AVR) to dampen the oscillation and improve the system's dynamic performance [10]. However, as RESs replace the conventional synchronous generators, more PSSs will be retired, which could negatively impact the damping of such oscillations. Power electronics-based devices such as high-voltage direct current (HVDC) transmission systems and flexible alternating current transmission systems (FACTS) can provide fast oscillation damping control [11, 12, 9]. With the growing deployment of Phasor Measurement Units (PMU) and the availability of wide-area measurements, wide-area power oscillation damping (POD) controllers have been effective techniques for suppressing low-frequency oscillations. Wide-area measurements can provide better observability than local measurements [13]. This dissertation aims to utilize the wide-area POD controller via VSC-HVDC to enhance the damping of low-frequency oscillations. The POD controller is implemented on the HIL setup. Realistic operating conditions are emulated to evaluate the controller's performance, including varying signal latencies, data package losses, and measurement noise.

Forced oscillation in the power system is usually a response to the external signal caused by cyclic load, equipment failure, or poor control design [14, 15]. Forced oscillation can pose a threat to the system's stability, especially when the forced oscillation frequency coincides with the dominant natural oscillation mode [16]. Multiple forced oscillation events around the world have been reported. On November 29, 2005, the western American power system experienced a force oscillation event due to steam extractor valve control failure at the Nova Joffre power plant in Alberta, Canada. The force oscillation energy was 20 MW, and the oscillation frequency was close to the system's natural mode of 0.25 Hz. Even though the natural mode was well-damped, the inter tie-line between California and Oregon experienced 200MW peak-to-peak oscillation energy [17]. Most of the existing studies focus on locating and identifying the force oscillation event, and few studies have been conducted on mitigating such events [18].

This dissertation proposes a general method for forced oscillation grid vulnerability analysis and mitigation through IBRs in large-scale power grids. To reduce the forced oscillation effect in the entire system, a forced oscillation damping controller at an effective IBR actuator can be activated before the exact forced oscillation source is identified and removed. First, a detailed location and frequency scanning method can identify critical areas/zones under different specified forced oscillation frequencies that can excite the most severe forced oscillation across a large-scale power system. These identified critical areas/zones are also effective locations as the actuators of forced oscillation damping controllers when the forced oscillation sources are narrowed down inside or close to the critical areas/zones. Secondly, a forced oscillation damping controller via IBRs was designed to reduce the impact of the forced oscillation event before the forced oscillation source is removed [15].

1.2 Contribution

The contributions of this dissertation are:

- Demonstrate the effectiveness of a wide-area POD controller via active power modulation of VSC-HVDC in enhancing the small-signal stability and damping the low-frequency oscillations.
- Demonstrate the performance of the POD controller in the HIL test setup based on hybrid TSAT-RTDS simulation.
- Demonstrate the performance of the POD controller under different communication impairments, including time delay, data package losses, and measurement noise.
- Propose a two-dimensional scanning forced oscillation grid vulnerability analysis method to identify the critical forced oscillation frequency and areas/zones.
- Analyze and compare the results of the grid vulnerability analysis method when the force oscillation events are excited by an external active or reactive power perturbation.
- Determine an effective IBR actuator location to forced oscillation damping controller based on the two-dimensional scanning method.
- Design and implementation of a forced oscillation damping controller to reduce the impact of a forced oscillation event to a safe level and provide the system operator sufficient time to locate and remove the forced oscillation source.

- Study the impact of mitigating forced oscillation through active, reactive and both active and reactive power modulation of IBR.
- Investigate the impact of increasing renewable penetration level on the oscillation frequency and damping ratio on a synthetic Texas power system model.

1.3 Dissertation Outline

This section presents an outline of each chapter covered in this dissertation.

- Chapter 2: provides a review of the low-frequency oscillations and their impact on the power system stability. It then presents an introduction to forced oscillations in a power system and the threat that they could pose to the system stability and some of the methods used in the literature to mitigate the impact of such oscillations. It is then followed by an introduction to the VSC-HVDC in the power transmission system. It is then followed by a review of the power oscillation damping controller is presented. The review includes some methods used to design the POD controller and actuators to damp the oscillations, and finally, some of the challenges are covered. Finally, an introduction to the Real-Time Digital Simulator (RTDS) and the TSAT-RTDS hybrid simulation is presented.
- Chapter 3: Describes the Great Britain (GB) model and method used to design the POD controller. The dynamic response of the TSAT-RTDS hybrid model was compared with the GB model in PSS/E and TSAT. Furthermore, the implementation of the POD controller on TSAT-RTDS hybrid software was presented.
- Chapter 4: Presents the implementation of the POD controller on hardware-in-the-loop (HIL) under different communication impairments.
- Chapter 5: Describes the proposed forced oscillation grid vulnerability analysis and mitigation method.

- Chapter 6: Presents the implementation of the forced oscillation grid vulnerability analysis method on the 2000-bus synthetic Texas power grid model when the forced disturbance is through active power disturbance of the generator. Furthermore, the selection of an effective IBR actuator location and the POD controller design is discussed. Then the performance of the POD controller via active power modulation of IBR in reducing the forced oscillation impact is investigated.
- Chapter 7: The forced oscillation grid vulnerability analysis method on the 2000-bus synthetic Texas power grid model when the forced disturbance is through active and reactive power disturbance of the load is discussed. Then the performance of the POD controller via reactive power modulation of IBR in reducing the forced oscillation impact is investigated and compared with active power modulation of IBR.
- Chapter 8: Investigate the impact of increasing renewable penetration level in the 2000-bus synthetic Texas power grid on the oscillation frequency and damping ratio. Demonstrate the performance of the POD controller with local measurement in damping the oscillation frequency at different renewable penetration levels.
- Chapter 9: Conclusion and Future Work.

Chapter 2

Literature Review

2.1 Natural Oscillation in Power System

Rotor angle stability is the capability of synchronous machines in an interconnected power system to retain synchronism following a disturbance. The ability of a power system to maintain synchronism following a small disturbance is called small signal stability, which is a subcategory of rotor angle stability [19, 20, 21, 22]. Following a disturbance, the electromagnetic torque of a synchronous machine can be split into two parts synchronizing torque and damping torque. Inadequate damping torque leads to oscillatory instability, while inadequate synchronizing torque leads to non-oscillatory instability. [19, 23, 24].

Low-frequency oscillation is of two types [24, 25]:

- Inter-area modes are linked to all of the generators in the system, divided into two parts where one-part swings against the other. The inter-area mode oscillation frequency ranges from 0.1 to 1 Hz.

- Local modes involve one machine or one plant in the system oscillating against the rest of the system. The local mode oscillation frequency ranges from 1 to 2 Hz.

The increased penetration and uncertainty of RESs and the displacement of synchronous machines can reduce system inertia and have a negative impact on the inter-area oscillations [26, 27, 28, 29]. Poorly damped inter-area oscillations can damage power system equipment, limit transfer capability, and lead to a blackout and cascading failure [30, 31, 32]. Many incidents have been related to low-frequency oscillations in the U.S and worldwide. In 1996, unstable inter-area oscillations caused the Western Electricity Coordinating Council (WECC) blackout. More than 7.5 million customers on the west side of the North American continent were affected by that event [33, 34]. Therefore, it is crucial to damp the electromechanical oscillations to ensure a secure and stable operation of the power system [35, 36].

2.2 Forced Oscillation in Power System

In power systems, forced oscillation is the response of the system due to an external periodic disturbance caused by inadequate control setting, cyclic load, or failing equipment [37, 38, 39, 40, 15]. Moreover, with the increase of variable load and high penetration of renewable energy resources with its intermittent nature, forced oscillation events could increase. Wind resource is a leading source of forced oscillation events within renewable energy resources because wind can fluctuate periodically due to wind shear and tower shadow effect [6, 7, 8, 41]. Multiple forced oscillation events were reported in the USA, China, and Canada. Forced oscillation events can sustain for minutes to hours. Consequently, forced oscillation can negatively impact the stability of the power system, degrade power quality, damage equipment, and reduce power transferring capability [42, 43]. On January 11, 2019, the Eastern Interconnection (EI) power grid experienced a forced oscillation event that lasted for 18 minutes before the plant operator removed the forced source. The forced oscillation is caused by a faulty input to the controller of the steam turbine. The frequency of the forced oscillation was near the 0.25 Hz EI natural oscillation mode, and the oscillation impacted the entire EI power grid [44]. Resonance could happen when the forced oscillation frequency is close to the system's natural oscillation mode with poor damping. As a result, the oscillation could propagate and spread across the entire power grid [45, 46].

Locating and removing the forced source from the power system is the most effective method for suppressing forced oscillation [47, 48]. However, it may be a time-consuming process to identify and eliminate the forced source once the event is detected. Damping control via IBR and other devices has been effectively utilized to suppress the natural oscillation [49, 50, 51]. Moreover, mitigating the impact of force oscillation via damping control can be an effective strategy to keep the system safe until the forced source is removed.

Few studies have been reported on mitigating forced oscillation through damping control. A static synchronous compensator with energy storage (E-STATCOM) with active and reactive power modulation is used to suppress the forced oscillation [52]. The author in [53] used a forced oscillation damping controller with an event-triggered control strategy to damp the forced oscillation, and it was tested on the IEEE 14-machine South East Australian. The author in [54] used voltage source converter-based high voltage direct current (VSC-HVDC) to mitigate the forced oscillation. Battery energy storage systems with active power modulation were implemented to mitigate the forced oscillation. [55]. Only [55] was tested on a large system among all the aforementioned strategies to mitigate forced oscillation.

2.3 VSC-HVDC in Power System Transmission

One of the challenges the present-day transmission system experiences is the large penetration of RESs such as wind and solar systems. The maximum potential location for wind is an offshore or rural area. The large-scale solar plant is often built in remote areas. Therefore, transmitting the power from RESs using the conventional AC transmission system is not economical, and the more cost-effective alternative is the utilization of HVDC [56, 57, 58].

HVDC transmission technology is mainly divided into two different technologies: traditional line commutated converter (LCC) HVDC and VSC-HVDC [59, 60]. The LLC-HVDC uses a thyristor which is triggered by a gate plus and turned off when the current drops to zero. This technology is well suited for long-distance and bulk power transmission systems. The VSC-HVDC uses Insulated Gate Bipolar Transistor (IGBT) or Insulated Gate Commutated Thyristor (IGCT), which is a self-commutated switch [61, 62].

The technical advantages of VSC-HVDC are as follows [63, 64]:

- Fast and independent control of active and reactive power can improve the dynamic performance of the grid under disturbance.
- The ability to connect weak systems.
- Power flow control flexibility.
- Suited for multi-terminal configuration. The direction of the power can be changed by changing the direction of the current and not the DC voltage polarity.
- Black start ability.
- Better transmission efficiency.

Many successful VSC-HVDC projects have been implemented, and others are under construction. The first VSC-HVDC project was built by ABB in Sweden in 1997 with a dc voltage of ±10 kV and a power rating of 3 MW. Table 2.1 shows the list of some VSC-HVDC projects worldwide [57, 65, 66, 67]. Most of the listed projects in Table 2.1 were developed by ABB. It can be noted from the table that with the advancement of VSC-HVDC technology over the years, the voltage levels and power ratings have increased significantly.

2.3.1 VSC-HVDC Components

A typical structure of VSC-HVDC with its key components is shown in Figure 2.1. and a brief description of each component is given below [68, 69, 70]:

- **Transformer**

  The AC grid is connected to the VSC-HVDC through the transformer. The primary purpose of the transformer is to convert the AC grid voltage to a level that the converter can withstand. The transformer reactance helps to limit the short circuit current.

- **Phase Reactor**

  The main purpose of the phase reactor is to facilitate the control of active and reactive power between the AC and DC sides. The phase reactor also filters the high-frequency

Table 2.1: VSC-HVDC projects across the world

Project name	**Location**	**Year**	**DC voltage (kV)**	**Power rating (MW)**
Hellsjön	Sweden	1997	±10	3
Gotland HVDC Light	Sweden	1999	±60	50
Tjaereborg	Denmark	2000	9	7
Troll A	Norway	2004	±60	2 x 40
Estlink	Estonia-Finland	2006	±150	350
Transbay	USA	2010	±200	400
Valhall	Norway	2011	150	78
East-West Interconnector	Ireland-UK	2012	±250	500
Skagerrak 4	Norway-Denmark	2014	500	700
INELFE	France-Spain	2015	±320	2000
NordBalt	Sweden-Lithuania	2015	±320	700
Caithness-Moray	UK	2018	±320	1200
Nemo	UK-Belgium	2019	±400	1000

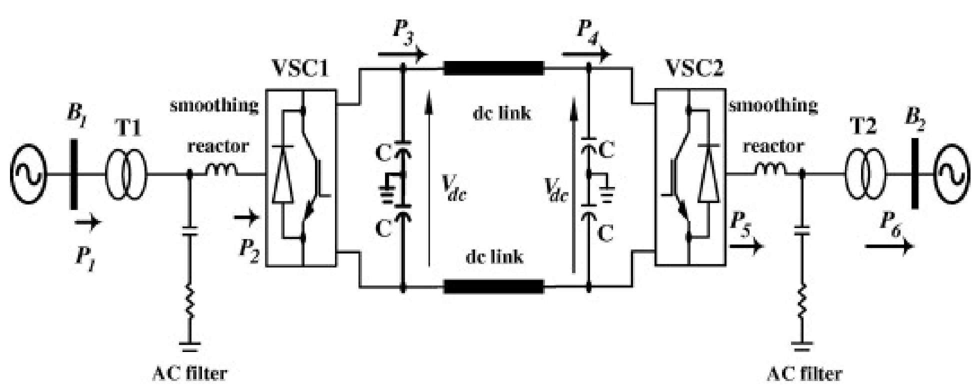

Figure 2.1: Structure of the VSC-HVDC [71].

harmonic component of the AC current caused by the VSC's switching operation. Another function of the phase reactor is limiting the short circuit current through the converters.

- **AC Filter**

  Harmonic components resulting from the switching of the VSC exist in the AC voltage output. These harmonics must be managed to avoid them being transmitted into the AC system and causing equipment malfunctions as well as radio and telecommunication problems. An AC high pass filter mitigates the harmonics.

- **Converter**

  The converters are fully controlled semiconductor devices based on transistors or thyristors. Table 2.2 shows an example of the high power and high voltage fully controlled switches [65].

- **DC Capacitor**

  The DC capacitor reduces the voltage ripple on the dc side. In addition, it serves as energy storage to maintain power balance during the transient. The desired DC voltage determines the size of the capacitor.

- **DC Cable**

  The cable used in VSC-HVDC applications is a newly developed type with an extruded polymer insulation specifically resistant to dc voltage. Polymeric cables are preferred for HVDC due to their mechanical strength, flexibility, and lightweight.

2.4 Power Oscillation Damping Control

A (PMU) is a device that measures the phasor value of the voltage and current [72, 73]. Wide-area measurement system (WAMS) applications commonly utilize the Synchrophasors estimated data by PMU. [74]. Implementing a synchrophasor-based WAMS can significantly improve the observability of power system dynamics, and the WAMS can be utilized to observe and damp the inter-area oscillation [75, 76].

Table 2.2: High power and high voltage fully controlled switches

Acronym	**Name**	**Type**
IGBT	Insulated Gate Bipolar Transistor	Transistor
IEGT	Injected Enhanced Gate Transistor	Transistor
IGCT	Integrated Gate Commutated Thyristor	Thyristor
GCT	Gate Commutated Turn-off Thyristor	Thyristor
GTO	Gate Turn-off Thyristors	Thyristor

Poorly damped inter-area oscillations in a power system may endanger system stability and lead to a blackout [30, 31]. Therefore, utilizing power oscillation damping (POD) control can improve system stability and damp the oscillations. Power system stabilizers (PSSs) are the most common and economical devices that enhance the damping of electromechanical oscillations. PSSs are feedback controllers installed at generators to modulate the voltage reference of automatic voltage regulators [77, 78, 79].

In certain situations, PSS may not offer sufficient performance to suppress oscillations. An example to illustrate such a situation in a large power system is the inter-area oscillation on a tie line or a long transmission line that is not close to a power plant. In such a circumstance, the suppression of power oscillations may need a complicated, coordinated design of several PSSs deployed at faraway power plants [80]. In addition, as RESs replace the synchronous generators and their associated PSSs, the synchronous generators' capacity in the grid decreases. The damping torque supplied by the excitation system is insufficient to suppress low-frequency oscillations [81]. An alternative to PSS is the use of POD control via Flexible AC Transmission Systems (FACTS) devices, High Voltage Direct Current (HVDC) and inverter-based resources (IBRs) [11, 82, 83, 84, 85, 86].

POD, through reactive power modulation via voltage control loop, uses a Static synchronous compensator (STATCOM) to damp low-frequency oscillation [26]. The residue-based method is used to design a POD controller for the Static VAR Compensator (SVC) [87]. The author in [88] uses an adaptive dynamic programming approach called goal representation heuristic dynamic programming (GrHDP) to design the supplementary damping controller via VSC-HVDC to damp the inter-area oscillations in the power system. Adaptive compensator-based POD through a PV plant is proposed in [89] to mitigate inter-area oscillations and reduce communication latency.

The primary goal of designing a damping controller is to obtain the maximum performance in damping the oscillation and minimizing the controller cost. Two main challenges in designing a damping control are selecting the optimal location and feedback signal and tuning the controller parameters [80]. Other challenges include the time delay of remote signals caused by measuring equipment, the sampling rate for phasor computation, and PMU processing time to convert the sample to phasors [90].

2.5 Real-Time Digital Simulator

The Real-Time Digital Simulator (RTDS) is an efficient tool for modeling and simulating power and control systems, developed at the HVDC research facility in Manitoba in the late 1980s. RTDS operates in real-time and accomplishes this by allocating the computing burden among several digital signal processors. Because the processors run in parallel, the system's size can be expanded without compromising the real-time functionality, provided the number of processor units increases proportionally [91, 92, 93].

The RTDS Simulator comprises hardware and software developed to conduct Electro-Magnetic Transient (EMT) simulations in real time. The RTDS software can be categorized into three distinct levels: graphical user interface (GUI), compiler system, and power system component models. The traditional stability and load flow programs can study the system within a narrow frequency range. However, RTDS can provide an accurate result under different ranges of frequencies from DC to 3 kHz. RTDS simulation timesteps are typically 25-50 μs, and for subnetworks with fast switching power devices, the timesteps can range from 1-4 μs. [91, 92, 94].

RTDS is commonly used for closed-loop testing of controllers for HVDC, Thyristor Controlled Series Compensation (TCSC), SVC, and FACTS devices. The RTDS is one of the best available tools to test protective relays. In addition, the performance of control devices can be validated using the HIL test in RTDS. Additionally, companies utilize RTDS for operator training. In RTDS, power electronic equipment such as HVDC and FACTS devices can be modeled in detail, but in traditional power system simulation, such modeling may not be available. [95, 96].

2.6 TSAT-RTDS Hybrid Simulation

Transient Security Assessment Tool (TSAT) is a time-domain simulation tool developed by Powertech Labs to assess the dynamic behavior of power systems. Moreover, TSAT is intended to address the rising issues the power sector has as a consequence of the increased need for the secure and reliable operation of bulk power systems [97]. One of the well-known applications of RTDS is to implement HIL testing to validate the performance of a physical device, such as power system controls or protection devices. Another application is the capability of building a detailed model for a power system or power electronic devices such as HVDC and FACTS. These two applications might not be available in pure electromechanical transients simulation tools such as TSAT [98]. However, it is very costly to model a large power system in RTDS because RTDS capacity depends on the available hardware. In this case, to fit a large system in RTDS, a large portion of the system must be reduced to an equivalent machine or source. This may drastically impact the system's behavior [99]. To overcome this issue, Powertech Labs developed a module called TSAT-RTDS Interface (TRI). TRI enables a hybrid and synchronized real-time co-simulation using RTDS and TSAT to study the dynamic behavior of a power system. In the TSAT-RTDS co-simulation, the system is divided into internal and external parts. The internal part of the system is in RTDS, including a detailed model of a small portion of the system under study. The external part is in TSAT, which contains the rest of the system. TSAT and RTDS exchanges result through an interface board at the end of each TSAT simulation timestep [98, 96].

Chapter 3

Model TSAT-RTDS Description and Validation for UK System

3.1 Great Britain Model Description

In this study, a reduced PSS/e model is used to study the Great Britain system. Figure 3.1 shows the Great Britain power system structure, consisting of 36 zones or terminals. There are five domestic HVDCs, as demonstrated in Table 3.1 and 11 international HVDCs. West Coast LCC-HVDC and East coast VSC-HVDC have a capacity of 3000 MVA. The VSC-HVDC at West Coast 2,3 and East Coast 2 have a capacity of 5000 MVA.

The system's total demand is 40 GW, and the renewable generations supply is around 40% of the total demand. All synchronous generators are equipped with generator (GENSAL), governor (TGOV1), exciter (ESAC4A) and power system stabilizer (IEEEST) models. Figure 3.2 shows bus frequency deviation at zone 1 when a temporary three-phase fault is applied on line 26-27W. The oscillation frequency was obtained using the Prony analysis. The dominant oscillation mode is 0.886 Hz between the northern and southern generators in the Great Britain grid, and the damping ratio is 2.8%. In this study, a POD controller is designed and implemented through West Coast 3 VSC-HVDC to suppress the oscillation.

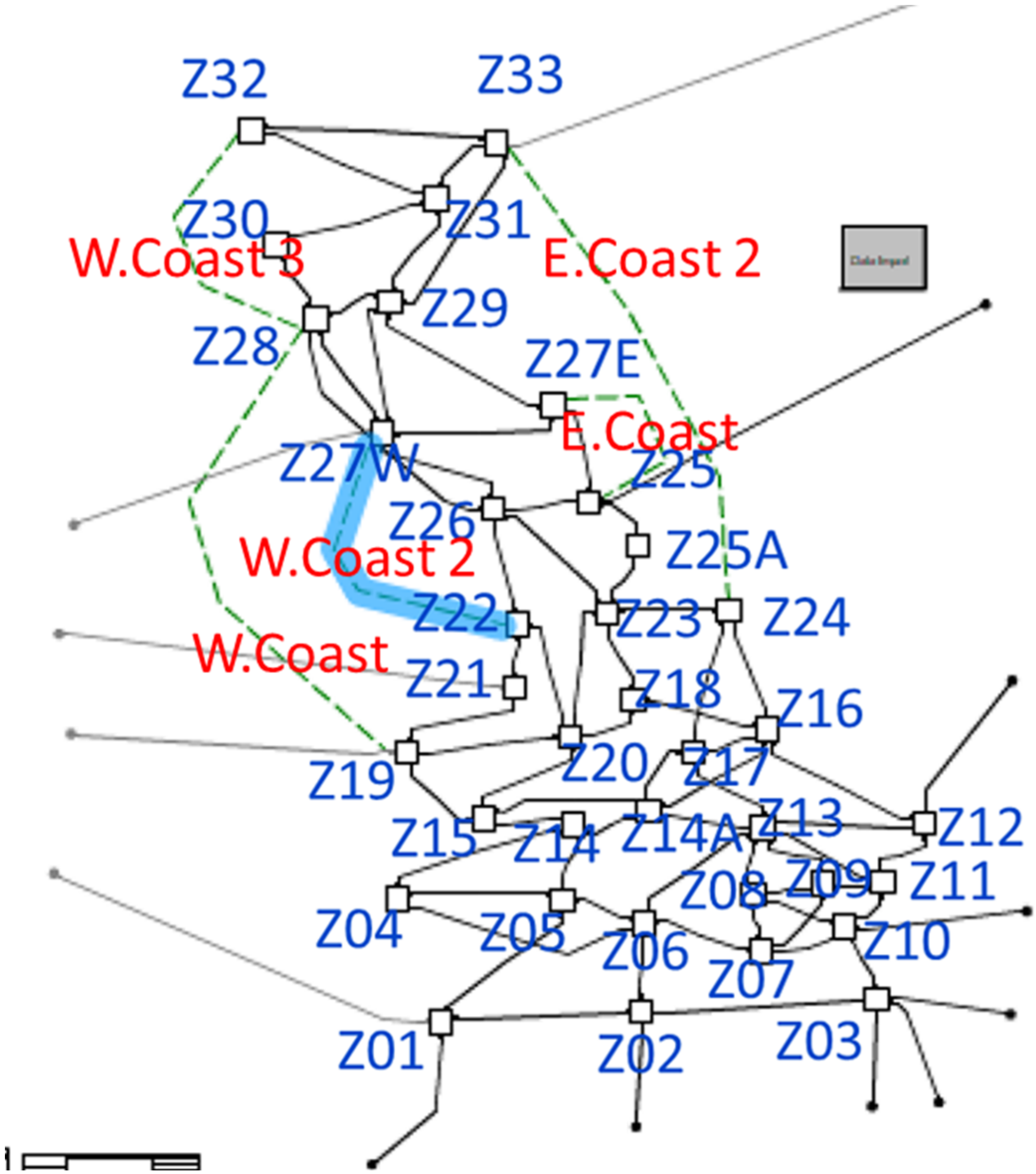

Figure 3.1: Great Britain system structure.

Table 3.1: Domestic HVDC links

HVDC	Capacity (MVA)	HVDC Type	Terminal 1	Terminal 2
West Coast	3000	LCC	Z19	Z28
West Coast 2	5000	VSC	Z22	Z27W
West Coast 3	5000	VSC	Z28	Z32
East Coast	3000	VSC	Z25	Z27E
East Coast 2	5000	VSC	Z24	Z33

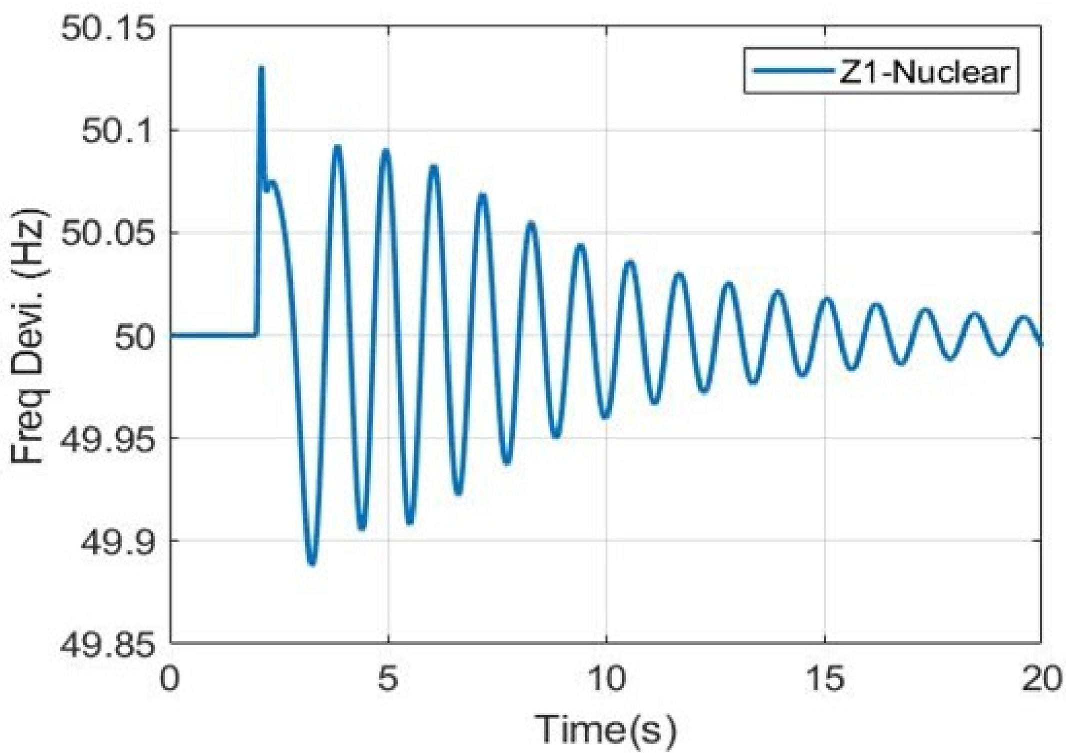

Figure 3.2: Bus frequency deviation at zone 1 when temporary three phase fault is applied on the line 26-27W.

3.2 POD Design

3.2.1 Selection of Optimal Observation Signal for POD

The selection of observation signals is critical in any POD controller design. Because of the growing installation of PMUs, a large power system has a considerable number of available observation signals for the analysis of oscillation mode. Nevertheless, a systematic mechanism is applied to choose the best observation signal of the targeted mode from all of the candidate observation signals since only a small number of them have good observability of the dominant mode [9, 100].

A Fourier analysis transforms sampling rate into frequency or vice versa. In order to compute such transformations quickly, The discrete Fourier transform matrix is transformed using the FFT algorithm into a product of sparse matrices. For N-dimensional vectors, the function Y=fft(x) is defined as follow [9]:

$$X(k) = \sum_{j=0}^{N-1} x(j)\omega_N^{jk} \qquad 0 \leq k \leq N-1 \tag{3.1}$$

where

$$\omega_N = e^{((-2\pi i)/N)} \tag{3.2}$$

represents the Nth root of unity.

FFT is utilized to convert the measurement signals to the frequency domain to determine the optimal damping control observation signals. The sampling rate is 100 per second and the time window is 20 seconds [9].

In this study, the targeted mode is excited through three-phase fault disturbances at several locations. The measurement signals were rated high to low for each disturbance based on their magnitudes at the dominant mode's frequency. Subsequently, the final rank was determined based on all the ranks for various scenarios. The optimal observation signal for the damping control is the signal with the highest ranking [9, 101].

3.2.2 Optimal Actuator Selection for POD

The controllability of system oscillation modes varies amongst various HVDC. Therefore, a sensitivity analysis of all potential actuation signals relative to the observation signal is established to determine the optimal actuation signals.

From the input u_i to the output y_j, the transfer function $g_{ij}(s))$ is derived and can be written as a sum of partial fractions [9, 102]:

$$g_{ij}\left(s\right) = \sum_{k=1}^{n} \frac{R_k}{s - \lambda_k} \tag{3.3}$$

where R_k is the residue corresponding to mode λ_k. The residue R_k reflects how the input u_i affects the mode λ_k and how mode λ_k is observable from the output y_j. Consequently, the residues can be an indication of the controllability and observability of a certain oscillation mode. This is why the use of residues in damping oscillation analysis is common [103, 9].

The residue is calculated using the state space realization [103]:

$$R_k = c_j \emptyset_k \varphi_k b_k \tag{3.4}$$

where $\emptyset_k$ and φ_k are the right and left eigenvectors, respectively, of the state matrix A that correspond to the eigenvalue λ_k.

The residues are generally complex numbers, and the highest magnitude of residues determines the optimal input-output signal [103].

3.2.3 POD Design Method

The POD controller in this study is based on a lead-lag structure that comprises a washout, a filter, phase compensations blocks, a gain, and a limiter [104, 105]. Figure 3.3 demonstrates the structure of the POD controller.

$\tau_\omega = 10$ seconds is the washout time constant, and the transfer function of the filter is defined as [104, 9]:

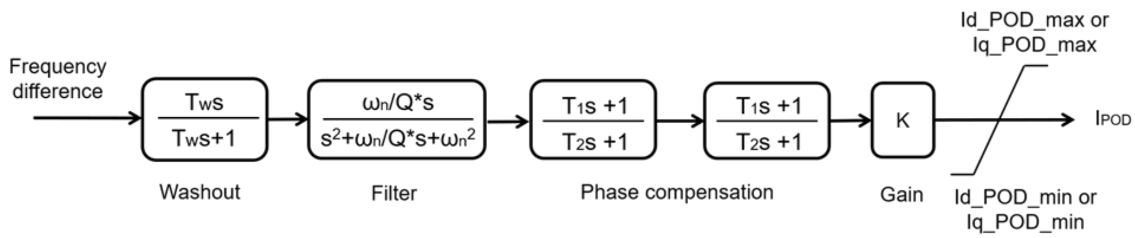

Figure 3.3: Block diagram of the POD controller.

$$K_f(s) = \frac{\frac{\omega_n}{Q}s}{s^2 + \frac{\omega_n}{Q}s + \omega_n^2} \tag{3.5}$$

where Q is the quality factor, typically set to 1, and ω_n is the targeted mode's oscillation frequency.

A controller's performance is primarily determined by its compensation phase and gain, which should be carefully designed. When modulating the reactive power or the active power of HVDC links, the phase compensation can be computed with the control gain based on the power system model's transfer function. The transfer function can be transformed as a sum of partial fractions in the following manner [9, 101]:

$$g_{ij}(s) = \sum_{k=1}^{n} \frac{R_k}{s - \lambda_k} \tag{3.6}$$

where R_k is the residue corresponding to mode λ_k. The residue R_k reflects how the input u_i affects the mode λ_k and how mode λ_k is observable from the output y_j.

R_k is the residue corresponds to the dominant oscillation mode λ_k, and the POD's compensation angle is [9]:

$$\angle K(j\omega_d) + \angle R_k = -180^\circ \tag{3.7}$$

and the amplitude satisfies

$$|K(j\omega_d)| \cdot |R_k| = |-(\zeta_* - \zeta_k)\omega_d| \tag{3.8}$$

where ω_d and ζ_k are the frequency and damping ratio of the dominant inter-area oscillation mode and ζ_* is the expected damping ratio.

The following formulas are used to compute the value of the parameters of K(s) [9, 106]:

$$\alpha = \frac{1 + sin\theta_{max}}{1 - sin\theta_{max}}, \quad \theta_{max} = \angle K(j\omega_d)/2 \tag{3.9}$$

$$T_1 = T_3 = \alpha T_2 \tag{3.10}$$

$$T_2 = T_4 = \frac{1}{\sqrt{\alpha}\omega_d} \tag{3.11}$$

$$K_w = \frac{|K\left(j\omega_d\right)|}{\left(\left|\frac{1+T_1 s}{1+T_2 s}\right|_{s=j\omega_d}\right)^2} \tag{3.12}$$

3.3 VSC-HVDC Setup in TSAT-RTDS

One of the main challenges in RTDS is to simulate a large scale power system due to the limited hardware resources of the RTDS. One of the solutions for this issue is to represent a large portion of the power system with an equivalent machine or source. However, this will affect the system's behavior and neglect the dynamic of a large part of the system. A more accurate and cost-effective solution is to use the TSAT-RTDS Hybrid simulation. The system will be divided into two parts, where the small part of the system that needs to be modeled in detail, such as HVDC or FACT devices, is modeled in RTDS. The rest of the system is simulated in TSAT to save computational resources [98, 107, 108, 99].

Figure 3.4 shows the procedure of setting up the VSC-HVDC model in the hybrid TSAT-RTDS. The setup procedure can be described in the following steps:

1. Split the System into TSAT and RTDS Parts

The method for dividing the system into RTDS and TSAT parts can be summarized as follows:

- Create two PSS/e files for the RTDS and the TSAT part.
- For the RTDS part, delete all the buses and components in the TSAT part.
- For the TSAT part, delete all the buses and components in the RTDS part.
- The interface or boundary buses are kept in both RTDA and TSAT.

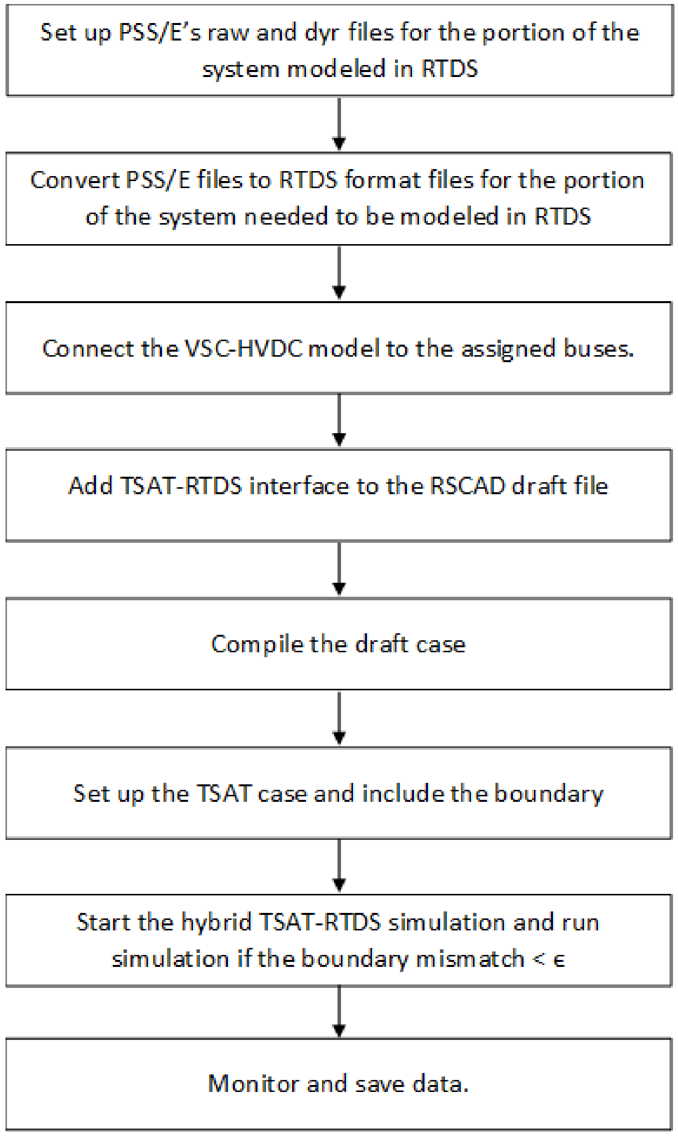

Figure 3.4: The procedure for setting up the VSC-HVDC model in the hybrid TSAT-RTDS.

In the hybrid TSAT-RTDS simulation, a small portion of the system is represented in RTDS, and the rest of the system is simulated in TSAT. The GB model is represented in PSS/e with the load flow description file with the extension (.raw) and the dynamic data file with the extension (.dyr). The West Coast 3 VSC-HVDC (actuator) is connected between the bus at zone 28 and zone 32, and the optimal observation signal as an input to the POD controller is the frequency signal of zone 1 and zone 32 (f1-f32). Therefore, PSS/e raw file is created, which only includes the bus at zone 28 and 32 that connect the VSC-HVDC and a bus from zone 1. The information on the three buses is the same as in the original PSS/e raw file. The dynamic file (.dyr) can be created if the PSS/e part converted to RTDS includes devices with dynamic representation. For example, If one of the buses represented in RTDS includes a synchronous generator with dynamic representation, then the .dyr file can be created, including the information of the generator dynamic model.

2. Convert PSS/e .raw File to RTDS Format

RTDS software contains a PSS/e Import utility tool, which imports data from PSS/e format files and transforms it to RSCAD/Draft-compatible format. The PSS/e conversion software accepts as input the load flow description (.raw), dynamic data (.dyr), and sequence data (.seq) files utilized by the PSS/e program. The. raw, .dyr, and .seq are in text format that describes the interconnection of the system buses and provides data for the power system's components [109, 110].

To convert the PSS/e raw file to a readable RSCAD/Draft file, first, click the convert icon on the graphical user interface (GUI) of RSCAD software, as seen in Figure 3.5. Then, from the RSCAD conversion utility window, select PSS/e to RSCAD as shown in Figure 3.6; the PSS/e conversion GUI's main window will pop up, as shown in Figure 3.7. The PSS/e conversion window includes multiple tabs, and before applying the conversion process, multiple inputs and selections must be set. The input includes the PSS/e raw file (mandatory), dyr file (optional), seq file (optional), and some of the main selections include selecting the PSS/e version, load model, system frequency and network allocation. After setting the input data and selections, the proceed bottom is selected to start the conversion process.

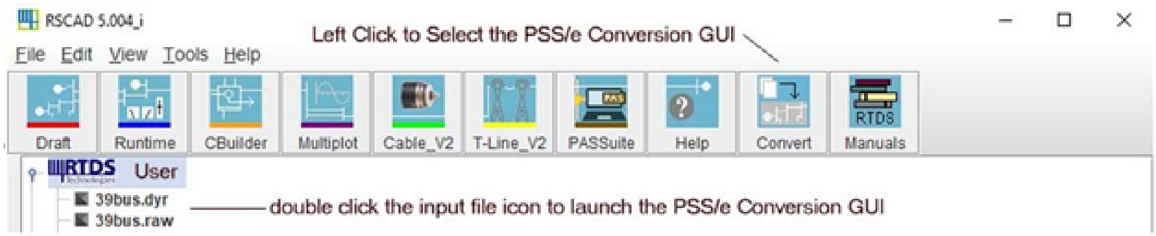

Figure 3.5: Launching the PSS/e Conversion GUI .

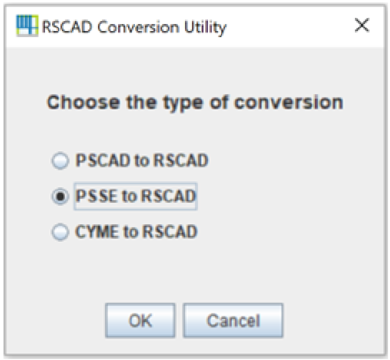

Figure 3.6: RSCAD conversion utility window.

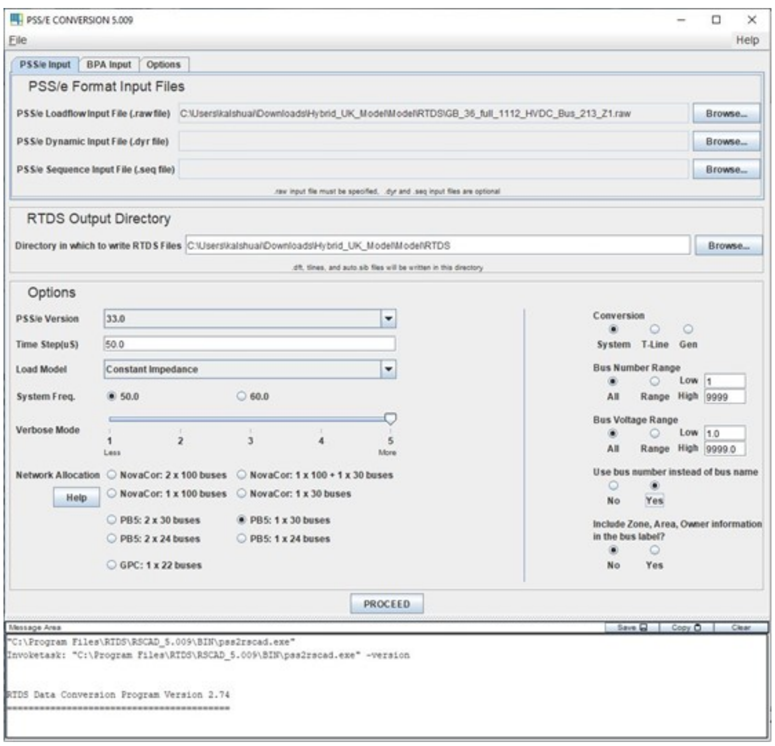

Figure 3.7: PSS/e conversion GUI's main window

If the conversion is successful, the following message appears in the message area "Conversion from PSS/e to RTDS completed successfully". After the conversion is completed, a couple of files will be generated, including the RSCAD/draft file (.sft) and RSCAD/ runtime file (.sib). The RSCAD draft file includes the layout of the components and parameters of the converted PSS/e file. The RSCAD draft file also has a library that contains power system, electronic, and control components. The RSCAD runtime file is used for multiple tasks such as running simulations, triggering events, monitoring signals and exporting data [109].

3. Connect the VSC-HVDC Model to the Assigned Buses

In this step, the VSC-HVDC model built in RTDS is added to the draft file and is connected between the zone 28 bus and the zone 32 bus.

4. Add TSAT-RTDS Interface to the RSCAD Draft File

TSAT-RTDS interface (TRI) is a tool that enables co-simulation between TSAT and RTDS. TRI is implemented using an FPGA installed in the user's PC's PCIe slot. This will allow RTDS and TSAT to exchange results at the end of every TSAT time step [111, 99]. Figure 3.8 shows the FPGA board, processing assignment, and TSAT Start signal. All three components are added to the RSCAD draft file. Figure 3.9 shows the TSAT interface connected to all the interface (boundary) buses between TSAT and RTDS.

5. Compile the Draft Case

After the system schematic is completed and all required components are added to the draft file, the draft file must be compiled. The compiling process checks if there are errors in the component parameters or connections and generate the executable code necessary to run the RTDS simulation [109].

6. Set Up the TSAT Case and Include the Boundary

This step is to set up the TSAT model and boundary. It is to be noted that the TSAT boundary should match the boundary in the RTDS.

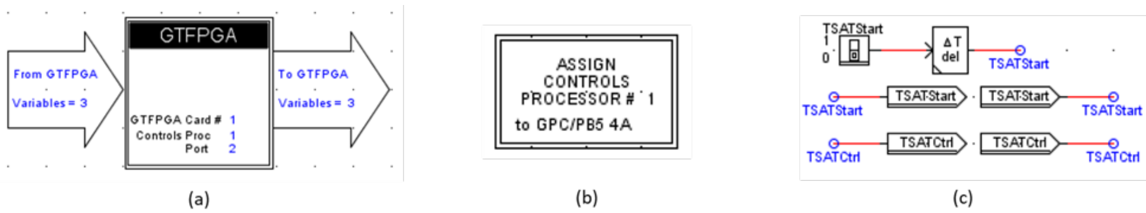

Figure 3.8: (a) FPGA board, (b) processing assignment, and (c) TSATStart signal.

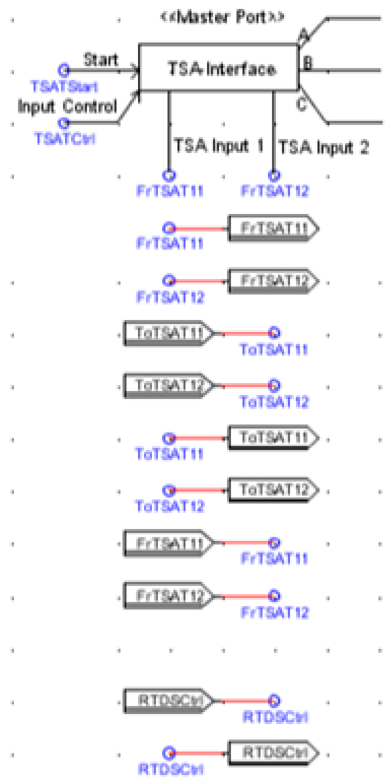

Figure 3.9: TSAT interface.

7. Start the Hybrid TSAT-RTDS Simulation and Run the Simulation if the Boundary Mismatch $< \epsilon$

The procedure to start and run the TSAT-RTDS hybrid simulation is summarized as follows:

- Open the RSCAD runtime and add the signal to be monitored and the switches, including the TSATStart switch. Make sure the TSATStart switch is set to off (0).
- Start the RTDS simulation by clicking the run case icon.
- In TSAT, run the hybrid simulation after clicking the "Run Hybrid Simulation" and then click start.
- When the boundary mismatch is small enough, switch TSATStart in the RSCAD runtime to on (1).

Figure 3.10 shows an example of the TSAT boundary mismatch window, and Figure 3.11 shows the RSCAD runtime window, including the TSATStart switch and Run case icon.

8. Monitor and Save Data

The last step is to monitor the signals and meters for bus frequency, voltage and power during and after disturbance. Also, it is possible to export the data from the RSCAD runtime.

Challenges in TSAT-RTDS Hybrid Model Development

- The number of buses and the type and quantity of models are limited to the capacity of the available RTDS hardware.
- High magnitude bus voltages fluctuation is observed after adding the VSC-HVDC. The cause of the voltage fluctuation is the absence of a high pass filter and reactor at the converter's terminal. The high pass filter, together with the reactor, filter out the switching harmonics. Also, when measuring the bus voltage in RTDS, a low pass filter is designed to further filter out the high-frequency harmonics.

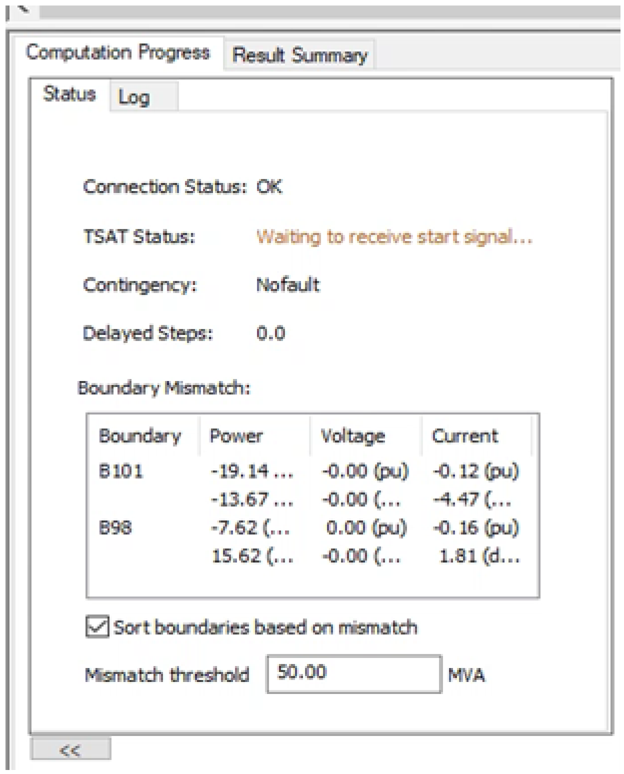

Figure 3.10: TSAT boundary mismatch window.

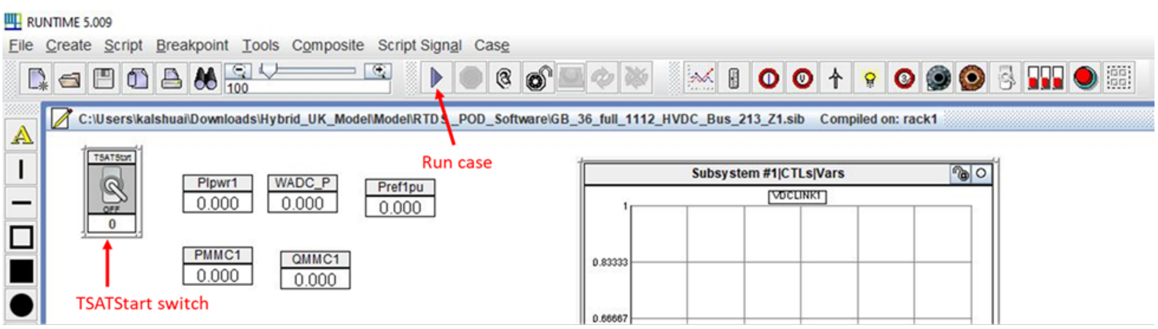

Figure 3.11: RSCAD runtime window.

3.4 Hybrid TSAT-RTDS Software Model Development

The dynamic response of the TSAT-RTDS hybrid model was compared with the reduced GB model in PSS/e and TSAT under a temporary three-phase fault on line 26-27W. Figure 3.12 to Figure 3.16 show the bus frequency response of the pump storage unit at zone 32, gas unit at zone 11 and 4, and nuclear unit at zone 27E and 1, respectively. The TSAT-RTDS hybrid model response is reasonably close to the pure PSS/e and TSAT models.

The dominant oscillation mode is calculated using Prony analysis in Table 3.2, where the oscillation frequency and damping ratio are close between the TSAT-RTDS hybrid model and pure PSS/e and TSAT models.

3.5 Software POD on TSAT-RTDS Hybrid Model

3.5.1 POD Structure

The POD structure via P modulation is designed in RTDS, as shown in Figure 3.17. The bus frequency difference of zone 1 and zone 32 is chosen as the input signal to the POD, and the POD output is added to the Pref of the VSC-HVDC active power controller.

The POD's parameters via P modulation of the VSC-HVDC are listed in Table 3.3. The output of the POD control is limited to ±10%. The phase shift block is bypassed because the phase shift angle of damping control of parallel HVDC links is close to zero [9, 101].

3.5.2 POD performance

Due to the limited capacity of the RTDS rack in UTK, the VSC-HVDC's total capacity of 5000 MVA or 3000 MVA cannot be accommodated. Therefore, a scaled-down VSC-HVDC model with a capacity of 800 MVA was used to test the POD controller performance.

The RTDS part, including the VSC-HVDC and POD controller, is shown in Figure 3.18. The performance of the POD controller via West Coast 3 VSC-HVDC has been validated for a temporary three-phase fault on bus 26-27W. The bus frequency deviations ($f_1 - f_{32}$)

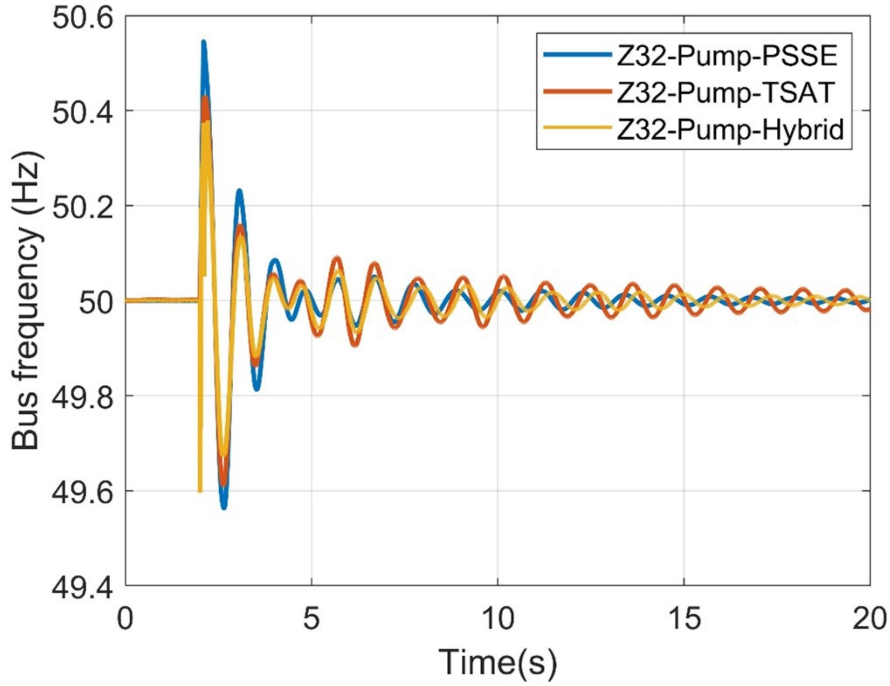

Figure 3.12: The bus frequency response of pump storage unit at zone 32 under temporary three-phase fault at line 26-27W.

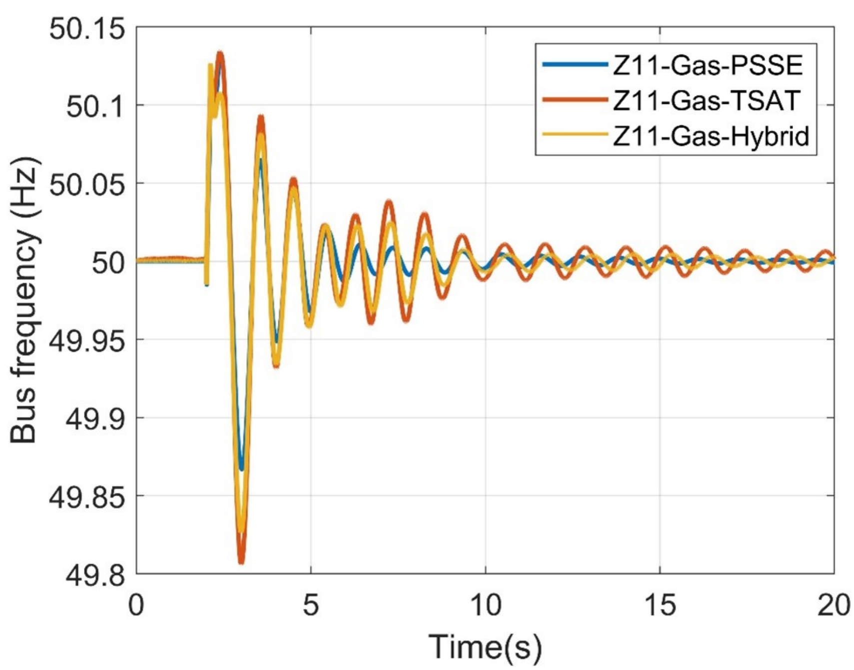

Figure 3.13: The bus frequency response of gas unit at zone 11 under temporary three-phase fault at line 26-27W.

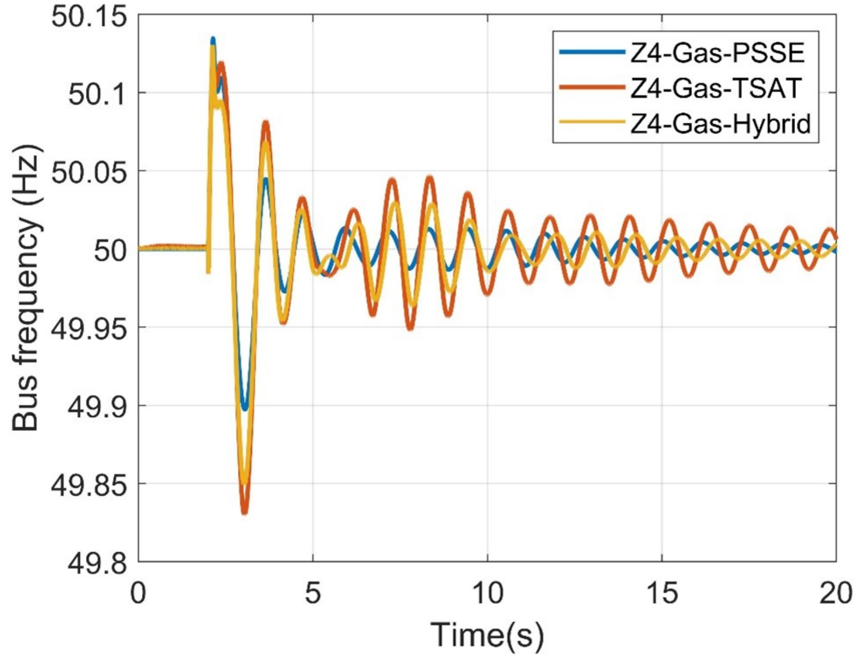

Figure 3.14: The bus frequency response of gas unit at zone 4 under temporary three-phase fault at line 26-27W.

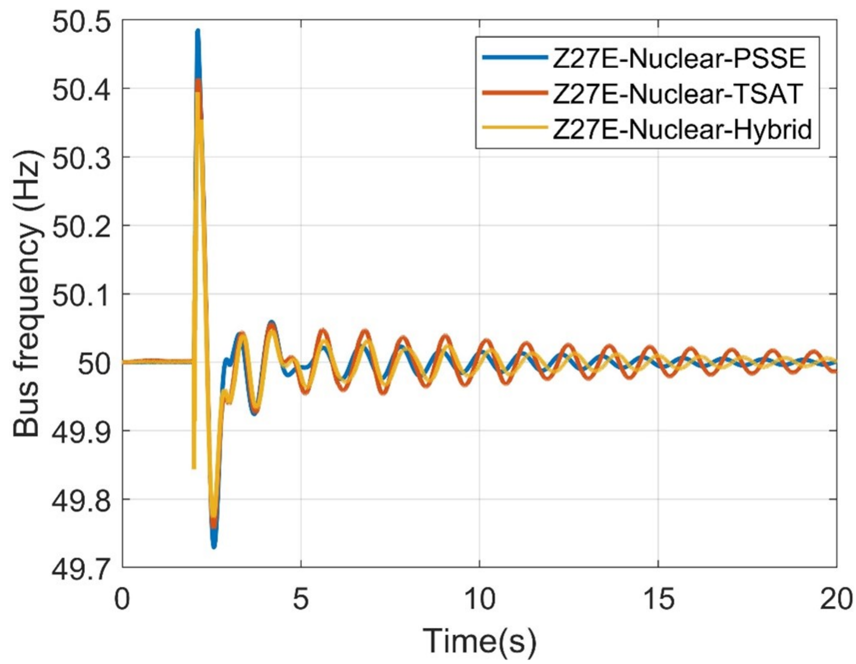

Figure 3.15: The bus frequency response of nuclear unit at zone 27E under temporary three-phase fault at line 26-27W.

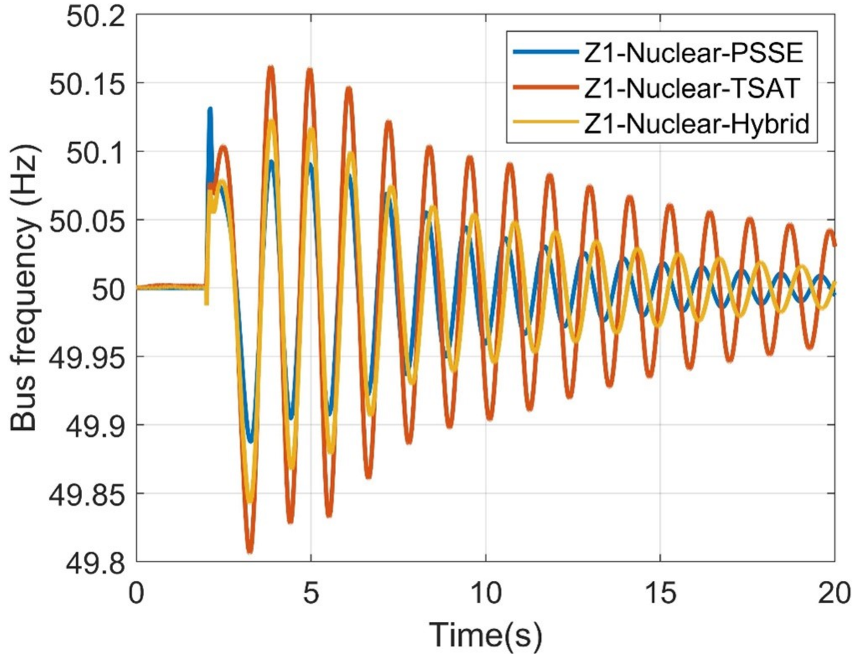

Figure 3.16: The bus frequency response of nuclear unit at zone 1 under temporary three-phase fault at line 26-27W.

Table 3.2: Prony analysis of the three models

Model	Frequency oscillation (Hz)	Damping ration (%)
PSS/e	0.886	2.8
TSAT	0.876	1.71
TSAT-RTDST hybrid	0.855	2.58

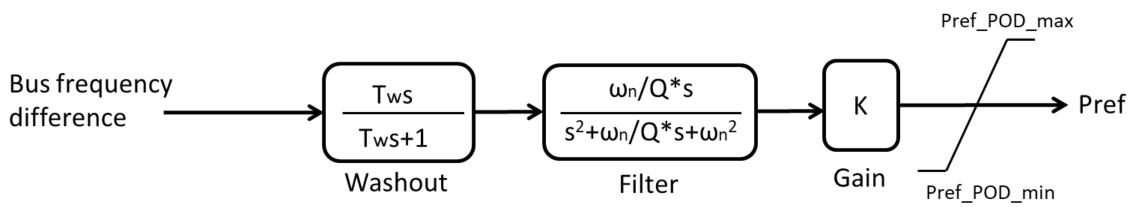

Figure 3.17: POD structure via P modulation.

Table 3.3: Parameters of POD via P modulation in RTDS

Tw (washout)	Wn (filter)	Q (filter)	K (control gain)
10	5.372	1	-150

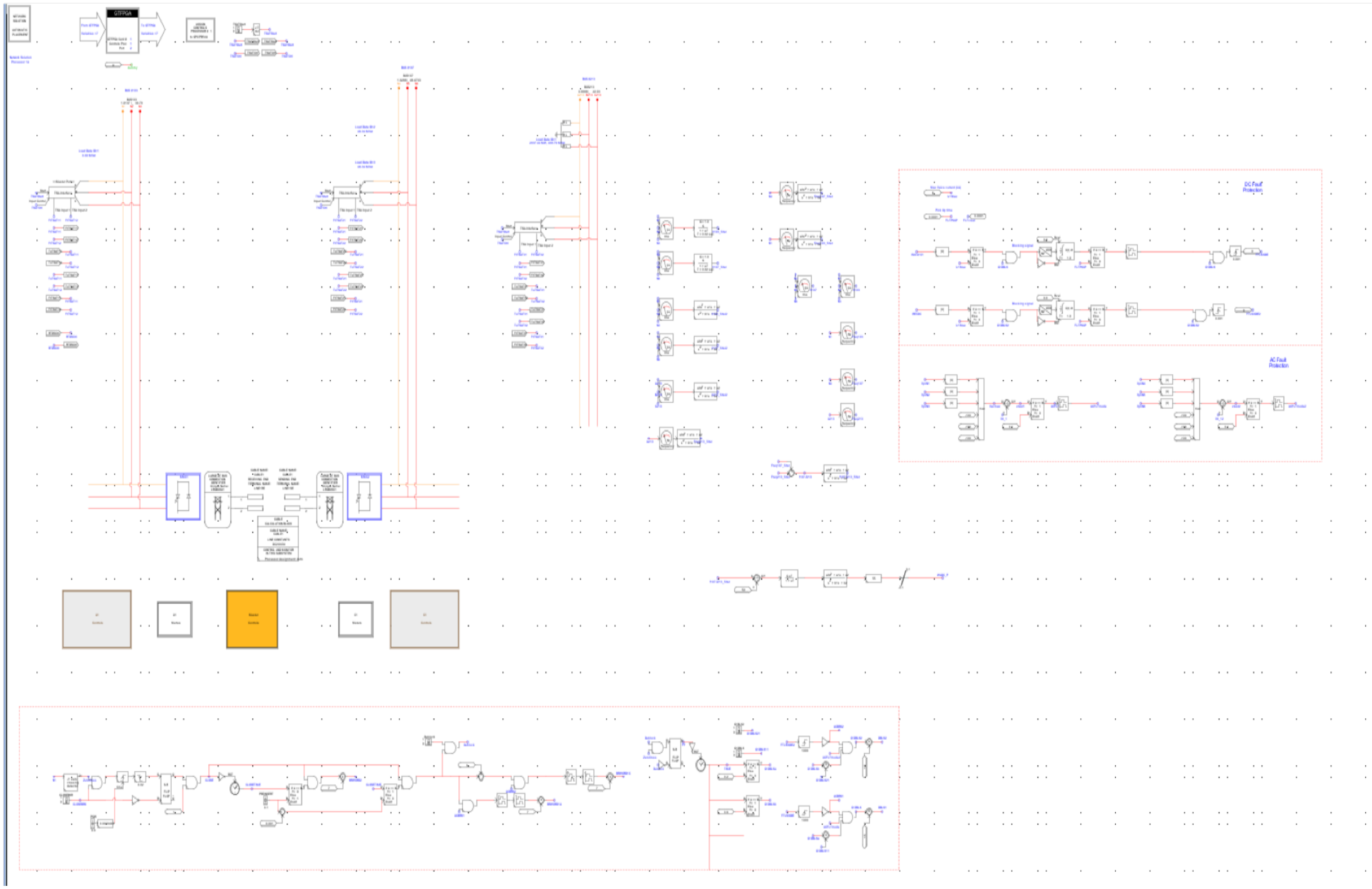

Figure 3.18: Screenshot of RTDS Part.

with and without POD via the West Coast 3 HVDC are given in Figure 3.19. It can be seen that POD, through active power modulation of the VSC-HVDC, can damp the oscillations.

Using Prony analysis, the oscillation frequency and damping ratio are calculated and shown in Table 3.4. After the implementation of the POD controller, the damping ratio increased from 2.58% to 7.57%. Figure 3.20 illustrates the POD output. It can be noted that the POD output hit the limit of $\pm 10\%$ from t=2 sec to t=10 sec, and this is reflected in the HVDC active power output as shown in figure 3.21, where the active power did not exceed the limit of $\pm 10\%$ or $\pm$ 80MW. Figure 3.22 depicts the HVDC DC voltage with and without POD.

3.6 Summary

The description of the GB model and the VSC-HVDC model setup in TSAT-RTDS were discussed. The dynamic response of the TSAT-RTDS hybrid model including the VSC-HVDC full model in RTDS was compared with the pure PSS/e and TSAT model under three-phase fault on line 26-27W. The result shows that the TSAT-RTDS hybrid model response is reasonably close to the pure PSS/e and TSAT model. Also, the performance of the wide-area POD controller through active power modulation of VSC-HVDC was investigated under a temporary three phase fault on line 26-27W. The simulation result shows that the POD via active power modulation of VSC-HVDC can effectively damp the oscillation and improve the damping ratio of the targeted oscillation mode.

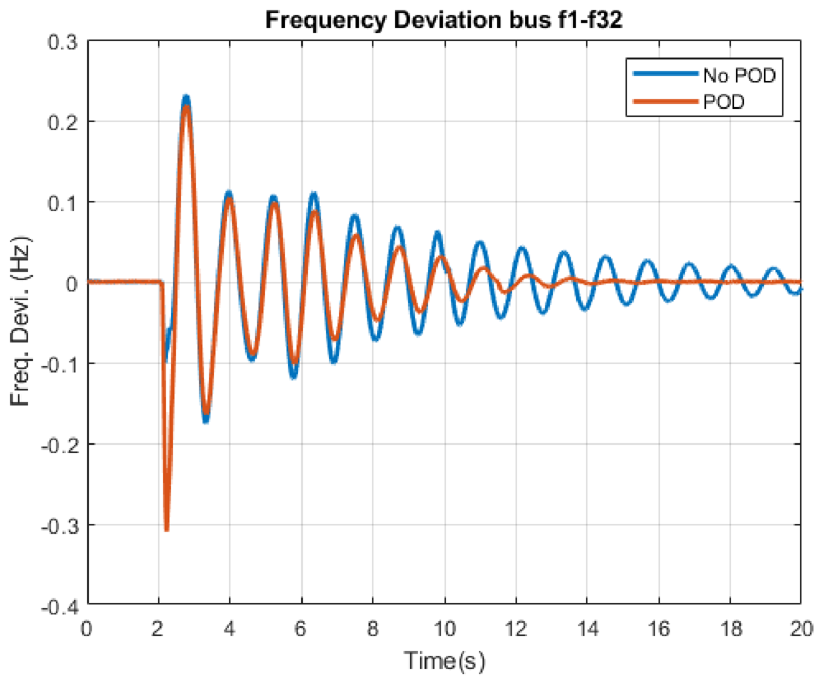

Figure 3.19: Frequency deviation of bus f1-f32 with and without POD.

Table 3.4: Oscillation frequency and damping ratio without POD and with POD with limit of ± 0.1

Test scenario	**Frequency deviation (Hz)**	**Damping ratio (%)**
Without POD	0.855	2.58
With POD ± 80 MW limit (± 0.1 p.u.)	0.887	7.57

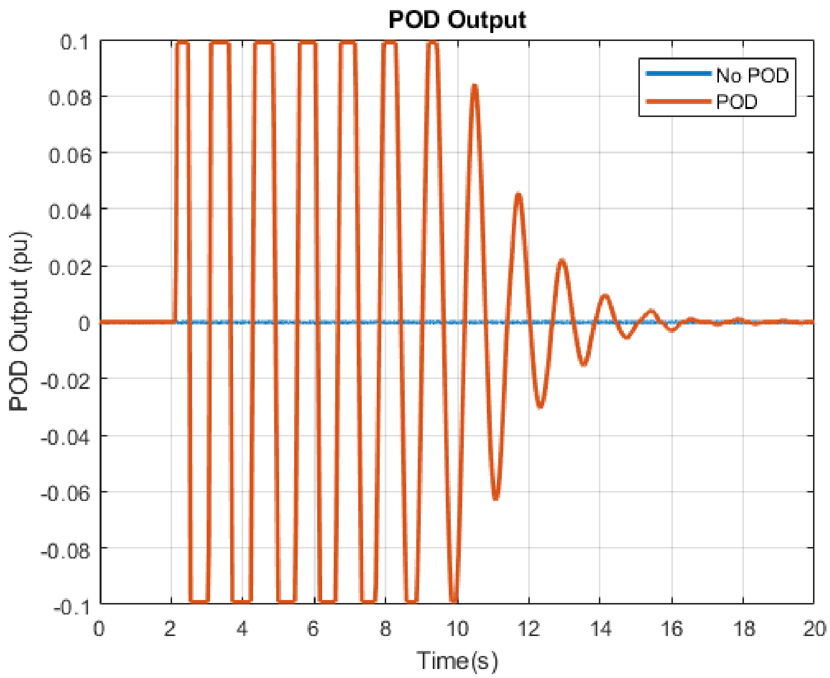

Figure 3.20: POD output with and without POD.

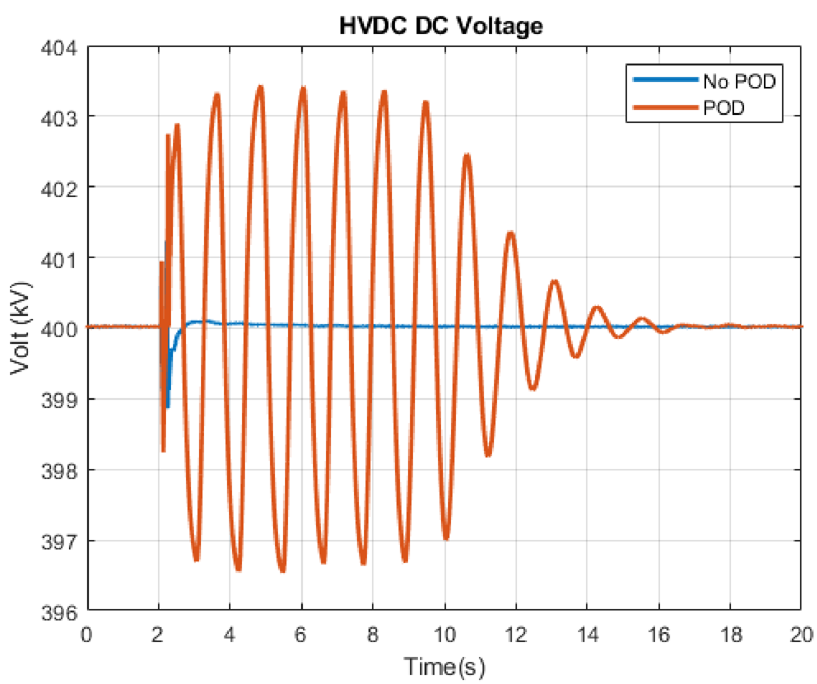

Figure 3.21: HVDC DC voltage with and without POD.

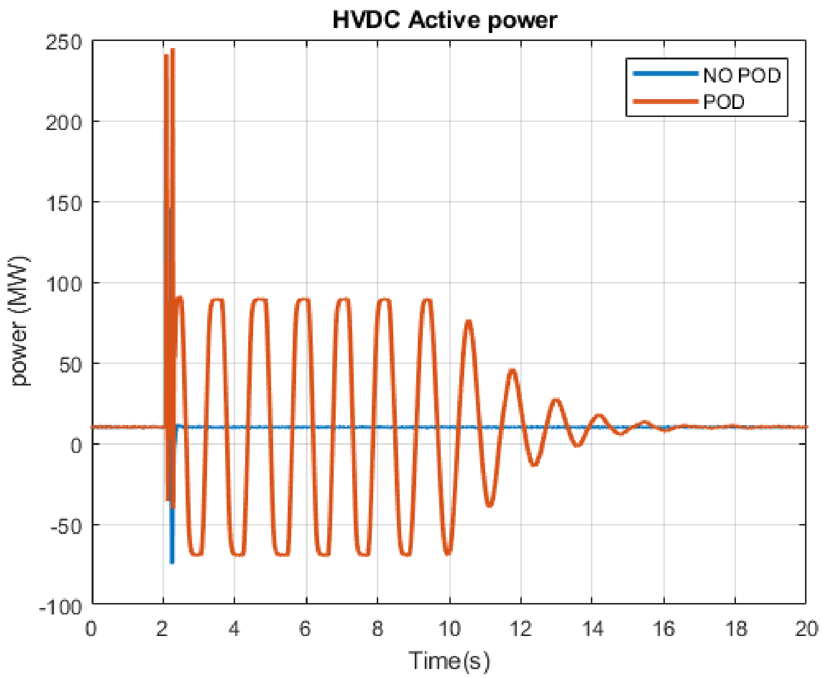

Figure 3.22: HVDC active power with and without POD.

Chapter 4

Hybrid TSAT-RTDS Hardware-In-the-Loop for UK system

4.1 POD implementation on CompactRio

The wide-area POD was employed on the National Instrument (NI) CompactRio real-time controller. The control is programmed using the LabVIEW programming environment. This section describes the function blocks of the cRIO-9035 [112].

4.1.1 Overview of Controller Structure

The wide-area POD controller structure is depicted in Figure 4.1. A brief description of each function block in Figure 1 is given below:

- The PMU data receiver utilizes BabelFish, a real-time data mediator. It includes features for receiving and processing numerical data in packages that comply with IEEE Standard C37.118.2-2011 for synchrophasor data transfer [113]. Because the damping controller needs to update the measurement in a timely manner and can tolerate occasional data loss, the BabelFish receiver was modified to support the User Datagram Protocol (UDP). As a result, the controller will not wait for lost packages and will proceed to the most recent accessible packages.

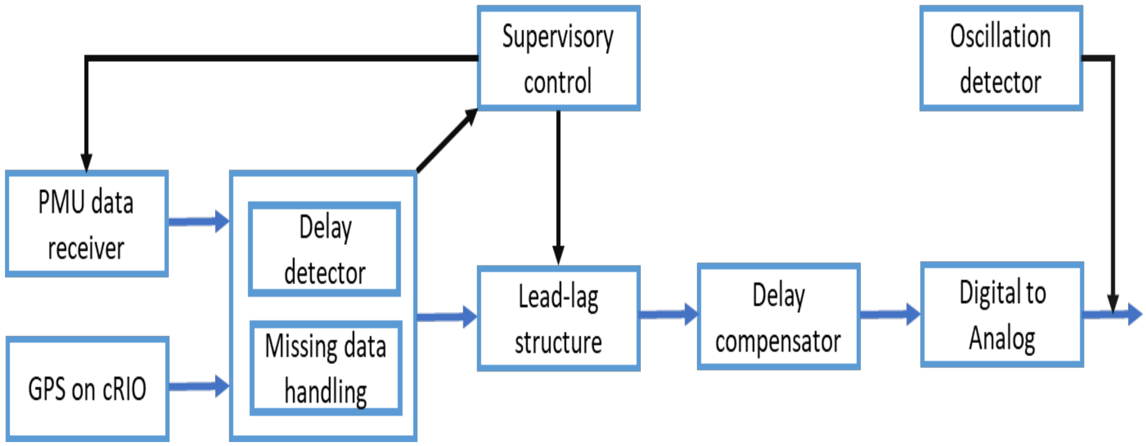

Figure 4.1: Overall structure of the controller.

- The GPS model, NI-9467, is utilized on the compactRIO to precisely monitor the communication delay between PMU and POD controller. The NI-9467 extension board is capable of generating a pulse-per-second (PPS) signal [114]. However, the wide-area POD controller needs a more precise step than the PPS. Therefore, to produce precise timestamps for the POD controller, an FPGA module is utilized to divide the PPS.

- The delay detector is utilized to measure the actual delay between the time the measurement is obtained from the PMU and the time the controller utilizes it. It is expected that a random delay to be introduced by the communication links during the HIL test or field test. Therefore, if the time delay is not appropriately compensated, it may cause a phase shift in the control output, resulting in degraded control performance. The actual delay can be determined by comparing the PMU and controller's timestamps as follow:

$$t_{actual-delay} = t_{PMU} + t_{CompactRIO} \tag{4.1}$$

- The missing data handling module handles the data loss resulting from data drop or congestion in the communication network.

- The supervisory control constantly observes the communication delay across all PMU channels and determines which channels are used for control.

- The lead-lag structure is an implementation of the transfer function.

- The delay compensator is responsible for monitoring the actual delay of the packages that are being utilized and selects the most effective parameters for the delay compensation.

- The oscillation detector is used to monitor and detect the oscillation in the grid and determine when to activate and deactivate the controller.

- The Digital to Analog conversion module is used to convert the controller output signal from digital to analog and send it to the RTDS.

4.2 Hybrid TSAT-RTDS Model Development

The GB model is divided into an internal and external system connected through boundary branches. The internal system is simulated in RTDS, and it consists of the VSC-HVDC detailed model for (W. Coast HVDC 3) and a bus from zone 1. The external system is the rest of the GB power system, and it is simulated in TSAT. The HIL test setup based on the hybrid TSAT-RTDS is given in Figure 4.2. As shown in Figure 4.2, the RTDS transmits a 10V analog signal to the amplifier, which then amplifies the signal to 120V before transmitting it to the PMU. The signal is then converted to a digital signal and forwarded to the network impairment simulator through a network switch. The communication network impairment simulator is utilized to evaluate the controller's performance under realistic conditions, including delay and data loss. The signal is then sent to the POD controller, and the POD controller's output is converted to analog before being sent back to the RTDS.

4.3 HIL Test Without Communication Impairment

In this section, the results of the hybrid RTDS-TSAT HIL test without communication impairment are presented. The communication network impairment simulator was bypassed to not introduce additional time delay and data drop. A temporary three-phase fault at line 26-27W is used as the disturbance. The performance of POD via P-modulation was investigated. The dynamic responses after the temporary three-phase fault at line 26-27W are shown in Figure 4.3 to Figure 4.6. Three cases are shown in in Figure 4.3 to Figure 4.6: no POD (blue), POD with limit +/- 80 MW via P-modulation on RTDS (red), and POD with limit +/- 80 MW P-modulation on CompactRIO (yellow). Using POD can improve the damping of the targeted oscillation. Furthermore, when POD is implemented on RTDS (software controller) or CompactRIO (hardware controller), the control effects are consistent.

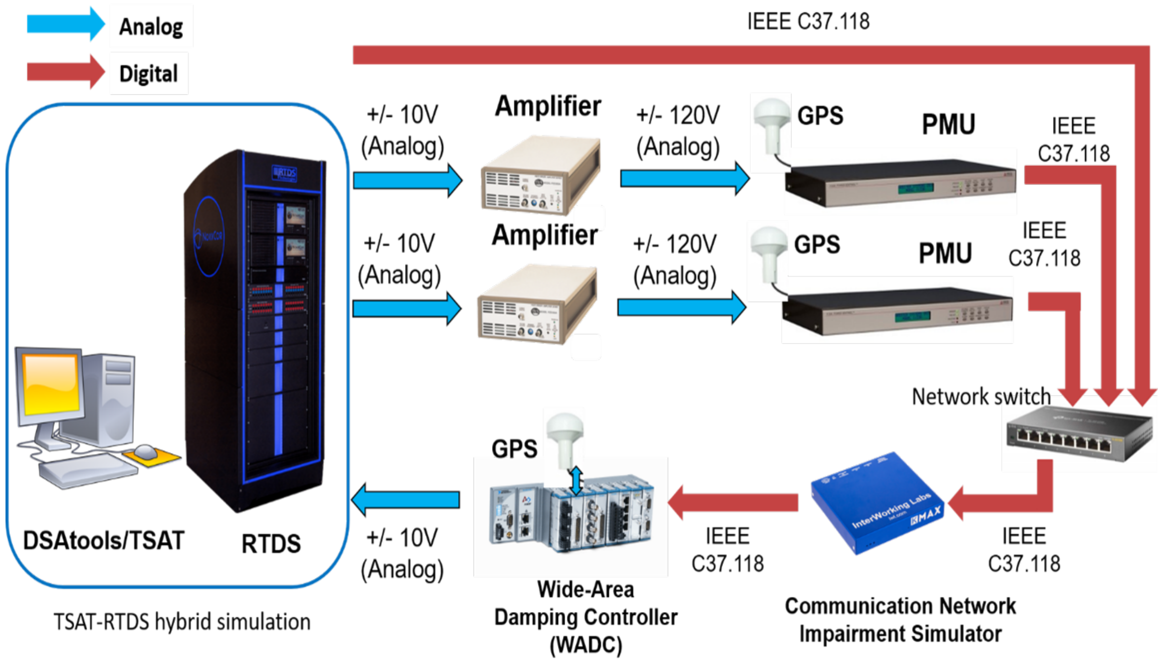

Figure 4.2: HIL test setup based on hybrid TSAT-RTDS simulation [115].

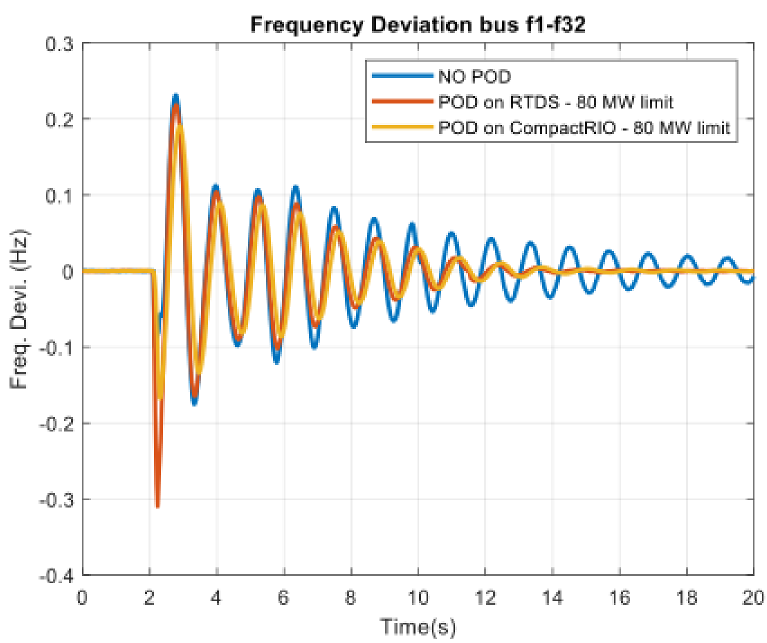

Figure 4.3: Frequency deviation of zone1 – zone 32 when POD with +/-80 MW limit via P-modulation is applied after a fault at line 26-27W.

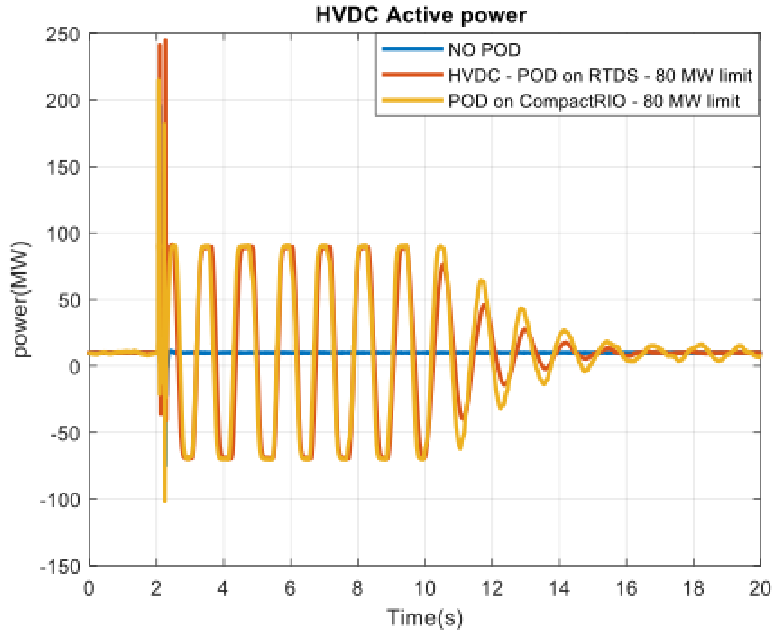

Figure 4.4: HVDC active power when POD with +/-80 MW limit via P-modulation is applied after a fault at line 26-27W.

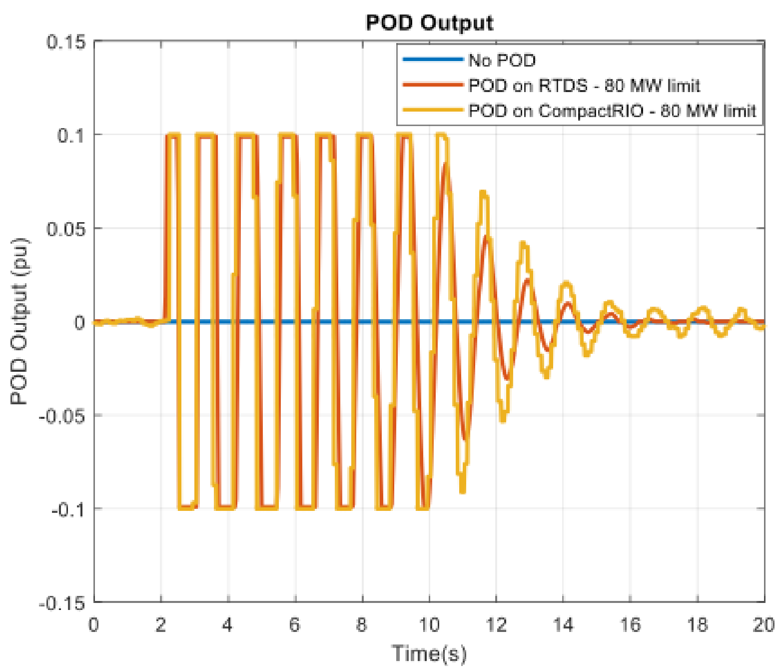

Figure 4.5: POD output when POD with +/-80 MW limit via P-modulation is applied after a fault at line 26-27W.

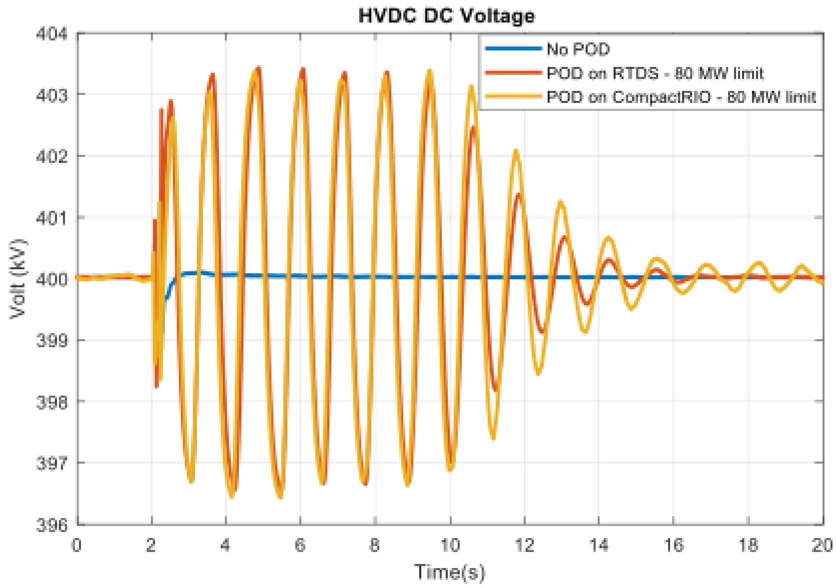

Figure 4.6: HVDC DC voltage when POD with +/-80 MW limit via P-modulation is applied after a fault at line 26-27W.

4.4 HIL Test with Communication Impairment

In this section, the POD was tested under different communication impairments. A POD with P-modulation during a temporary three-phase fault at line 26-27W was tested in all the communication impairment scenarios.

4.4.1 Constant Time Delay

The POD via P-modulation during a temporary three-phase fault at line 26-27W was tested when a constant time delay is applied to the communication impairment simulator without delay compensation in the controller. The test results are shown in Figure 4.7, in which four cases are compared: No POD (blue), POD via P-modulation without delay (red), POD via P-modulation with 400 ms delay (yellow), and POD via P-modulation with 600 ms delay (purple). When the time delay (e.g., 400ms, 600 ms) is not compensated, it could reduce the damping and excite the oscillation.

One method to determine the time delay that leads to instability is through the small signal stability analysis. The authors in [116] incorporated the wide-area damping control with the time delay in driving the small signal stability model. Moreover, by using the small signal state space model to perform eigenvalue analysis and by varying the time delay, the time delay that causes that dominant eigenvalue to cross the imaginary axis is the time delay that causes the system to be unstable.

The detrimental effects of time delay, on the other hand, can be mitigated by using delay compensation. As shown in Figure 4.8, the POD can provide sufficient damping after the delay compensator is applied. The control effect is similar to POD without time delay. The delay compensator parameters were set for 400 ms or 600 ms accordingly.

4.4.2 Random Time Delay

The POD was further evaluated when a random time delay is introduced. The buffer-based delay compensator was used, and the buffer size is 400 ms. The test results are shown in Figure 4.9, in which three cases are compared: No POD (blue), POD via P-modulation

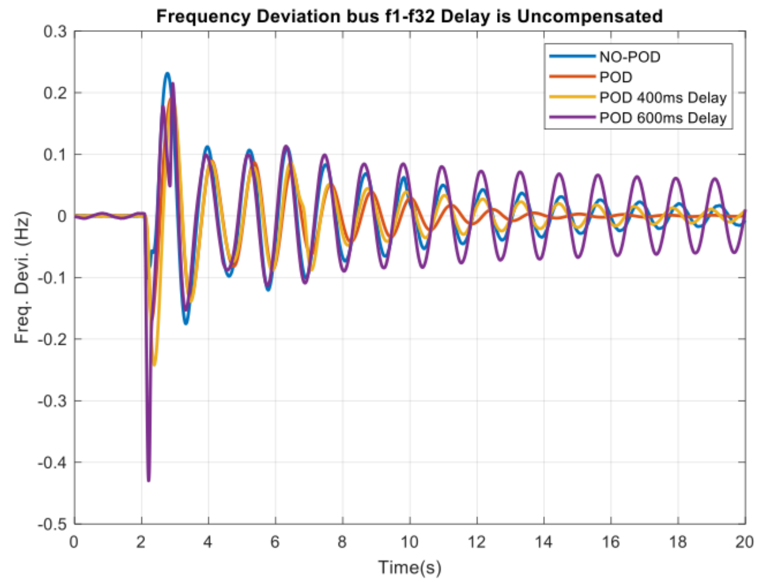

Figure 4.7: Control effect of POD via P-modulation with constant delay.

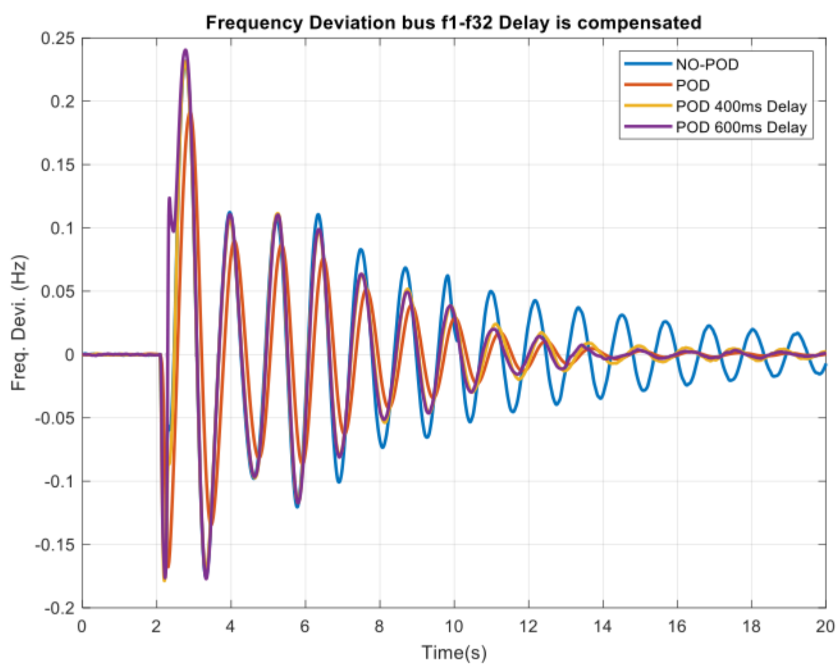

Figure 4.8: Control effect of POD via P-modulation with constant delay and delay compensation.

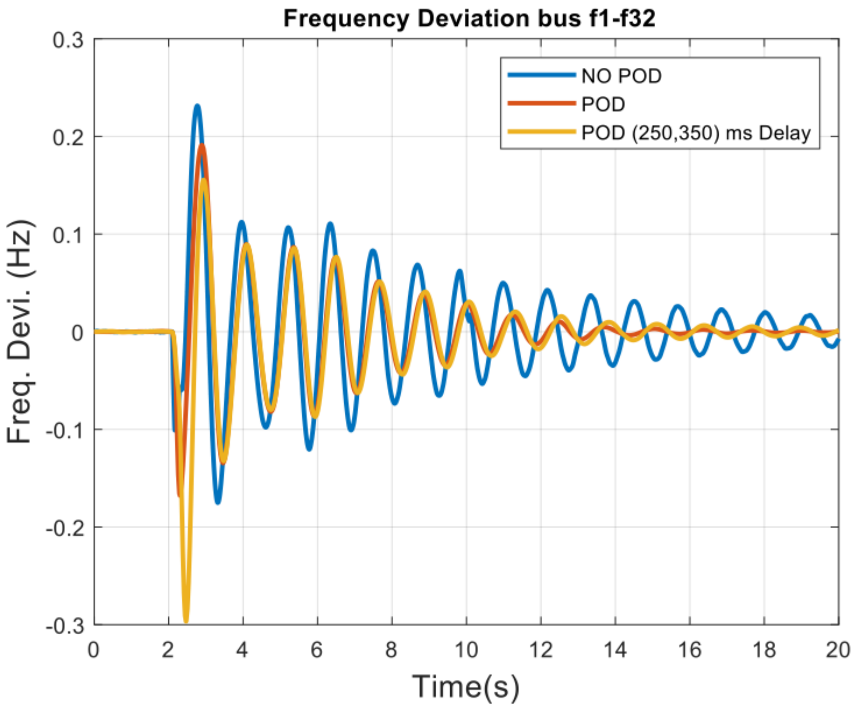

Figure 4.9: Control effect of POD via P-modulation with random time delay.

without delay (red), and POD via P-modulation with a time delay of (250-350) ms (yellow). Under the random time delay, the control effect can be guaranteed if the time delay is less than the buffer size of 400 ms.

4.4.3 Random Time Delay and Occasional Data Drop

The POD was evaluated under random time delay, and occasional data drop. The buffer-based delay compensator was used, and the buffer size is 400 ms. The test results are shown in Figure 4.10. When the data drop rate is 50%, the POD can still provide sufficient damping. In the other case, the POD was verified under the random delay (250-350) ms and data drop rate of 50%. The POD can function well to provide sufficient damping to suppress the oscillation mode, as shown in Figure 4.11.

4.4.4 Intolerable Time Delay with Supervisory Control

When the delay is larger than the buffer size, the controller cannot fully compensate for the time delay resulting in a poor control effect. In this situation, the developed supervisory control module can switch the primary PMU to a backup PMU, allowing the controller to generate control commands based on the PMU measurements with better data quality. The test results are shown in Figure 4.12. When the random time delay is (600 to 1000) ms, if there is no supervisory control module, an oscillation with poor damping could appear. However, if the supervisory control module can switch to a backup PMU, the oscillation can be suppressed, and the control effect is similar to the no time delay case.

4.4.5 Consecutive Data Drop with Supervisory Control

Similarly, when consecutive data drop occurs in the primary PMU, it is necessary to switch to a backup PMU to guarantee the control effect. The test results under consecutive data loss with and without the supervisory control module are compared in Figure 4.13. With the supervisory control module, the control effect is guaranteed. It should be noted that the case with consecutive data drop and supervisory control (purple) is slightly better than the

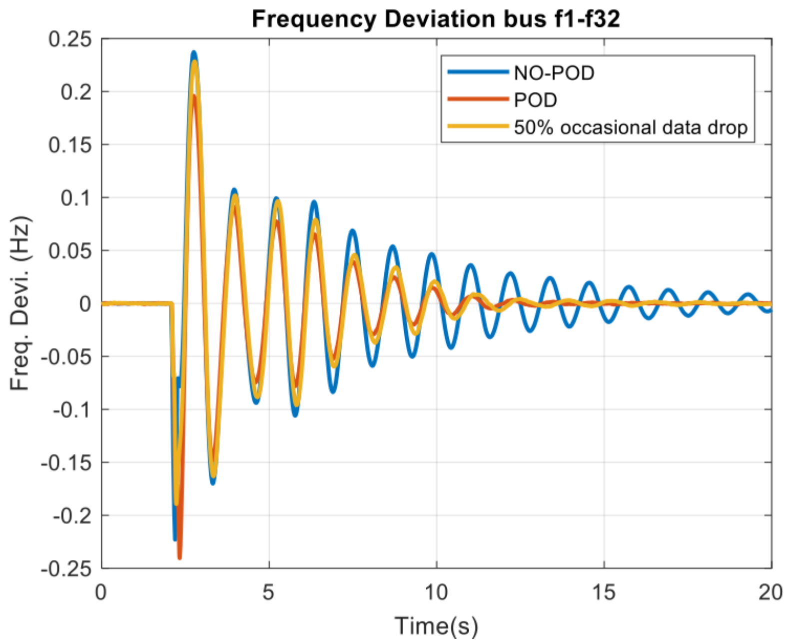

Figure 4.10: Control effect of POD via P-modulation with occasional data drop.

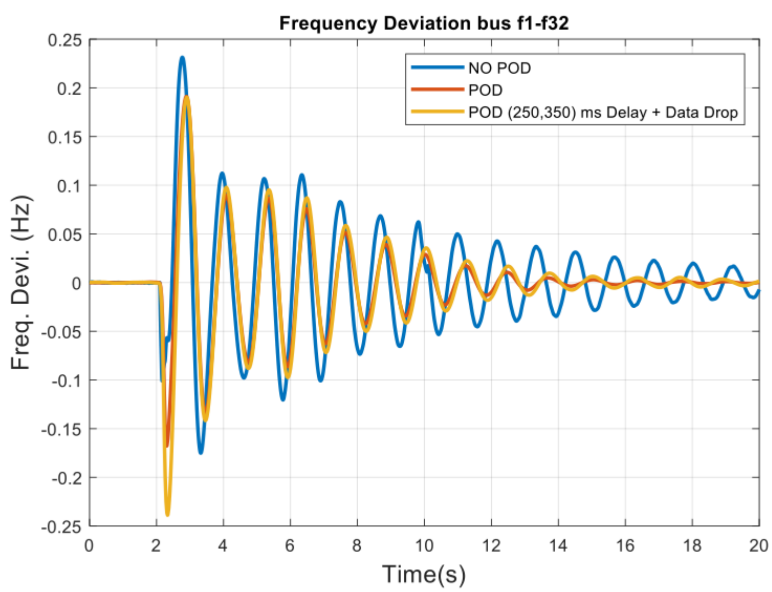

Figure 4.11: Control effect of POD via P-modulation with random time delay and occasional data drop.

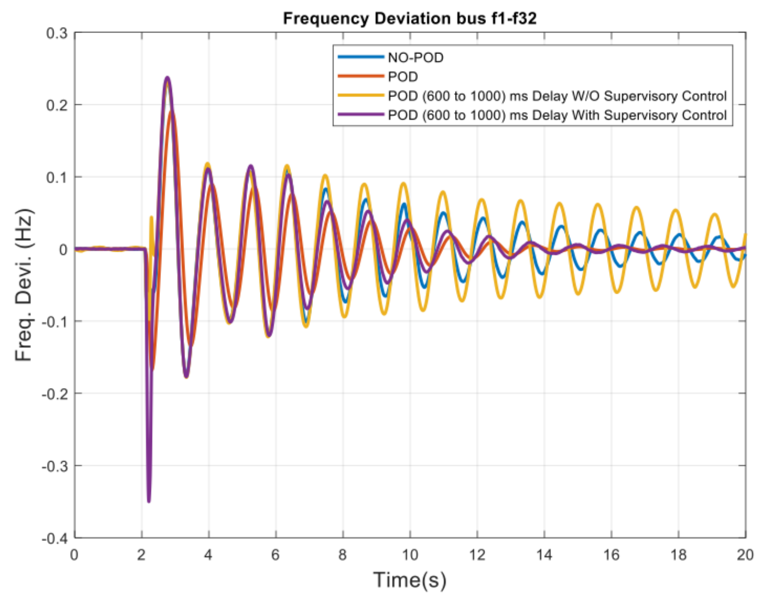

Figure 4.12: Control effect of POD via P-modulation with random time delay and supervisory control.

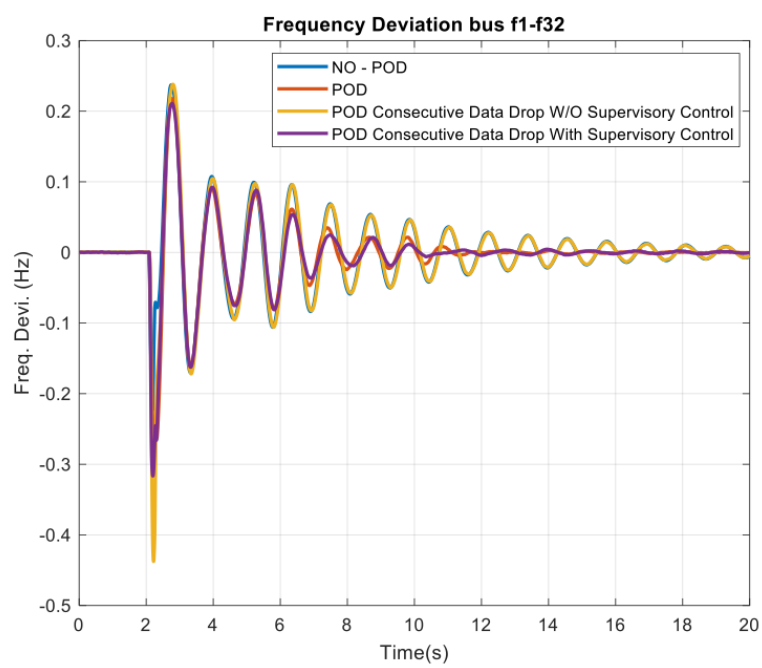

Figure 4.13: Control effect of POD via P-modulation under consecutive data loss with supervisory control.

base case without consecutive data drop (red). The reason is that the case with consecutive data drop and supervisory control (purple) uses the backup virtual PMU, which has better data quality than the primary PMU. In addition, it should be noted that the consecutive data loss from 1s to 20 sec. It is also to be noted that the POD controller output limit is increased in this case.

4.5 Summary

The developed POD controller via VSC-HVDC was implemented on a general-purpose hardware platform CompactRIO and tested on a HIL test setup based on the TSAT-RTDS interface with actual PMU devices and a communication network impairment simulator. Realistic operating conditions are considered in the HIL tests, including measurement error/noise, occasional/consecutive data package losses, constant/random time delays, and multiple backups PMUs. The results indicate that the POD controller is capable of providing adequate damping to suppress the targeted oscillation mode.

Chapter 5

Forced Oscillation Vulnerability Analysis and Mitigation

5.1 Introduction

This chapter proposes a general method for forced oscillation grid vulnerability analysis and mitigation through IBRs in large-scale power grids [15]. To reduce the forced oscillation effect in the entire system, a forced oscillation damping controller at an effective IBR actuator can be activated before the exact forced source is identified and removed. First, critical areas/zones under different specified forced oscillation frequencies that can excite the most severe forced oscillation across a large-scale power system can be identified by using a detailed location and frequency scanning method. These identified critical areas/zones under the specified forced oscillation frequencies are also effective locations as the actuators of forced oscillation damping controllers when the forced oscillation sources are narrowed down inside or close to the critical areas/zones. Secondly, a forced oscillation damping controller through active power modulation control via IBRs is designed to reduce the impact of the forced oscillation event before the forced source is removed.

5.2 Framework of the Algorithm

Figure 5.1 shows the framework of the proposed method to identify the critical areas/zones under different forced oscillation frequency events and the damping control of the forced oscillation.

To mimic the forced oscillation events in the simulation model, a sinusoidal signal with a specified frequency can be added to the active power set point of the governor model or to the voltage set point of the exciter model at a synchronous generator. In addition, forced oscillation can also be mimicked in simulation by modulating the active or reactive power of the load with a specified frequency. A two-dimensional (frequency and location) scanning method is utilized for the forced oscillation vulnerability analysis to identify the critical areas/zones and the oscillation frequencies that could excite the most severe forced oscillation. The frequency dimension scanning is performed by changing the forced oscillation frequency in a specific range (e.g., from 0.1 Hz to 1.5 Hz) at a fixed source location. A high-voltage bus frequency deviation in each area/zone is used as the indicator of the forced oscillation energy in each area/zone. The location dimension scanning is performed by changing the forced oscillation source location across the system under different specified forced oscillation frequencies. The critical frequency and critical locations that can excite the maximum bus frequency deviation are determined through frequency dimension scanning and location dimension scanning.

Once the critical areas/zones under different forced oscillation frequencies are identified, a local forced oscillation damping controller can be designed and implemented at IBRs in these areas as candidates to mitigate the forced oscillation event. The ideal location of the damping controller/actuator would be the same as the external source to reduce the forced oscillation energy. However, when the forced source location can be quickly narrowed down in the relative area that is inside or close to the critical areas/zones with the forced damping controller, the damping controller can be activated to reduce the forced oscillation impact before the accurate forced source is identified and removed. In other

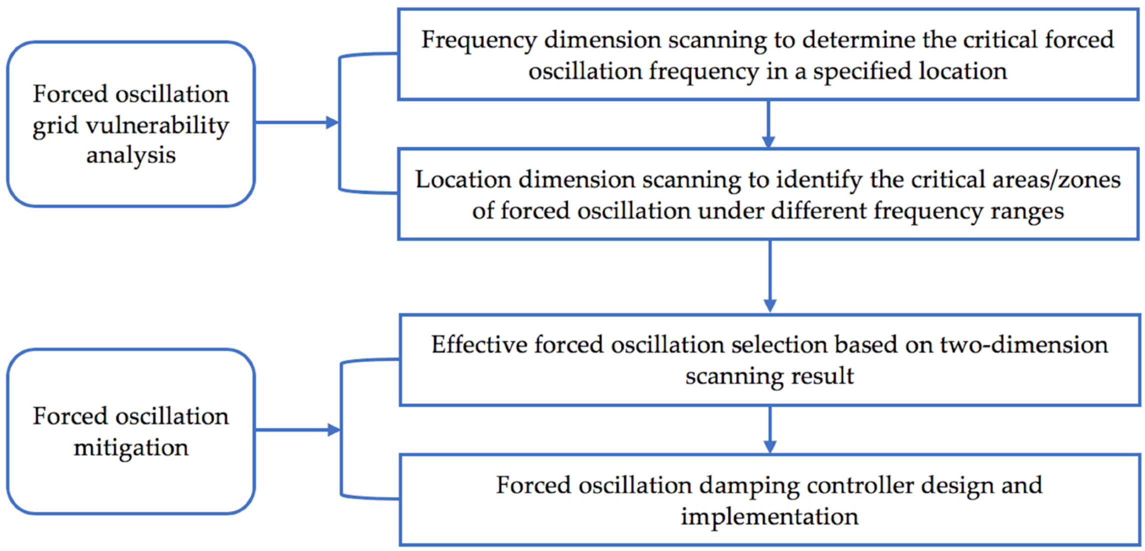

Figure 5.1: Framework of the forced oscillation identification and mitigation procedure.

words, the identified critical areas/zones are the effective locations of the actuator with a forced oscillation damping controller.

5.3 Two-dimensional scanning

The two-dimensional scanning grid vulnerability method is used to identify the critical areas/zones and frequencies to forced oscillation in a power grid. The two-dimensional scanning method comprises of frequency dimension scanning and location dimension scanning. This section presents an explanation of the frequency and location dimension scanning.

5.3.1 Forced Oscillation Frequency Scanning

The frequency dimension scanning is performed by changing the forced oscillation frequency with a small, fixed step size in a specified range of frequencies at a fixed source location. For each specified oscillation frequency, the bus frequency signals at the high voltage substations in each zone/area are recorded to calculate their peak–to–peak frequency deviation. The maximum peak–to–peak bus frequency deviation in each zone is used as an indicator of the severity of a forced event impact in each zone. By comparing the peak–to–peak bus frequency deviation in all these zones/areas, the maximum value will be chosen to represent the peak–to–peak frequency deviation under this specified oscillation frequency. The peak–to–peak frequency deviations for the different frequencies are sorted in ascending order, and the frequency with the largest frequency deviation is determined as the most critical forced oscillation frequency at this fixed source location.

5.3.2 Forced Oscillation Location Scanning

Location dimension scanning is conducted by changing the source location through the entire grid with the same forced energy. The peak–to–peak frequency deviations under different forced sources are then compared to identify the critical location to the forced oscillation event. The largest synchronous generator at each zone or a load added at the bus of the largest synchronous generator at each zone is selected as the forced source. The above-mentioned frequency dimension scanning procedure is repeated at each selected generator. For each selected forced oscillation source, the maximum peak–to–peak bus frequency deviation under each specified forced oscillation frequency can be obtained. After the location dimension scanning, the peak–to–peak frequency deviations under each specified forced oscillation frequency at different forced oscillation sources are sorted in ascending order, and the source location with the largest frequency deviation is identified as the most critical location for the forced oscillation event with the specified forced oscillation frequency in the power system.

5.4 Forced Oscillation Generation in Simulation

This section presents how the forced oscillation can be excited in simulation through the generator's or load's active or reactive power disturbance. To fairly compare the bus frequency deviation in the frequency and location dimension scanning, the forced oscillation disturbance energy is modified to the same peak-to-peak amplitude for all forced sources. In this study, the peak-to-peak forced oscillation disturbance energy is set to 100 MW or 100 Mvar to excite a severe forced oscillation in the system.

5.4.1 Forced Oscillation Generation through Active Power Modulation of Generator

Forced oscillation in simulation is mimicked by changing the active power set point of the generator's governor. Figure 5.2 shows TGOV1, the steam-turbine governor model, with a sinusoidal waveform applied to the active power set point of the governor. The sine signal is described as:

$$\Delta P(t) = A\, sin(2\pi f t) \tag{5.1}$$

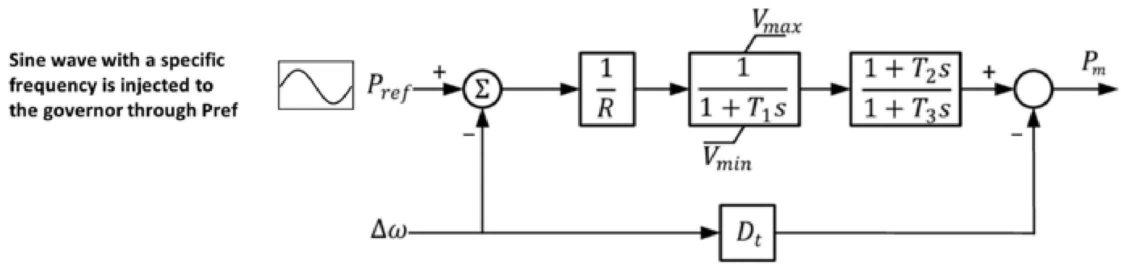

Figure 5.2: Sinusoidal signal added to governor turbine model TGOV1.

Where A is the amplitude of the sinusoidal signal, f is the forced oscillation frequency, and ΔP(t) is the active power that is applied to the governor active power set point.

Figure 5.3 illustrates an example of the generator's active power output at 0.4 Hz forced oscillation frequency and 100 MW peak-to-peak forced oscillation energy.

5.4.2 Forced Oscillation Generation through Active Power Modulation of Load

In this study, a load is added at the bus of the largest generator in each area/zone during the simulation of the forced oscillation event. The active and reactive power is set to zero, and when the forced event starts, the active power of the load is modulated with a specified frequency to mimic the force oscillation event. The peak-to-peak forced oscillation energy is set to 100 MW. Figure 5.4 illustrates an example of the active power output of the added load when the forced oscillation frequency is 0.67 Hz, and the peak-to-peak forced oscillation energy is 100 MW. It is to be noted that the reason for adding the load at the bus of the synchronous generator with the largest capacity in each area/zone is to create a close system frequency response to when the forced oscillation disturbance is through active power modulation of the generator.

5.4.3 Forced Oscillation Generation through Reactive Power Modulation of Generator

Forced oscillation through reactive power modulation of the generator can be excited in simulation by varying the voltage set point of the exciter model. A sinusoidal signal is applied to the exciter voltage set point, as shown in Figure 5.5. Figure 5.6 illustrates an example of the generator's active power output at 0.4 Hz forced oscillation frequency and 100 Mvar peak-to-peak forced oscillation energy.

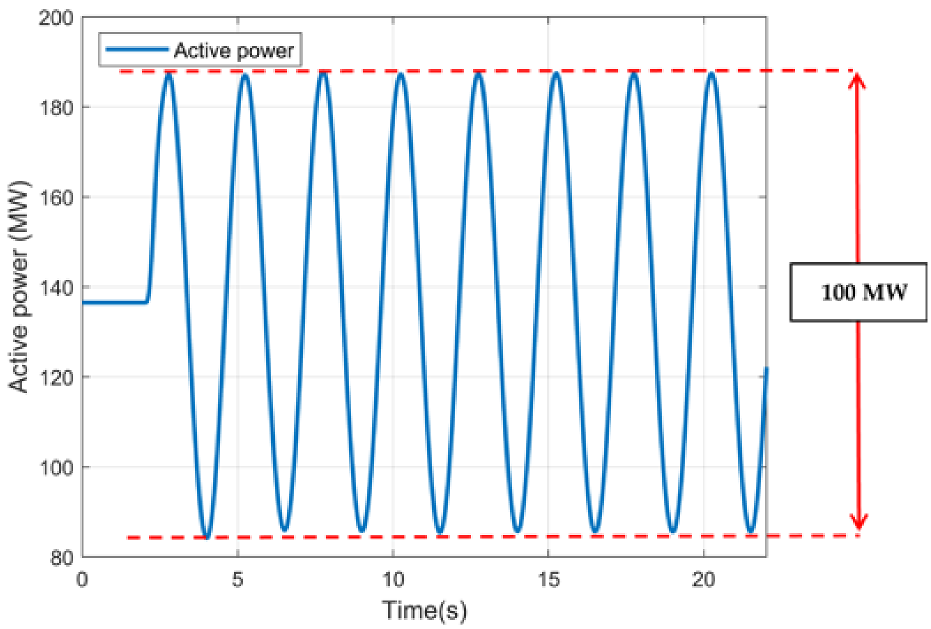

Figure 5.3: A generator's active power output in MW oscillates with a 0.4 Hz forced oscillation frequency.

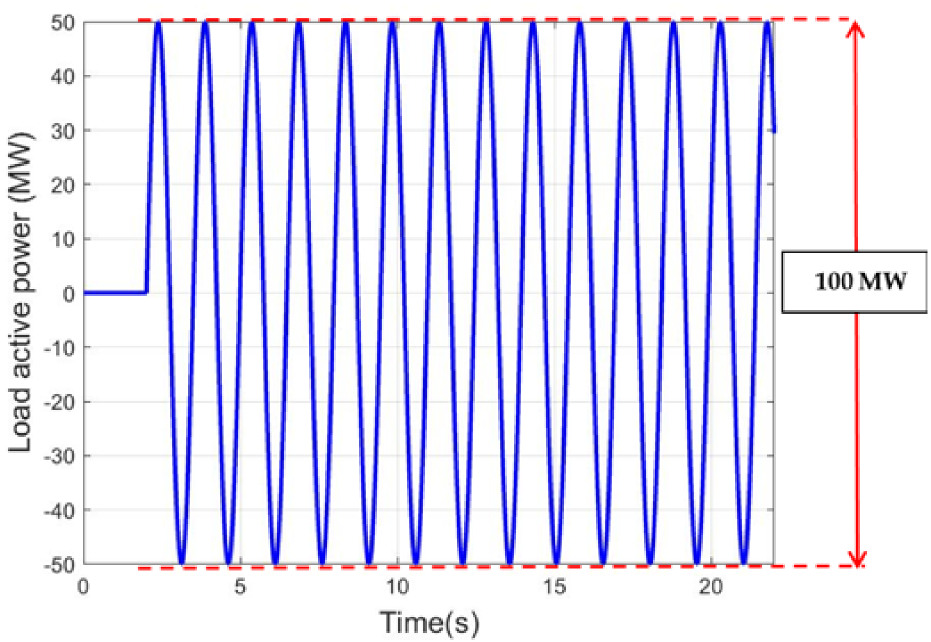

Figure 5.4: Active power output in MW of an added load with a 0.67 Hz oscillation frequency.

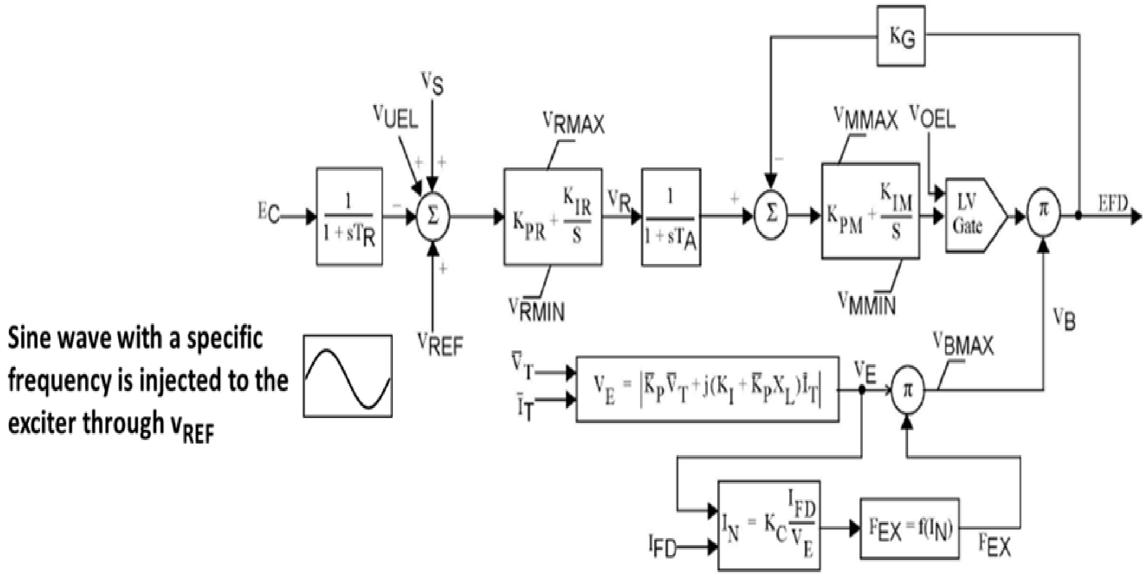

Figure 5.5: Sinusoidal signal added to exciter model ESST4B. [117].

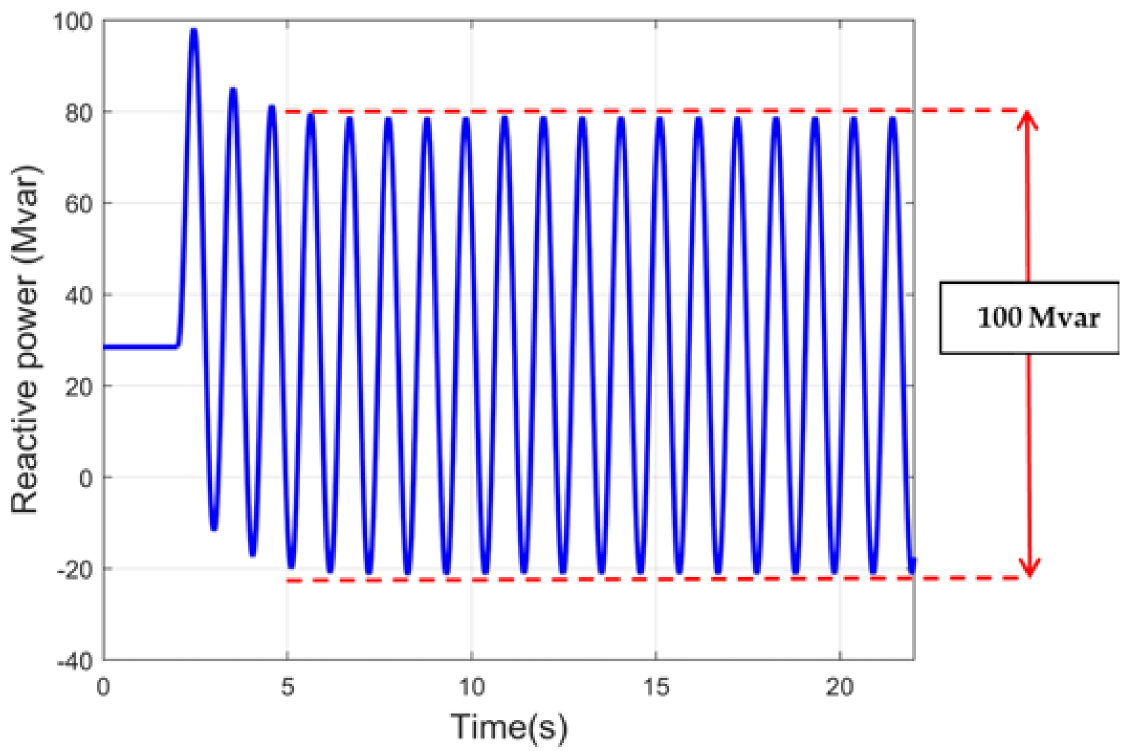

Figure 5.6: A generator's reactive power output in Mvar oscillates with a 0.95 Hz forced oscillation frequency.

5.4.4 Forced Oscillation Generation through Reactive Power Modulation of Load

In this study, forced oscillation is excited through reactive power modulation of load by adding a load added at the bus of the largest generator in each area/zone during the simulation of the forced oscillation event. The active and reactive power is set to zero, and when the forced event starts, the reactive power of the load is modulated with a specified frequency to mimic the force oscillation event. The peak-to-peak forced oscillation energy is adjusted to 100 Mvar.

5.5 Actuator Selection of Forced Oscillation Controller via IBRs

Based on the above two-dimension scanning results, the critical locations to the forced oscillation event under different specified oscillation frequencies can be further considered as the candidate effective actuator location of the oscillation damping controller to reduce the critical forced oscillation impact in the whole system.

Since the oscillation frequency and the relatively large area with the forced source can be quickly estimated, the effective candidate actuators (IBRs) that are close to or in the forced source areas can be activated to reduce the forced source impact before the accurate forced source is located and removed.

5.6 Forced Oscillation Damping Controller Design through IBR

This section presents the design of the forced oscillation damping control through active and reactive power modulation of IBR. The proposed forced oscillation damping control is through a utility-scale inverter-based wind/solar model. The IBRs are modeled using dynamic models developed by the Western Electricity Coordinating Council (WECC) Renewable Energy Modeling Task Force [118].

Figure 5.7 shows the proposed controller, which is a droop controller with the frequency deviation of its local high voltage bus as input. The dynamic models of IBR consist of the generator/converter model (REGCAU2) and the electrical control model (REECCU1). For active power modulation of IBR, the controller's output is added at Paux to modulate the active current of the IBR, as shown in Figure 5.8. For reactive power modulation of IBR, the controller's output is added at pfaref to modulate the reactive current of the IBR, as shown in Figure 5.9. Variables PfFlag, VFlag, and QFlag are set to be 1.

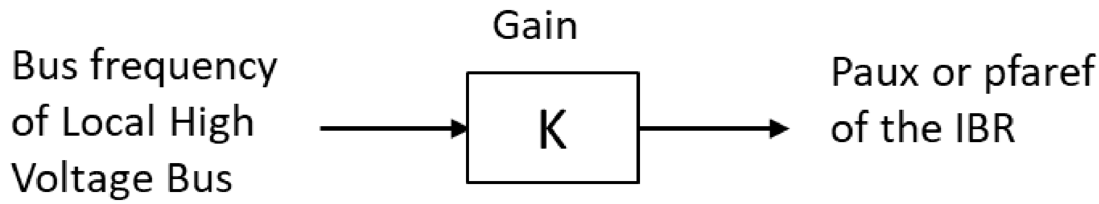

Figure 5.7: Controller structure.

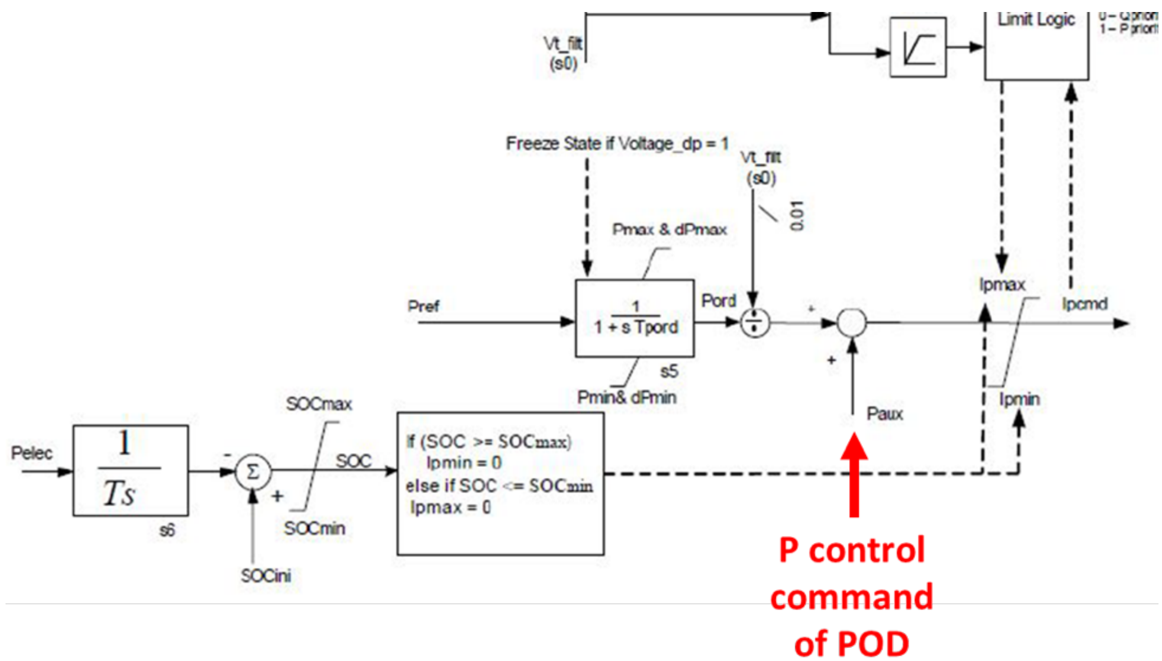

Figure 5.8: Diagram of active power modulation of IBRs [117].

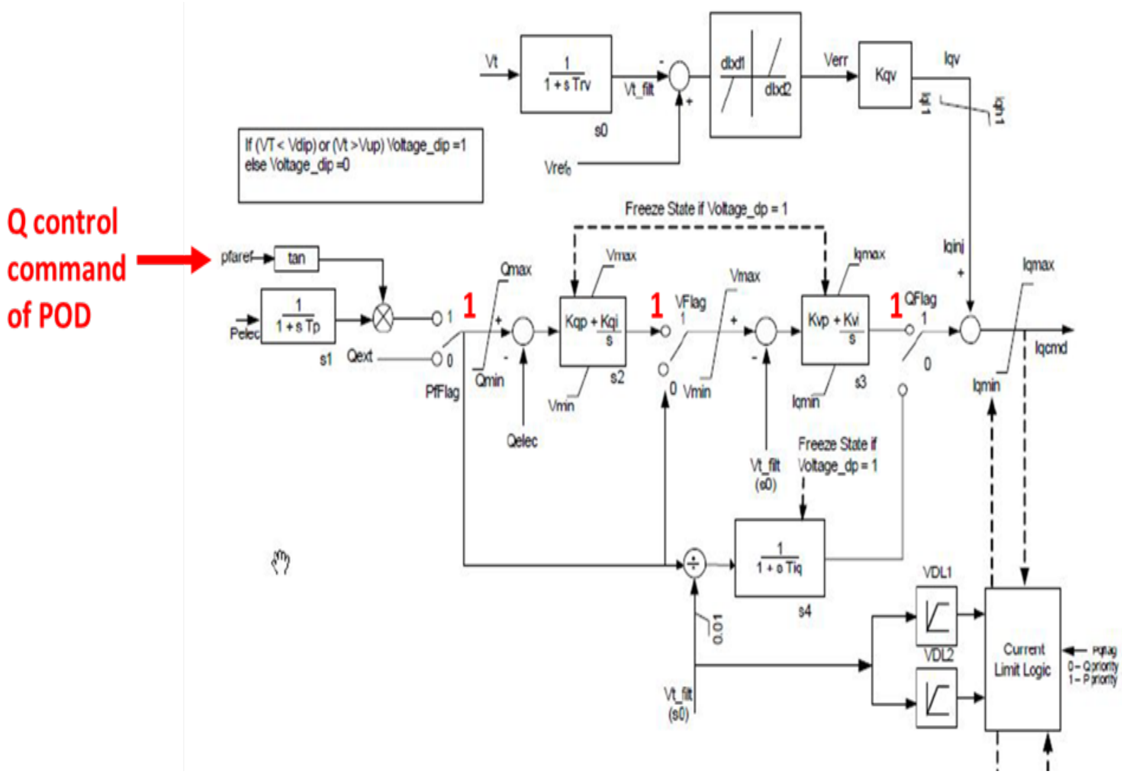

Figure 5.9: Diagram of reactive power modulation of IBRs [117].

Chapter 6

Grid Vulnerability Analysis of Active power Forced Disturbance through Generator: Texas Case Study

In this chapter, the proposed method for forced oscillation grid vulnerability analysis and mitigation is implemented and validated in the 2000-bus synthetic Texas power grid model when the forced disturbance is excited by changing the active power set point of the generator's governor [15].

6.1 Synthetic Texas Power System Model Description

The 2000-bus synthetic Texas, power grid PSS/e model, was used in this work. The model has been built from publicly available information by Texas A&M University [119]. The model consists of 432 in-service machines with a maximum generation capacity of 84.1 GW that partially supply a total load of 67.1 GW. In these 432 machines, there are 81 renewable resources with a maximum capacity of 11.83 GW and an actual generation of 8.9 GW. In addition, there are 2345 transmission lines and four high voltage levels: 500, 230, 161, and 115 kV. Each synchronous generator is equipped with a PSS, a governor, and an exciter. The generic models developed by WECC, specifically the generator/converter model and the electrical control model, were utilized for the dynamic models of renewables. As shown in Figure 6.1, The system is divided into 8 areas, each of which has one or more zones, for a total of 28 zones. Area 5 is the load center. The red arrows indicate the power flow directions among these areas. There is a large power transfer from Area 7 (Coast) and Area 8 (East) to Area 5 (North Central) [120]. The renewables are placed in Areas 1 to 5, with a 13.92% renewable penetration level based on the system's maximum MW capacity.

Small-signal stability analysis using the DSAtools/SSAT tool shows that there are two dominant oscillation modes, as shown in Table 6.1. The first oscillation model is 0.67 Hz with a damping ratio of 5.31% between Area 4 and Area 7, as illustrated in Figure 6.2. The other oscillation mode is 0.6 Hz with a damping ratio of 6.31% between Areas 1, 2, 3, 4, 5, and parts of Area 8 and Area 7.

The generators with a high participation factor of the two dominant oscillation modes are shown in Table 6.2. It can be seen that Area 4 has the highest participation factor in the 0.67 Hz oscillation mode.

6.2 Grid Vulnerability Analysis - Active Power Forced Disturbance through Generator

This section presents the grid vulnerability analysis in the Texas system using the proposed two-dimensional scanning method. The purpose of the scanning is to compare the forced oscillation energy at different frequencies and forced source locations in order to identify the areas that can excite the largest frequency deviation. In this study, the forced oscillation starts at t = 2 sec and is simulated for 20 sec. The conventional generator (coal, oil, nuclear, and hydro) with the maximum capacity at each zone in the Texas system was selected as the source of the forced oscillation. To excite sufficient frequency deviations in the system, the oscillation energy at each source location was set to 100 MW peak-to-peak for all the events.

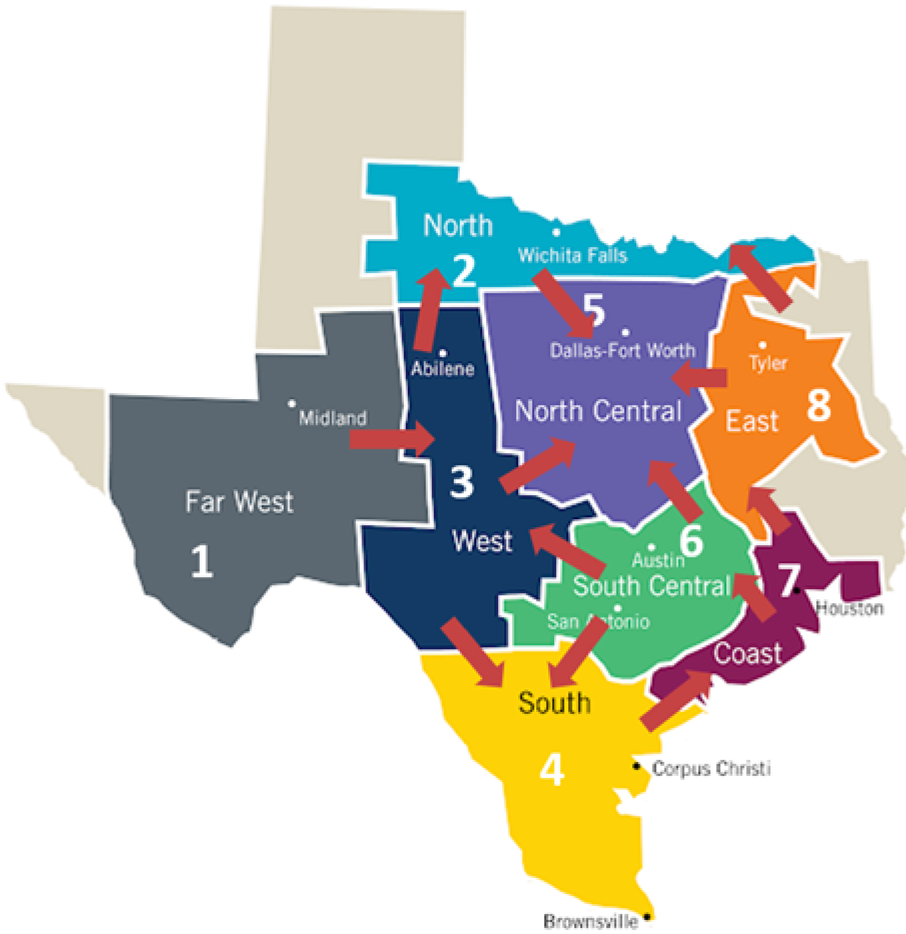

Figure 6.1: Area map of synthetic Texas power grid model [120].

Table 6.1: Dominant oscillation mode

Mode	**Frequency (Hz)**	**Damping ratio (%)**
Mode 1	0.67	5.31
Mode 2	0.60	6.31

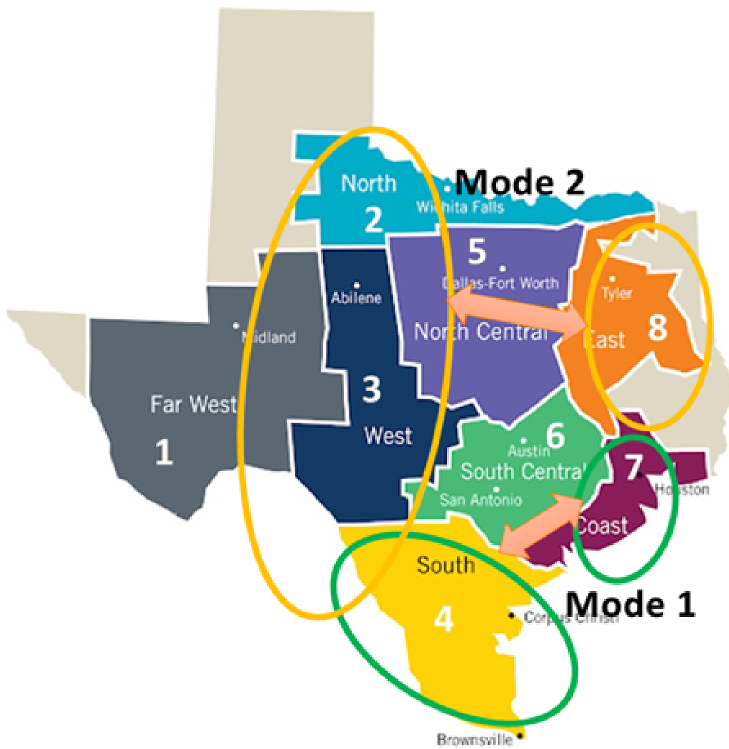

Figure 6.2: Mode shape of the two dominant modes.

Table 6.2: Dominant oscillation mode

Generator Location	Generator Bus NO.	Participation Factor (0.67 Hz)	Participation Factor (0.60 Hz)
Area 4 Zone 19	4192	1.00	0.14
Area 4 Zone 21	4058	0.72	0.01
Area 4 Zone 20	4115	0.40	0.22
Area 8 Zone 8	8080	0.19	0.77
Area 1 Zone 9	1051	0.18	1.00
Area 5 Zone 12	5063	0.18	0.01
Area 2 Zone 11	2023	0.18	0.76
Area 5 Zone 18	5319	0.17	0.73

6.2.1 Frequency Dimension Scanning

The frequency dimension scanning procedure involves changing the forced oscillation frequency at a fixed source location. In this study, the oscillation frequency ranges from 0.1 Hz to 1.5 Hz with a step size of 0.05 Hz. A high voltage bus frequency response at each zone was selected to calculate its peak-to-peak bus frequency deviation by using its last 1.5 oscillation cycles. By comparing the peak-to-peak bus frequency deviation among the buses in different zones, the maximum peak-to-peak bus frequency deviation under each specified forced oscillation frequency was identified.

Figure 6.3 shows the maximum peak-to-peak bus frequency deviation under different frequencies when the forced oscillation source was located at Area 4 Zone 19. Figure 6.4 illustrates the frequency response of the selected high voltage buses at each zone in the Texas system when the 0.67 Hz oscillation source was located at Area 4 Zone 19. As shown in Figure 6.3, when the oscillation frequency goes to around 0.67 Hz (the natural oscillation frequency), the most severe oscillation deviation can be observed in the system than other forced oscillation frequencies.

6.2.2 Location Dimension Scanning

The location dimension scanning is to vary the location of the forced oscillation source across the system with different forced oscillation frequencies. Figure 6.5 shows the location scanning results of the forced oscillation source with the top five frequency deviations. Regardless of the forced source location, compared to other forced oscillation frequency ranges, the maximum frequency deviation can always be observed in the Texas synthetic system when the forced oscillation frequency is equal or close to the natural oscillation at 0.67 Hz. This proves that the forced oscillation impact on the power system stability is magnified when the forced oscillation frequency coincides with the natural oscillation frequency. What's more, when the forced oscillation source was located at zones that have high participation of the natural 0.67 Hz oscillation, a larger frequency deviation can be observed in the system than other forced oscillation sources.

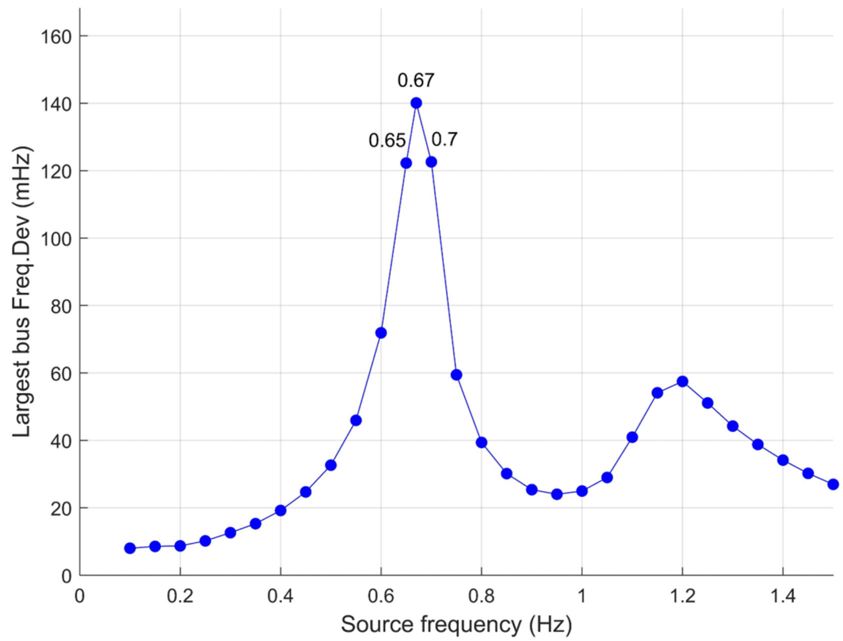

Figure 6.3: Frequency dimension scanning results when the forced source at Area 4 Zone 19.

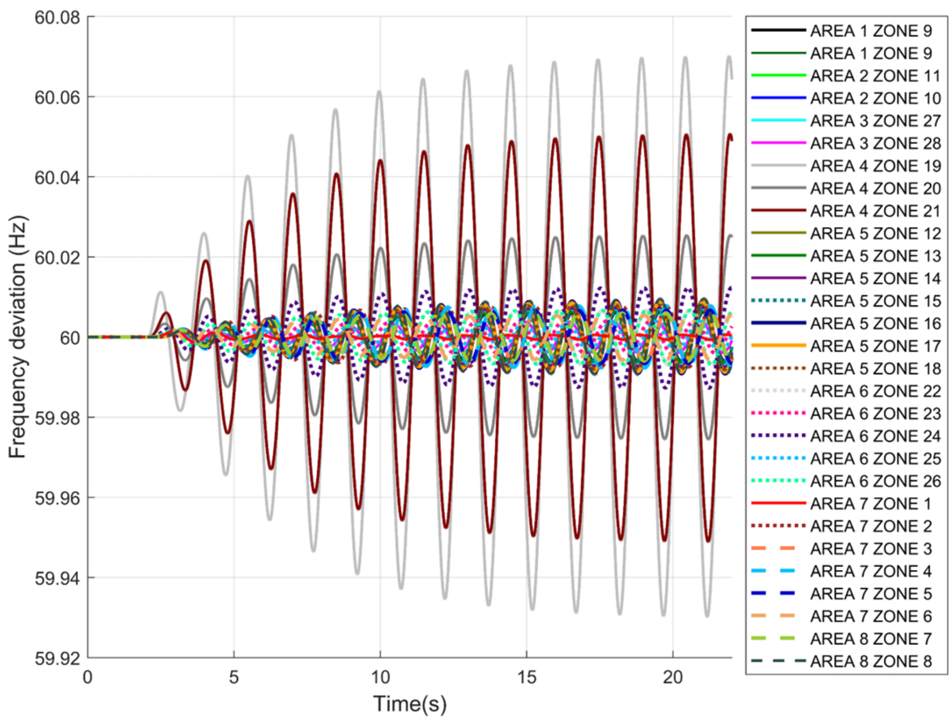

Figure 6.4: Bus frequency of selected high voltage buses at each zone in response to 0.67 Hz forced oscillation from a source located at Area Zone 19.

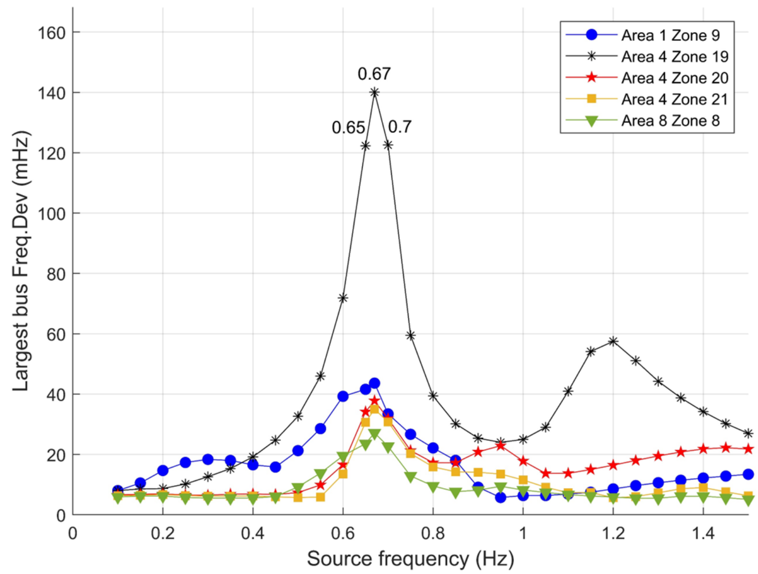

Figure 6.5: Location dimension scanning results of the forced oscillation source with the top five zones with generators that has high participation factor to the natural mode of 0.67 Hz.

Table 6.3 shows an example of the location dimension scanning results under the critical 0.67 Hz forced oscillation. It can be observed that Area 4 Zone 19 is the critical source location that can excite the maximum peak-to-peak bus frequency deviation in the system. This is consistent with the participation factor sorting of 0.67 Hz natural oscillation in Table 6.2.

6.3 Actuator Selection of Forced Oscillation Controller via IBR

Based on the two-dimension scanning, the critical areas/zones under different frequency range are summarized in Table 6.4. This table is useful for selecting the effective actuators to install the oscillation damping controller and reduce the forced oscillation in the power system. Based on Table 4, IBRs in Area 1 Zone 9 were effective in suppressing oscillations from 0.10 Hz to 0.35 Hz; IBRs in Area 4 Zone 19 were effective in suppressing oscillations around 0.4 Hz and from 0.5 Hz to 0.85 Hz and 1.10 Hz to 1.3 Hz; and IBRs in Area 3 Zone 28 were effective in suppressing oscillations around 0.45 Hz and from 0.90 Hz to 1.05 Hz and 1.35 Hz to 1.50 Hz. The IBRs with a large capacity in these areas are recommended to implement forced oscillation damping controllers.

When the forced oscillation frequency is monitored, the actuators that are effective to damp the oscillations can be identified from Table 6.4. Once the forced source is narrowed down within a relatively large area, the effective actuators (IBRs) that are close to or in the forced source areas can be activated to reduce the impact of the forced source energies before the accurate forced source is located.

6.4 Forced Oscillation Control via IBR

This section demonstrates the performance of the forced oscillation damping controller. The aim of the controller is to reduce the impact of the forced oscillation until the forced oscillation source is located and removed. The controller performance is validated under the most

Table 6.3: Location dimension scanning results when the critical forced oscillation frequency is 0.67 Hz

Source Location	Area—Zone with Largest Bus Frequency Deviation	Peak-to-Peak Bus Frequency Deviation (mHz)
Area 4 Zone 19	Area 4 Zone 19	140.090
Area 1 Zone 9	Area 4 Zone 19	43.622
Area 4 Zone 20	Area 4 Zone 19	37.798
Area 4 Zone 21	Area 4 Zone 19	34.996
Area 8 Zone 8	Area 4 Zone 19	30.780
Area 5 Zone 12	Area 4 Zone 19	27.221
Area 7 Zone 4	Area 4 Zone 19	27.125
Area 2 Zone 11	Area 4 Zone 19	26.910
Area 7 Zone 3	Area 4 Zone 19	25.536
Area 5 Zone 18	Area 4 Zone 19	24.451
Area 7 Zone 2	Area 4 Zone 19	23.359
Area 3 Zone 28	Area 3 Zone 28	23.172
Area 8 Zone 7	Area 4 Zone 19	19.345
Area 7 Zone 5	Area 4 Zone 19	18.532
Area 5 Zone 14	Area 4 Zone 19	18.099
Area 5 Zone 16	Area 4 Zone 19	17.938
Area 6 Zone 22	Area 4 Zone 19	17.764
Area 5 Zone 13	Area 4 Zone 19	17.663
Area 5 Zone 17	Area 4 Zone 19	15.185
Area 6 Zone 26	Area 4 Zone 19	13.886
Area 7 Zone 6	Area 4 Zone 19	12.948
Area 6 Zone 25	Area 4 Zone 19	11.598
Area 6 Zone 23	Area 4 Zone 19	9.652
Area 7 Zone 1	Area 7 Zone 4	9.191

Table 6.4: The critical areas/zones under different frequency range based on two-dimensional scanning.

Source Location	Oscillation Frequency (Hz)	Area—Zone with Largest Bus Frequency Deviation	Peak-to-Peak Bus Frequency Deviation (mHz)
Area 1 Zone 9	0.1	Area 7 Zone 4	8.00
Area 1 Zone 9	0.15	Area 7 Zone 4	10.53
Area 1 Zone 9	0.2	Area 7 Zone 4	14.67
Area 1 Zone 9	0.25	Area 7 Zone 4	17.33
Area 1 Zone 9	0.3	Area 7 Zone 4	18.35
Area 1 Zone 9	0.35	Area 7 Zone 4	18.00
Area 4 Zone 19	0.4	Area 4 Zone 19	19.19
Area 3 Zone 28	0.45	Area 3 Zone 28	25.22
Area 4 Zone 19	0.5	Area 4 Zone 19	32.63
Area 4 Zone 19	0.55	Area 4 Zone 19	45.95
Area 4 Zone 19	0.6	Area 4 Zone 19	71.88
Area 4 Zone 19	0.65	Area 4 Zone 19	122.30
Area 4 Zone 19	0.67	Area 4 Zone 19	140.09
Area 4 Zone 19	0.7	Area 4 Zone 19	122.58
Area 4 Zone 19	0.75	Area 4 Zone 19	59.45
Area 4 Zone 19	0.8	Area 4 Zone 21	39.37
Area 4 Zone 19	0.85	Area 4 Zone 21	30.16
Area 3 Zone 28	0.9	Area 3 Zone 28	30.35
Area 3 Zone 28	0.95	Area 3 Zone 28	31.79
Area 3 Zone 28	1	Area 3 Zone 28	31.78
Area 3 Zone 28	1.05	Area 3 Zone 28	33.20
Area 4 Zone 19	1.1	Area 4 Zone 19	40.93
Area 4 Zone 19	1.15	Area 4 Zone 19	54.10
Area 4 Zone 19	1.2	Area 4 Zone 19	57.49
Area 4 Zone 19	1.25	Area 4 Zone 19	51.09
Area 4 Zone 19	1.3	Area 4 Zone 19	44.23
Area 3 Zone 28	1.35	Area 3 Zone 28	46.49
Area 3 Zone 28	1.4	Area 3 Zone 28	48.79
Area 3 Zone 28	1.45	Area 3 Zone 28	51.21
Area 3 Zone 28	1.5	Area 3 Zone 28	53.53

serious resonance case, i.e., when the forced source is at Area 4 Zone 19 with the forced oscillation frequency coinciding with the natural oscillation mode 1 (0.67 Hz). Based on the results in Tables 6.3 and 6.4, the effective location for a forced oscillation damping controller is at Area 4 Zone 19. The 243.6 MVA IBR at bus 4183 in Area 4 Zone 19 is then selected as the actuator and the feedback signal is the 230 kV bus 4070 that is located in Area 4 Zone 19.

In this study, the droop controller gain was set to be -190. Figure 6.6 depicts the Area 4 Zone 19 frequency deviation improvement and the active power output of the actuator when the forced source at Area 4 Zone 19 before and after implementing the control. Table 6.5 illustrates the peak-to-peak frequency deviation improvement of the selected high voltage buses at each zone in the Texas system after implementing the controller. The largest deviation of the entire system can be reduced to less than ±36 mHz (66.6 mHz) with -190 control gain and 17% limiter. The peak-to-peak actuator output is 50.05 MW which is around ±16.44% of the actual active power of the actuator of 152.25 MW. Table 6.5 shows when the actuator is at the same zones of the forced source, the peak-to-peak bus frequency deviation is reduced at all the zones in the system.

Considering that the governors in the system have a ±36 m Hz deadband before being activated, the forced oscillation damping controller is helpful to ensure the system response is limited in the deadband of governors and reduces the forced oscillation impact on the entire system.

The frequency deviation of Area 4 Zone 19 in Figure 6.6 (a) can be reduced further if the actuator has a higher capacity or the controller limit is set to a high value. Figure 6.7 shows Area 4 Zone 19 frequency deviation improvement when the forced source and actuator at Area 4 Zone 19 and the peak-to-peak active actuator power is 50MW and 85MW. The frequency deviation in Area 4 Zone 19 can be reduced from 140.09 mHz to 13.67 mHz with a peak-to-peak actuator active power output of 85MW.

When the controller is far from the forced source, the forced oscillation may not be mitigated at all the zones in the system. Figure 6.8 illustrates Area 4 Zone 19 frequency deviation and the active power output of the actuator when the forced source at Area 4

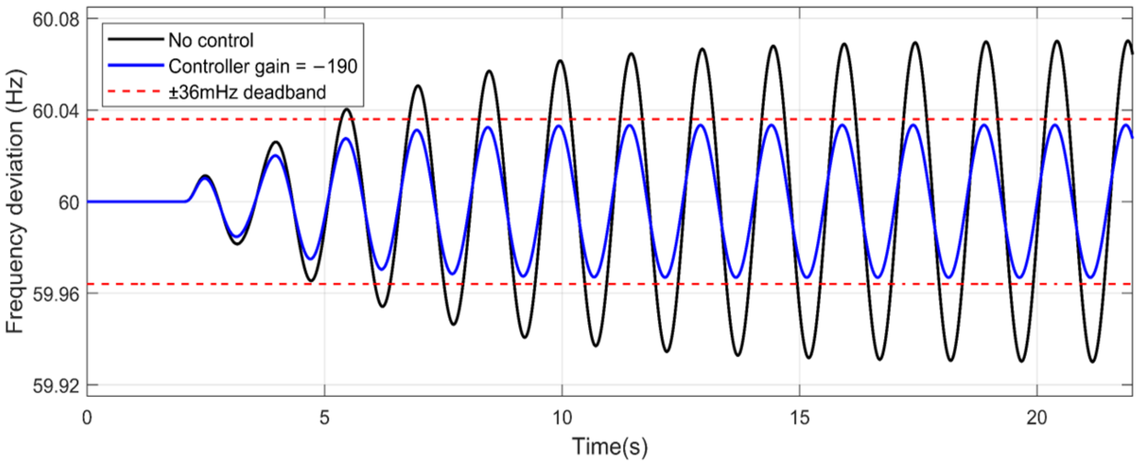

(a)

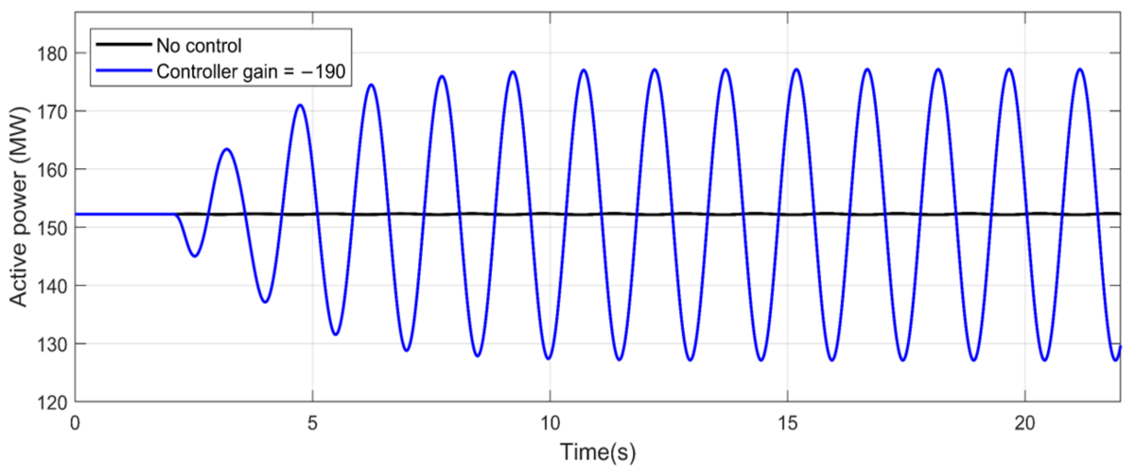

(b)

Figure 6.6: (a) Area 4 Zone 19 frequency deviation improvement. (b) Active power output of the actuator at Area 4 Zone 19 when the forced source is at Area 4 Zone 19.

Table 6.5: The peak-to-peak bus frequency deviation improvement before and after implementing the forced oscillation damping controller.

Area-Zone	Peak-to-Peak Bus Frequency Deviation (mHz)		Bus Frequency Deviation Reduction (mHz)
	No Control	With Control	
Area 1 Zone 9	13.00	5.99	7.01
Area 2 Zone 11	18.41	8.53	9.88
Area 2 Zone 10	14.74	6.76	7.98
Area 3 Zone 27	13.44	6.19	7.25
Area 3 Zone 28	7.83	3.62	4.21
Area 4 Zone 19	140.09	66.60	73.49
Area 4 Zone 20	51.11	23.64	27.47
Area 4 Zone 21	101.95	47.10	54.85
Area 5 Zone 12	16.07	7.43	8.65
Area 5 Zone 13	12.95	5.99	6.95
Area 5 Zone 14	15.29	7.08	8.21
Area 5 Zone 15	12.01	5.55	6.46
Area 5 Zone 16	18.39	8.52	9.87
Area 5 Zone 17	17.52	8.11	9.41
Area 5 Zone 18	16.24	7.51	8.72
Area 6 Zone 22	13.46	6.24	7.22
Area 6 Zone 23	8.19	3.78	4.40
Area 6 Zone 24	25.01	11.57	13.44
Area 6 Zone 25	7.85	3.63	4.23
Area 6 Zone 26	13.53	6.27	7.26
Area 7 Zone 1	1.27	0.54	0.73
Area 7 Zone 2	14.98	6.94	8.03
Area 7 Zone 3	13.10	6.07	7.03
Area 7 Zone 4	15.47	7.17	8.30
Area 7 Zone 5	13.27	6.15	7.12
Area 7 Zone 6	11.20	5.19	6.01
Area 8 Zone 7	11.97	5.54	6.43
Area 8 Zone 8	19.28	8.93	10.35

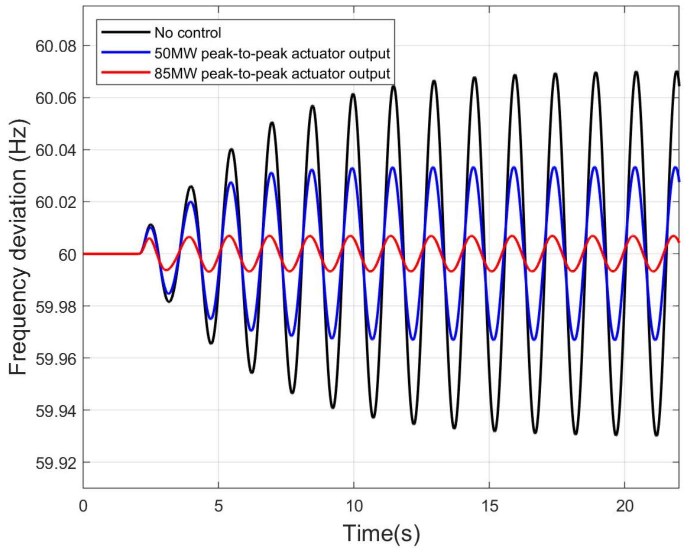

Figure 6.7: Area 4 Zone 19 frequency deviation improvement when the forced source and actuator is at Area 4 Zone 19.

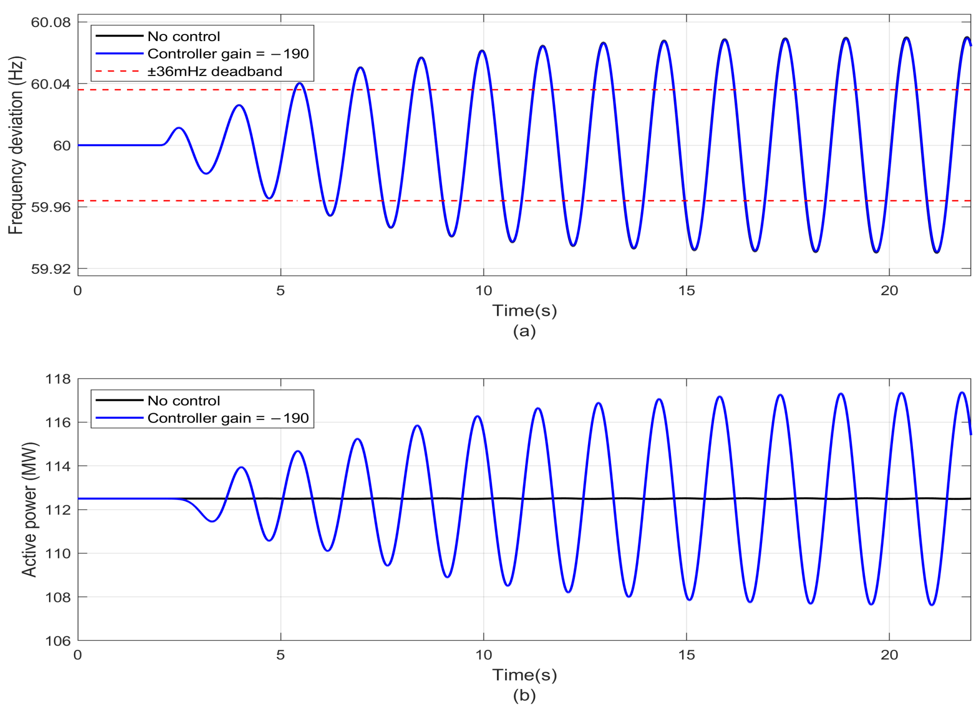

Figure 6.8: (a) Area 4 Zone 19 frequency deviation improvement. (b) Active power output of the actuator at Area 2 Zone 11 when the forced source is at Area 4 Zone 19.

Zone 19 and the actuator at Area 2 Zone 11. When the actuator is at Area 2 Zone 11, far from the forced source, the frequency deviation at Area 4 Zone 19 reduces by only 1.3 mHz. In addition, the frequency deviation did not reduce at all the zones in the system, and the frequency deviation increased slightly at some zones.

Figure 6.9 illustrates Area 4 Zone 19 frequency deviation improvement and the active power output of the actuator when the forced source at Area 4 Zone 20 before and after implementing the control. In this case, the peak-to-peak forced oscillation energy is increased to 160 MW in order for the peak-to-peak bus frequency deviation to exceed the deadband of the governor (±36 mHz). Area 4 Zone 19 had the largest peak-to-peak frequency deviation, and it can be reduced to 40.51 mHz. The peak-to-peak actuator output was 30.73 MW which is around ±10.1% of the actual active power of the actuator of 152.25 MW

6.5 Summary

A two-dimension scanning forced oscillation grid vulnerability analysis method in large-scale power grids was proposed. Based on the grid vulnerability analysis results, the effective location for forced oscillation damping controller can be selected. Active power modulation control through IBRs at the effective location with local measurement was also designed to mitigate forced oscillation under serious forced oscillation cases. The key findings are summarized below:

- Based on frequency dimension scanning, forced oscillation at or close to the natural oscillation excites the largest peak-to-peak frequency deviation in the entire system.
- When the forced oscillation source is located at the areas that have high participation of the natural oscillations, the forced oscillation will be further magnified throughout the system and significantly impact the system stability.
- Active power modulation control through IBRs with local measurement was effective in reducing the frequency deviation that was caused by the forced oscillation. This will allow the operator to have sufficient time to locate and disconnect the forced source.

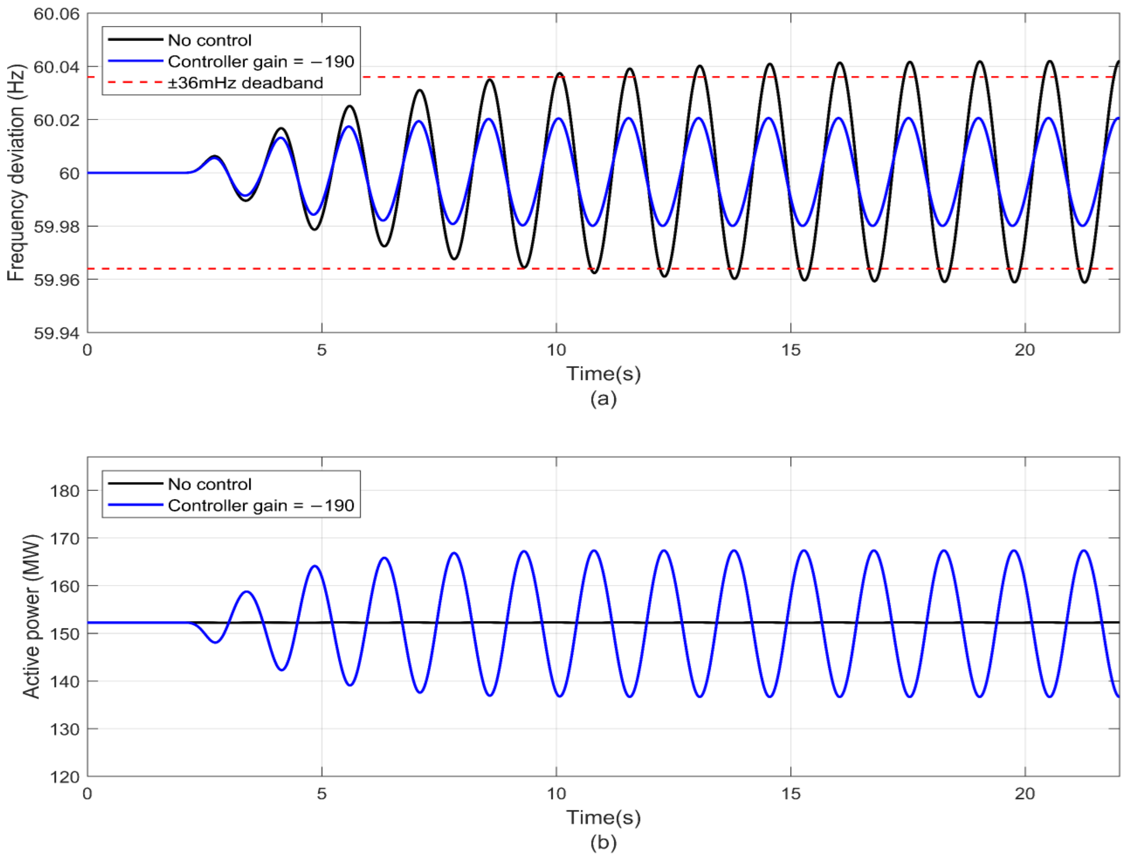

Figure 6.9: (a) Area 4 Zone 19 frequency deviation improvement. (b) Active power output of the actuator at Area 4 Zone 19 when the forced source is at Area 4 Zone 20.

- The proposed forced oscillation controller can reduce all the zones' frequency deviation to a safety level in the synthetic Texas power grid when the actuator is close to the forced source. The largest peak–peak bus frequency deviation can be reduced by more than 50%, to 66.6 mHz (in the range of governor deadband ±36 mH) with appropriate control gain.

Chapter 7

Grid Vulnerability Analysis of Active and Reactive Power Forced Disturbance through Load: Texas Case Study

In this chapter, the system frequency response of selected high voltage buses is compared when the forced source is a synchronous generator and a load is added at the same bus of these generators. The comparison is made through active and reactive power modulation of the generator and the load with oscillation energy of 100 MW and 100 Mvar, respectively. Furthermore, the proposed two-dimension scanning forced oscillation grid vulnerability analysis method is demonstrated in the synthetic Texas power grid model when the forced disturbance is through the active and reactive power of the load. The performance of the damping control is assessed when the forced disturbance is through the active and reactive power of the load. A control damping comparison between active and reactive power modulation of the IBR is discussed.

7.1 Different Types of Forced Source Comparison

7.1.1 Comparison of Active Power Forced Oscillation Disturbance at Generator and Load

The main objective of this part is to compare the system frequency response between the force source at the largest synchronous generator of the selected zones and the load added at the same bus. The forced oscillation frequency and energy are kept the same. Table 7.1 shows the Area/Zone of the largest frequency deviation and the value of the peak-to-peak frequency deviation when the forced source is the generator and the added load at the same bus of the generator at selected zones and different oscillation frequencies. In the three cases, the location of the largest frequency deviation of the system is the same for the generator and load at the same bus. The largest frequency deviation is also close to each other when a generator and a load are at the same bus.

Figures 7.1, 7.2, and 7.3 compare the peak-to-peak frequency deviation of selected high voltage buses at each zone in the Texas grid when the forced source at the generator and the load. The forced source locations are Area 1 Zone 9, Area 4 Zone 19, and Area 6 Zone 22, and oscillation frequencies are 0.3 Hz, 0.67 Hz, and 0.95 Hz, respectively. In Figure 7.1, the force source location is at Area 1 Zone 9, and the oscillation frequency is 0.3 Hz. Moreover, the largest frequency deviation is observed at Area 7 Zone 4, and the generator as a forced source can excite a higher frequency deviation than the load. In Figure 7.2, the force source location is at Area 4 Zone 19, the oscillation frequency is at the resonance of 0.67 Hz, and the largest frequency deviation is observed at Area 4 Zone 19. The force source location in Figure 7.3 is at Area 6 Zone 22, the oscillation frequency is 0.95 Hz, and the largest frequency deviation is observed at Area 6 Zone 22. It can be observed in both Figures 7.2 and 7.3 that the load as a forced source can excite a higher frequency deviation than the generator.

Table 7.1: Comparison of active power forced oscillation disturbance at generator and load at selected Areas/Zones.

Case #	Forced Source Area/Zone	Oscillation Frequency (Hz)	Comparing Between Different Forced Sources					
			Generator with Largest Capacity			Added Load at Generator with the Largest Capacity		
			Bus	Largest Deviation Location	Freq.Dev (mHz)	Bus	Largest Deviation Location	Freq.Dev (mHz)
1	Area 1 Zone 9	0.3	1072	A7 Z4	18.35	1072	A7 Z4	15.64
2	Area 4 Zone 19	0.67	4192	A4 Z19	140.09	4192	A4 Z19	163.13
3	Area 6 Zone 22	0.95	6147	A6 Z22	16.55	6147	A6 Z22	22.96

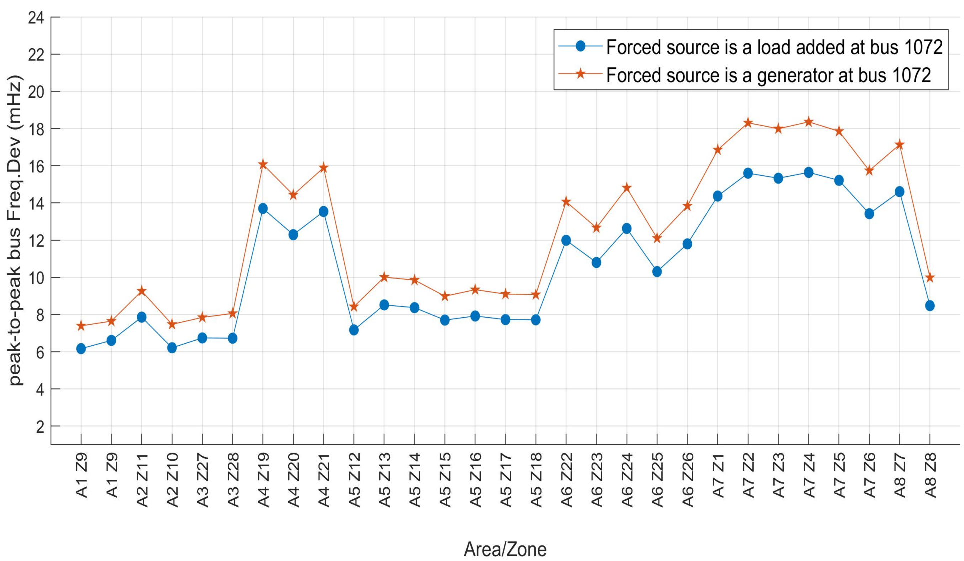

Figure 7.1: Comparison of the peak-to-peak frequency deviation of selected high voltage buses at each zone in the Texas grid when the forced source perturbation is through active power modulation of the largest generator and a load at Area 1 Zone 9 and oscillation frequency of 0.3 Hz.

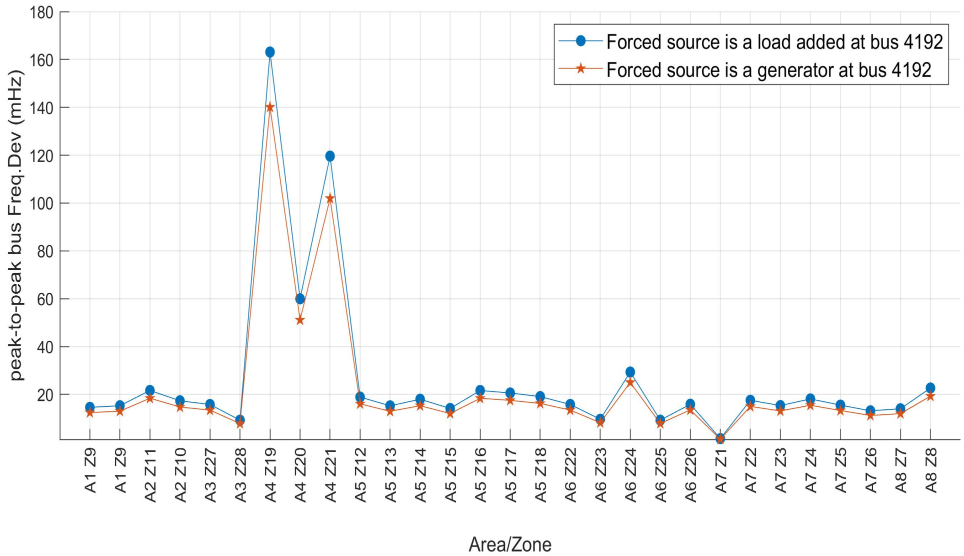

Figure 7.2: Comparison of the peak-to-peak frequency deviation of selected high voltage buses at each zone in the Texas grid when the forced source perturbation is through active power modulation of the largest generator and a load at Area 4 Zone 19 and oscillation frequency of 0.67 Hz.

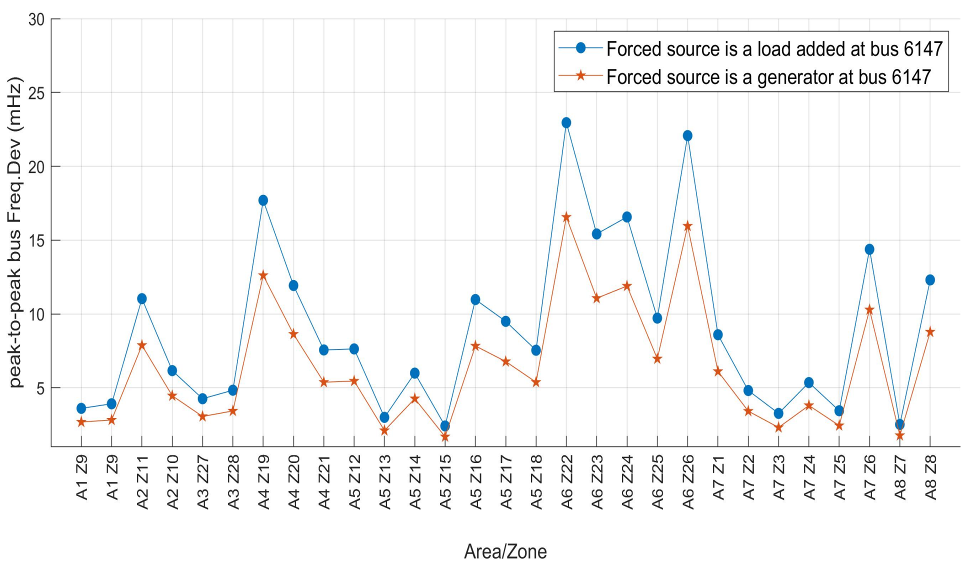

Figure 7.3: Comparison of the peak-to-peak frequency deviation of selected high voltage buses at each zone in the Texas grid when the forced source perturbation is through active power modulation of the largest generator and a load at Area 6 Zone 22 and oscillation frequency of 0.95 Hz.

7.1.2 Comparison of Reactive Power Forced Oscillation Disturbance at Generator and Load

The system frequency response was also compared when the forced source is through reactive power perturbation of the largest generator and an added load at the same bus of the generator at selected zones in the system. Table 7.2 illustrates the largest frequency deviation caused by forced event excited through reactive power perturbation of the largest generator and load at a selected Area/Zone under different oscillation frequencies. The oscillation energy is set to a peak-to-peak of 100 Mvar. Similar as the active power disturbances, when the forced source is at a generator or a load of the same bus, the location of the largest frequency deviation is the same in the three cases.

Figure 7.4, 7.5 and 7.6 show the system frequency response when the forced source is through reactive power perturbation of the generator and load at Area 1 Zone 9, Area 4 Zone 19, and Area 6 Zone 22 with an oscillation frequency of 0.3 Hz, 0.67 Hz and 0.95 Hz, respectively. In the three cases, the generator as a forced source causes a higher frequency deviation than the load.

7.2 Grid Vulnerability Analysis - Active Forced Disturbance through Load

7.2.1 Frequency Dimension Scanning

The frequency dimension scanning process is implemented by fixing the forced source location and varying the forced oscillation frequency. The forced oscillation frequency varies from 0.1 to 1.5 Hz with a step size of 0.05 Hz, and the dominant natural oscillation mode of 0.67 Hz is also included. The frequency response of selected high voltage buses from each zone was recorded to compute the bus peak-to-peak frequency deviation using the last 1.5 oscillation cycles. For each forced oscillation frequency, the largest peak-to-peak frequency deviation was computed by comparing the peak-to-peak frequency deviation in all zones.

Table 7.2: Comparison of reactive power forced oscillation disturbance at generator and load at selected Areas/Zones.

Case #	Forced Source Area/Zone	Oscillation Frequency (Hz)	Comparing Between Different Forced Sources					
			Generator with Largest Capacity			Added Load at Generator with the Largest Capacity		
			Bus	Largest Deviation Location	Freq.Dev (mHz)	Bus	Largest Deviation Location	Freq.Dev (mHz)
1	Area 1 Zone 9	0.3	1072	A7 Z4	10.75	1072	A7 Z4	9.19
2	Area 4 Zone 19	0.67	4192	A4 Z19	89.60	4192	A4 Z19	72.49
3	Area 6 Zone 22	0.95	6147	A6 Z22	12.29	6147	A6 Z22	5.00

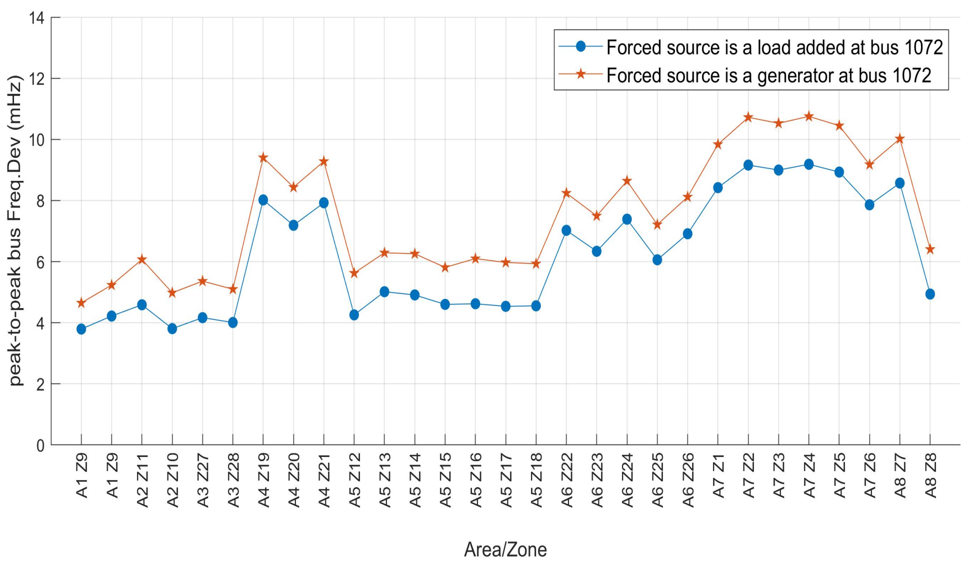

Figure 7.4: Peak-to-peak frequency responses comparison between forced source through reactive power perturbation of the generator and load at Area 1 Zone 9 and oscillation frequency of 0.3 Hz.

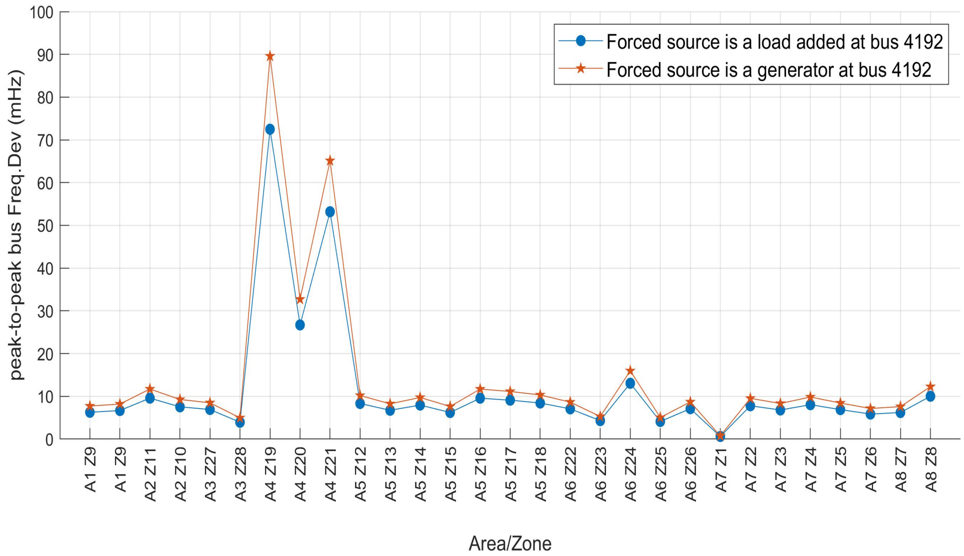

Figure 7.5: Peak-to-peak frequency responses comparison between forced source through reactive power perturbation of the generator and load at Area 4 Zone 19 and oscillation frequency of 0.67 Hz.

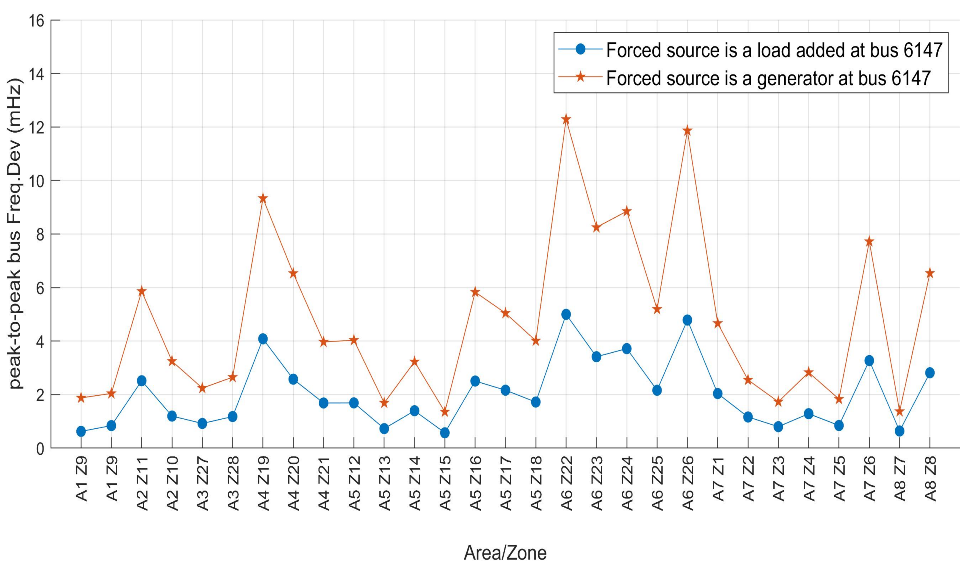

Figure 7.6: Peak-to-peak frequency responses comparison between forced source through reactive power perturbation of the generator and load at Area 6 Zone 22 and oscillation frequency of 0.95 Hz.

Figure 7.7 depicts the largest peak-to-peak bus frequency variation when the forced source at Area 4 Zone 19 under different oscillation frequency ranges. Figure 7.8 depicts the bus frequency of selected high voltage buses at each zone in response to 0.67 Hz forced oscillation from a source located at Area Zone 19. Figure 7.7 illustrates that the most severe frequency deviation occurs when the forced oscillation frequency coincides with the system's dominant natural mode of 0.67 Hz.

7.2.2 Location Dimension Scanning

The location dimension scanning is to change the forced source location across the system under different forced oscillation frequencies. Figure 7.9 shows the location scanning results of the forced oscillation source with the top five zones with generators with a high participation factor to the natural mode of 0.67 Hz. In the synthetic Texas grid model, despite the location of the forced source, the largest peak-to-peak bus frequency deviation is always observed when the forced oscillation frequency is equal to or near to the system's natural mode of 0.67 Hz. This demonstrates that when the forced oscillation frequency is close to the system's natural oscillation frequency, the negative effect on power system stability is amplified. Furthermore, a severe frequency deviation can be observed when the location of the forced source is at a zone with a high participation factor to the system's natural oscillation frequency of 0.67 Hz (see Table 6.2).

The location dimension scanning result at the most critical forced oscillation frequency of 0.67 Hz is shown in Table 7.3. It can be noted that the largest peak-to-peak bus frequency deviation is observed when the forced source is at the critical location of Area 4 Zone 19. This corresponds with the 0.67 Hz natural oscillation participation factor sorted in Table 6.2.

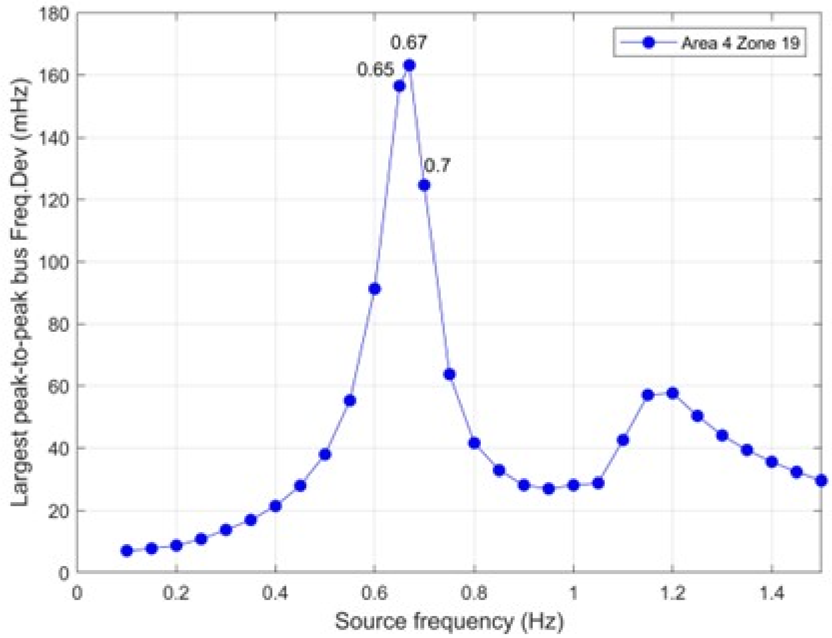

Figure 7.7: Frequency dimension scanning results when the forced source at Area 4 Zone 19.

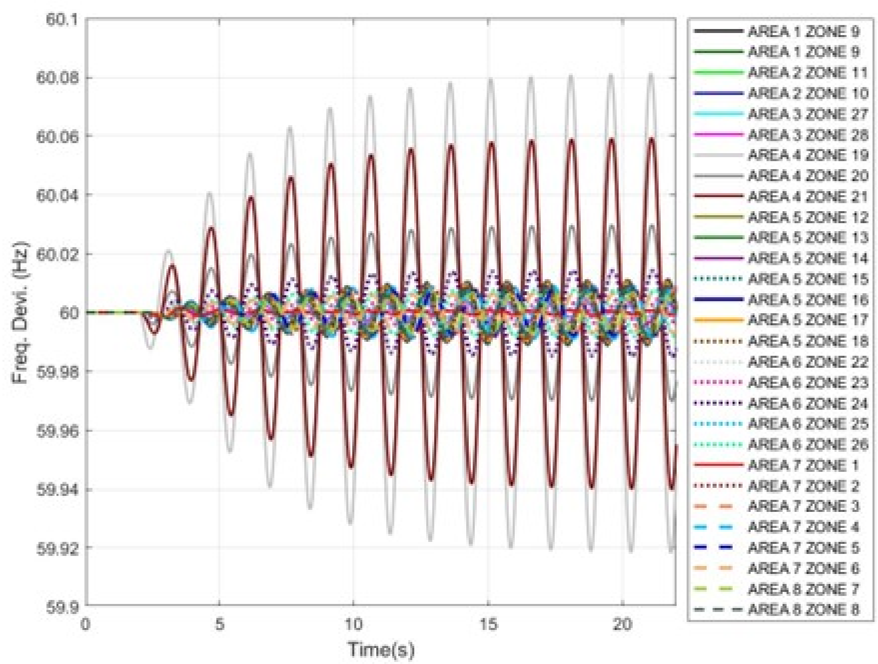

Figure 7.8: Bus frequency of selected high voltage buses at each zone in response to 0.67 Hz forced oscillation from a source located at Area Zone 19.

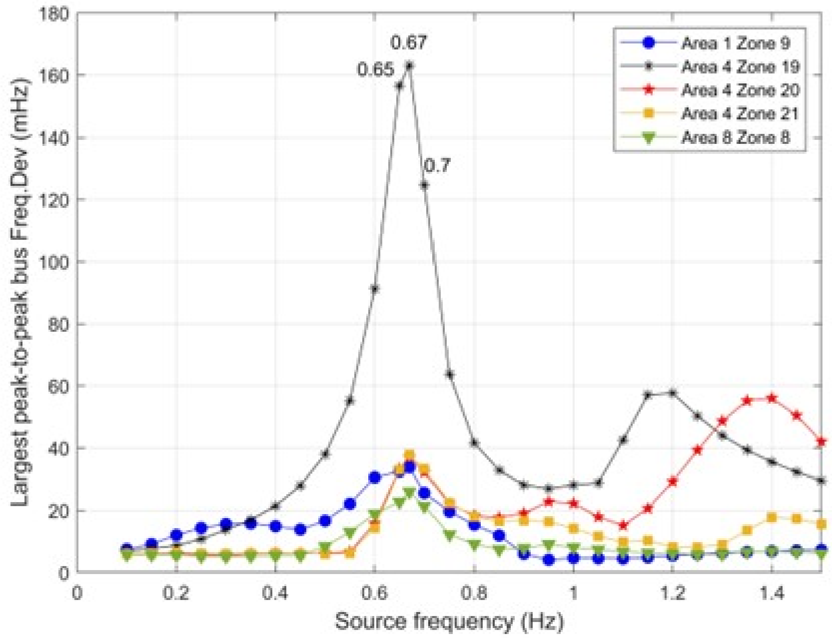

Figure 7.9: Location dimension scanning results of the forced oscillation source with the top five zones with generators that has a high participation factor to the natural mode of 0.67 Hz.

Table 7.3: Location dimension scanning results when the critical forced oscillation frequency is 0.67 Hz.

Source Location	**Area—Zone with Largest Bus Frequency Deviation**	**Peak-to-Peak Bus Frequency Deviation (mHz)**
Area 4 Zone 19	Area 4 Zone 19	163.13
Area 4 Zone 21	Area 4 Zone 19	37.90
Area 4 Zone 20	Area 4 Zone 19	37.07
Area 1 Zone 9	Area 4 Zone 19	33.80
Area 2 Zone 11	Area 4 Zone 19	31.13
Area 7 Zone 4	Area 4 Zone 19	28.86
Area 7 Zone 3	Area 4 Zone 19	27.02
Area 5 Zone 12	Area 4 Zone 19	26.99
Area 8 Zone 8	Area 4 Zone 19	26.01
Area 7 Zone 2	Area 4 Zone 19	24.53
Area 5 Zone 18	Area 4 Zone 19	23.88
Area 6 Zone 22	Area 4 Zone 19	22.02
Area 8 Zone 7	Area 4 Zone 19	21.91
Area 5 Zone 16	Area 4 Zone 19	21.43
Area 5 Zone 17	Area 4 Zone 19	20.30
Area 7 Zone 5	Area 4 Zone 19	18.21
Area 5 Zone 14	Area 4 Zone 19	18.09
Area 5 Zone 13	Area 4 Zone 19	18.00
Area 6 Zone 26	Area 4 Zone 19	16.24
Area 3 Zone 28	Area 4 Zone 19	14.53
Area 7 Zone 6	Area 4 Zone 19	13.12
Area 6 Zone 25	Area 4 Zone 19	12.19
Area 6 Zone 23	Area 4 Zone 19	10.86
Area 7 Zone 1	Area 7 Zone 4	10.76

7.3 Grid Vulnerability Analysis - Reactive Forced Disturbance through Load

7.3.1 Frequency Dimension Scanning

The frequency dimension scanning procedure mentioned earlier when the forced disturbance through active power of the load was implanted in this section but using the reactive power of the load as a forced disturbance. Figure 7.10 shows the maximum peak-to-peak bus frequency deviation under different frequencies when the forced oscillation source was located at Area 4 Zone 19. The largest frequency deviation is observed when the oscillation frequency coincides with the dominant oscillation mode of 0.67 Hz. Figure 7.11 shows the frequency response of the selected high voltage buses at each zone in the Texas system when the 0.67 Hz oscillation source was located at Area 4 Zone 19. Comparing Figure 7.11 with Figure 7.8, at the beginning of the forced event, the bus frequency drops below 60 Hz when the forced disturbance is through the active power of the load, while the bus frequency increases when the forced disturbance is through the reactive power of the load.

7.3.2 Location Dimension Scanning

Figure 7.12 shows the location scanning results of the forced oscillation source with the top five zones with generators with a high participation factor to the natural mode of 0.67 Hz. As in active power disturbance, the maximum frequency deviation is observed when the oscillation frequency is close to the natural domination mode of 0.67 Hz. Table 7.4 shows an example of the location dimension scanning results under the critical 0.67 Hz forced oscillation. The most server peak-to-peak frequency deviation is observed at Area 4 Zone 19, where a generator at this zone (see Table 6.2) has the highest participation factor to the natural mode of 0.67 Hz.

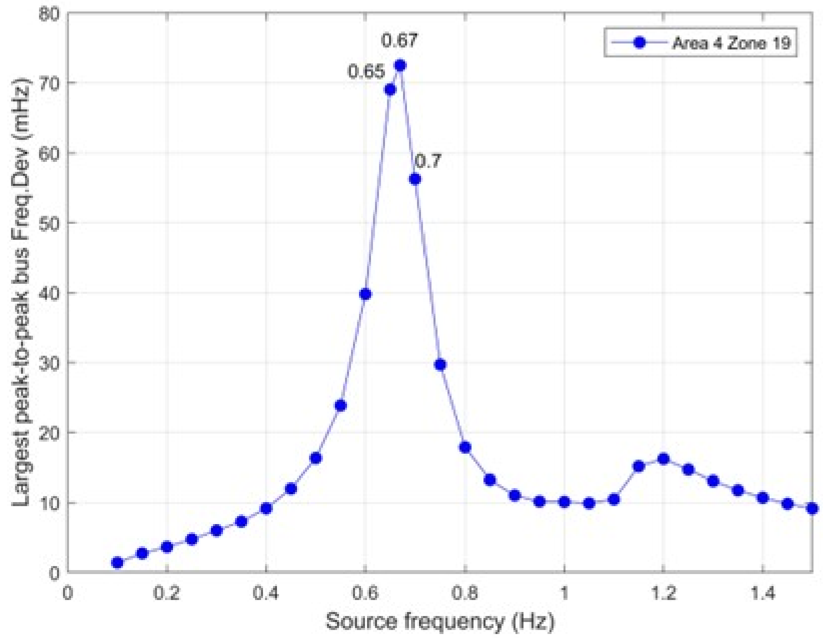

Figure 7.10: Frequency dimension scanning results when the forced source at Area 4 Zone 19.

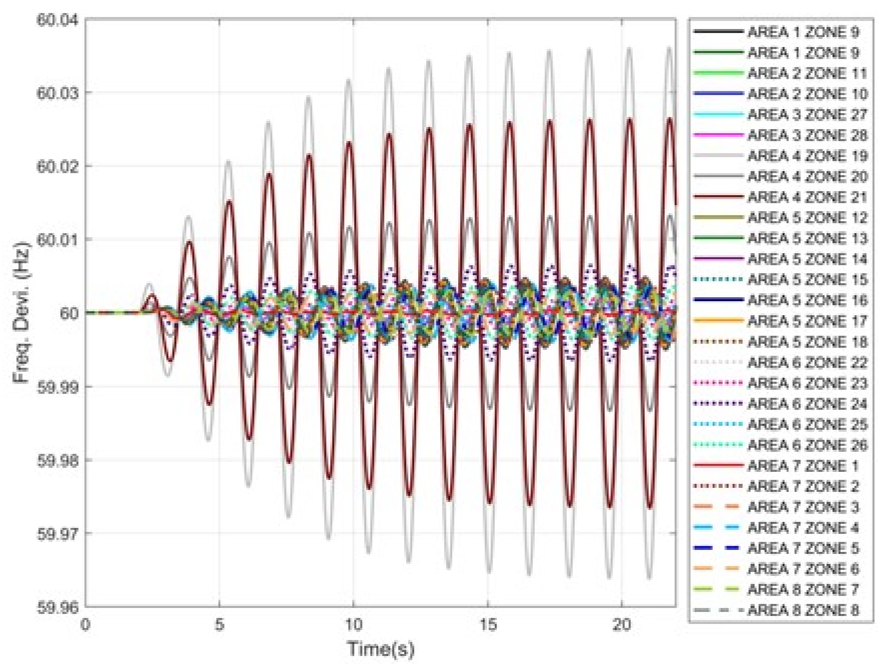

Figure 7.11: Bus frequency of selected high voltage buses at each zone in response to 0.67 Hz forced oscillation from a source located at Area Zone 19.

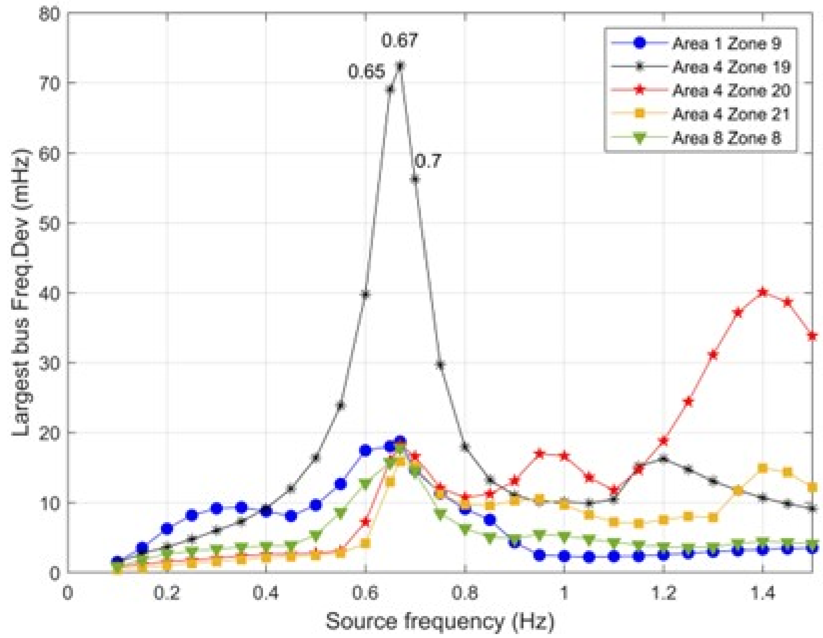

Figure 7.12: Location dimension scanning results of the forced oscillation source with the top five zones with generators that has a high participation factor to the natural mode of 0.67 Hz.

Table 7.4: Location dimension scanning results when the critical forced oscillation frequency is 0.67 Hz.

Source Location	**Area—Zone with Largest Bus Frequency Deviation**	**Peak-to-Peak Bus Frequency Deviation (mHz)**
Area 4 Zone 19	Area 4 Zone 19	72.49
Area 1 Zone 9	Area 4 Zone 19	18.69
Area 4 Zone 20	Area 4 Zone 19	18.27
Area 8 Zone 8	Area 4 Zone 19	17.78
Area 5 Zone 12	Area 4 Zone 19	16.60
Area 4 Zone 21	Area 4 Zone 19	15.84
Area 2 Zone 11	Area 4 Zone 19	15.67
Area 5 Zone 17	Area 4 Zone 19	15.42
Area 5 Zone 14	Area 4 Zone 19	15.16
Area 5 Zone 16	Area 4 Zone 19	14.67
Area 5 Zone 18	Area 4 Zone 19	14.18
Area 7 Zone 5	Area 4 Zone 19	13.88
Area 3 Zone 28	Area 3 Zone 28	12.36
Area 7 Zone 4	Area 4 Zone 19	10.59
Area 7 Zone 2	Area 4 Zone 19	10.33
Area 8 Zone 7	Area 4 Zone 19	9.93
Area 6 Zone 26	Area 4 Zone 19	8.70
Area 7 Zone 3	Area 4 Zone 19	8.38
Area 6 Zone 23	Area 4 Zone 19	5.61
Area 5 Zone 13	Area 4 Zone 19	5.11
Area 6 Zone 22	Area 4 Zone 19	5.08
Area 6 Zone 25	Area 4 Zone 19	4.47
Area 7 Zone 1	Area 7 Zone 4	2.98
Area 7 Zone 6	Area 7 Zone 4	2.83

7.4 Grid Vulnerability Analysis Comparison between Active and Reactive Forced Disturbance

Two-dimension scanning compression between forced disturbance through active and reactive power of the load is presented in Table 7.5. The table shows the location of the forced source and the area/zone with the largest peak-to-peak frequency deviation under 30 scenarios when the oscillation frequency ranges from 0.1 Hz to 1.5 Hz with a step size of 0.05 Hz, including the 0.67Hz oscillation frequency. When the forced disturbance is through active or reactive power of the load, the most critical location that excites the most severe frequency deviation is at Area 4 Zone 19, when the oscillation frequency is 0.67 Hz. It also can be observed from Table 7.5 that in each of the 30 oscillation frequency scenarios, the largest peak-to-peak frequency deviation caused by forced source through active power of the load is higher than the reactive power of the load.

When comparing the two-dimensional scanning result in Table 7.5 between forced disturbance through active and reactive power of the load, four categories can be observed based on the location of the forced source and the area of the largest frequency deviation, and these categories are as follow:

- Category 1: the area with the largest deviation through active power forced disturbance is the same as the reactive power forced disturbance, and the forced source area triggered the largest deviation is the same.
- Category 2: the area with the largest deviation through active power forced disturbance is the same as the reactive power forced disturbance; however, the forced source area that triggered the largest deviation is different.
- Category 3: the area with the largest deviation through active power forced disturbance is different from the reactive power forced disturbance, and the forced source area that triggered the largest deviation is the same.

Table 7.5: Two-dimensional scanning comparison between forced disturbance through active and reactive.

<table>
<tr><th>Oscillation freq (Hz)</th><th>Area - Zone with Largest Deviation (P modulation)</th><th>Deviation (mHz) (P modulation)</th><th>Area - Zone with Largest Deviation (Q modulation)</th><th>Deviation (mHz) (Q modulation)</th><th>Largest Deviation (P VS Q)</th><th>Forced source location (P modulation)</th><th>Forced location source (Q modulation)</th><th>Forced location source</th></tr>
<tr><td>0.1</td><td>Area 7 Zone 4</td><td>7.49</td><td>Area 7 Zone 4</td><td>2.27</td><td>Same zone
Dev_P>Dev_Q</td><td>Area 1 Zone 9</td><td>Area 8 Zone 7</td><td>Not the same area</td></tr>
<tr><td>0.15</td><td>Area 7 Zone 4</td><td>9.16</td><td>Area 7 Zone 4</td><td>3.54</td><td rowspan="4">Same zone
Dev_P>Dev_Q</td><td>Area 1 Zone 9</td><td>Area 1 Zone 9</td><td rowspan="4">Same zone</td></tr>
<tr><td>0.2</td><td>Area 7 Zone 4</td><td>12.09</td><td>Area 7 Zone 4</td><td>6.28</td><td>Area 1 Zone 9</td><td>Area 1 Zone 9</td></tr>
<tr><td>0.25</td><td>Area 7 Zone 4</td><td>14.37</td><td>Area 7 Zone 4</td><td>8.20</td><td>Area 1 Zone 9</td><td>Area 1 Zone 9</td></tr>
<tr><td>0.3</td><td>Area 7 Zone 4</td><td>15.64</td><td>Area 7 Zone 4</td><td>9.19</td><td>Area 1 Zone 9</td><td>Area 1 Zone 9</td></tr>
<tr><td>0.35</td><td>Area 4 Zone 19</td><td>16.95</td><td>Area 7 Zone 4</td><td>9.33</td><td>Not the same area</td><td>Area 4 Zone 19</td><td>Area 1 Zone 9</td><td>Not the same area</td></tr>
<tr><td>0.4</td><td>Area 4 Zone 19</td><td>21.44</td><td>Area 4 Zone 19</td><td>9.19</td><td rowspan="9">Same zone
Dev_P>Dev_Q</td><td>Area 4 Zone 19</td><td>Area 4 Zone 19</td><td rowspan="9">Same zone</td></tr>
<tr><td>0.45</td><td>Area 4 Zone 19</td><td>27.99</td><td>Area 4 Zone 19</td><td>12.01</td><td>Area 4 Zone 19</td><td>Area 4 Zone 19</td></tr>
<tr><td>0.5</td><td>Area 4 Zone 19</td><td>37.91</td><td>Area 4 Zone 19</td><td>16.32</td><td>Area 4 Zone 19</td><td>Area 4 Zone 19</td></tr>
<tr><td>0.55</td><td>Area 4 Zone 19</td><td>55.26</td><td>Area 4 Zone 19</td><td>23.85</td><td>Area 4 Zone 19</td><td>Area 4 Zone 19</td></tr>
<tr><td>0.6</td><td>Area 4 Zone 19</td><td>91.26</td><td>Area 4 Zone 19</td><td>39.80</td><td>Area 4 Zone 19</td><td>Area 4 Zone 19</td></tr>
<tr><td>0.65</td><td>Area 4 Zone 19</td><td>156.45</td><td>Area 4 Zone 19</td><td>69.02</td><td>Area 4 Zone 19</td><td>Area 4 Zone 19</td></tr>
<tr><td>0.67</td><td>Area 4 Zone 19</td><td>163.13</td><td>Area 4 Zone 19</td><td>72.49</td><td>Area 4 Zone 19</td><td>Area 4 Zone 19</td></tr>
<tr><td>0.7</td><td>Area 4 Zone 19</td><td>124.67</td><td>Area 4 Zone 19</td><td>56.28</td><td>Area 4 Zone 19</td><td>Area 4 Zone 19</td></tr>
<tr><td>0.75</td><td>Area 4 Zone 19</td><td>63.73</td><td>Area 4 Zone 19</td><td>29.70</td><td>Area 4 Zone 19</td><td>Area 4 Zone 19</td></tr>
<tr><td>0.8</td><td>Area 4 Zone 21</td><td>41.56</td><td>Area 4 Zone 19</td><td>17.87</td><td>Same area
Dev_P>Dev_Q</td><td>Area 4 Zone 19</td><td>Area 4 Zone 19</td><td>Same zone</td></tr>
<tr><td>0.85</td><td>Area 4 Zone 21</td><td>32.82</td><td>Area 4 Zone 21</td><td>13.25</td><td>Same zone
Dev_P>Dev_Q</td><td>Area 4 Zone 19</td><td>Area 4 Zone 19</td><td>Same zone</td></tr>
<tr><td>0.9</td><td>Area 4 Zone 21</td><td>28.17</td><td>Area 4 Zone 19</td><td>13.11</td><td>Same area
Dev_P>Dev_Q</td><td>Area 4 Zone 19</td><td>Area 4 Zone 20</td><td>Same area</td></tr>
<tr><td>0.95</td><td>Area 4 Zone 21</td><td>27.01</td><td>Area 6 Zone 24</td><td>16.93</td><td rowspan="2">Not the same area</td><td>Area 4 Zone 19</td><td>Area 4 Zone 20</td><td rowspan="2">Same area</td></tr>
<tr><td>1</td><td>Area 4 Zone 21</td><td>28.16</td><td>Area 6 Zone 22</td><td>16.62</td><td>Area 4 Zone 19</td><td>Area 4 Zone 20</td></tr>
<tr><td>1.05</td><td>Area 4 Zone 21</td><td>28.83</td><td>Area 3 Zone 28</td><td>15.96</td><td rowspan="4">Not the same area</td><td>Area 4 Zone 19</td><td>Area 3 Zone 28</td><td rowspan="4">Not the same area</td></tr>
<tr><td>1.1</td><td>Area 4 Zone 19</td><td>42.54</td><td>Area 3 Zone 28</td><td>18.85</td><td>Area 4 Zone 19</td><td>Area 3 Zone 28</td></tr>
<tr><td>1.15</td><td>Area 4 Zone 19</td><td>57.05</td><td>Area 3 Zone 28</td><td>22.84</td><td>Area 4 Zone 19</td><td>Area 3 Zone 28</td></tr>
<tr><td>1.2</td><td>Area 4 Zone 19</td><td>57.64</td><td>Area 3 Zone 28</td><td>27.94</td><td>Area 4 Zone 19</td><td>Area 3 Zone 28</td></tr>
<tr><td>1.25</td><td>Area 7 Zone 1</td><td>64.32</td><td>Area 3 Zone 28</td><td>33.20</td><td>Not the same area</td><td>Area 7 Zone 1</td><td>Area 3 Zone 28</td><td>Not the same area</td></tr>
<tr><td>1.3</td><td>Area 3 Zone 28</td><td>77.84</td><td>Area 3 Zone 28</td><td>36.39</td><td>Same zone
Dev_P>Dev_Q</td><td>Area 3 Zone 28</td><td>Area 3 Zone 28</td><td>Same zone</td></tr>
<tr><td>1.35</td><td>Area 3 Zone 28</td><td>74.64</td><td>Area 6 Zone 24</td><td>37.14</td><td rowspan="2">Not the same area</td><td>Area 3 Zone 28</td><td>Area 4 Zone 20</td><td rowspan="2">Not the same area</td></tr>
<tr><td>1.4</td><td>Area 3 Zone 28</td><td>62.68</td><td>Area 6 Zone 24</td><td>40.08</td><td>Area 3 Zone 28</td><td>Area 4 Zone 20</td></tr>
<tr><td>1.45</td><td>Area 6 Zone 24</td><td>50.47</td><td>Area 6 Zone 24</td><td>38.64</td><td rowspan="2">Same zone
Dev_P>Dev_Q</td><td>Area 4 Zone 20</td><td>Area 4 Zone 20</td><td rowspan="2">Same zone</td></tr>
<tr><td>1.5</td><td>Area 6 Zone 24</td><td>42.08</td><td>Area 6 Zone 24</td><td>33.85</td><td>Area 4 Zone 20</td><td>Area 4 Zone 20</td></tr>
</table>

- Category 4: the area with the largest deviation through active power forced disturbance is different from the reactive power forced disturbance, and the forced source area that triggered the largest deviation is different.

Table 7.6 provides a summary of the four categories. More than 60% of the cases in Table 7.5 show that the areas of the largest frequency deviation and the corresponding forced source that triggered the largest deviation through either active or reactive forced energy are the same. Moreover, around 27% of the cases show that the areas of the largest frequency deviation and the corresponding forced source location that triggered the largest deviation through active or reactive forced energy are all different.

7.5 Controller Performance Validation

The purpose of the forced oscillation damping controller is to mitigate the impact of the forced event until the forced source is located and removed. The POD performance comparison between active and reactive power modulation of IBR in mitigating the forced oscillation through active power and reactive power disturbance of the load is discussed.

7.5.1 Damping Control Performance Comparison between Active and Reactive Power Modulation of IBR When the Forced Disturbance through Reactive Power of the Load

This section presents the damping control performance comparison between active and reactive power modulation of the IBR when the forced disturbance through reactive power of the load. Three cases are discussed to active and reactive power modulation of the IBR. The location of the forced source and actuator is the same for the three cases, and the locations are Area 4 Zone 19, Area 1 Zone 9, and Area 2 Zone 11, respectively. Table 7.7 shows the three cases of damping control performance comparison between active and reactive power modulation of the IBR. In the three cases, the forced oscillation frequency is 0.67 Hz, and the peak-to-peak forced oscillation energy is 100 MVar. As shown in Table 7.7, active

Table 7.6: Summary of the four categories two-dimensional scanning result based on the location of the forced source and the area of the largest frequency deviation.

Scenario #	The Largest Deviation Location (P VS Q)	Forced Source Location that Triggered Largest Deviation (P VS Q)	Number of cases	Percentage
Scenario 1	Same	Same	19	63.33%
Scenario 2	Same	Different	1	3.33%
Scenario 3	Different	Same	2	6.67%
Scenario 4	Different	Different	8	26.67%
Total			30	100%

Table 7.7: Summary of the forced oscillation damping control performance when forced disturbance through reactive power of the load.

Case #	Forced Source Area/Zone	No Control Frequency Deviation (mHz)	P Modulation of Actuator		Q Modulation of Actuator		P&Q Modulation of Actuator	
			Peak to Peak					
			Actuator Output (MW)	Freq.Dev (mHz)	Actuator Output (MVar)	Freq.Dev (mHz)	Actuator Output (MW)+(MVar)	Freq.Dev (mHz)
1	Area 1 Zone 9	72.49	20	44.11	20	55.64	20+20	26.54
2	Area 4 Zone 19	18.69	15	14.47	15	16.47	15+15	12.18
3	Area 2 Zone 11	15.67	15	11.78	15	13.42	15+15	9.17

power modulation of the IBR can improve frequency deviation better than reactive power modulation of the IBR. When combining the active and reactive power modulation of the IBR, the frequency deviation could improve significantly, as shown in case 1. In some cases, the actuator's active or reactive power may have a limit, and combining them could provide more damping.

Figures 7.13, 7.14, and 7.15 show the frequency deviation improvement at Area 4 Zone 19 and the active and reactive power output of the actuator before and after implementing the controller for the three cases when the forced source and actuator is at Area 4 Zone 19, Area 1 Zone 9, and Area 2 Zone 11 respectively.

7.5.2 Damping Control Performance Comparison between Active and Reactive Power Modulation of IBR When the Forced Disturbance through Active Power of the Load

This section presents the damping control performance comparison between active and reactive power modulation of the IBR when the forced disturbance through active power of the load. Three cases are discussed to active and reactive power modulation of the IBR. The location of the forced source and actuator is the same for the three cases, and the locations are Area 4 Zone 19, Area 1 Zone 9, and Area 2 Zone 11, respectively. Table 7.8 shows the three cases of damping control performance comparison between active and reactive power modulation of the IBR. In the three cases, the forced oscillation frequency is 0.67 Hz, and the peak-to-peak forced oscillation energy is 100 MW. As shown in Table 7.8, active power modulation of the IBR can improve frequency deviation better than reactive power modulation of the IBR. When combining the active and reactive power modulation of the IBR, the frequency deviation could further improve, as shown in case 1.

Figures 7.16, 7.17, and 7.18 show the frequency deviation improvement at Area 4 Zone 19 and the active and reactive power output of the actuator before and after implementing the controller for the three cases when the forced source and actuator is at Area 4 Zone 19, Area 1 Zone 9, and Area 2 Zone 11 respectively.

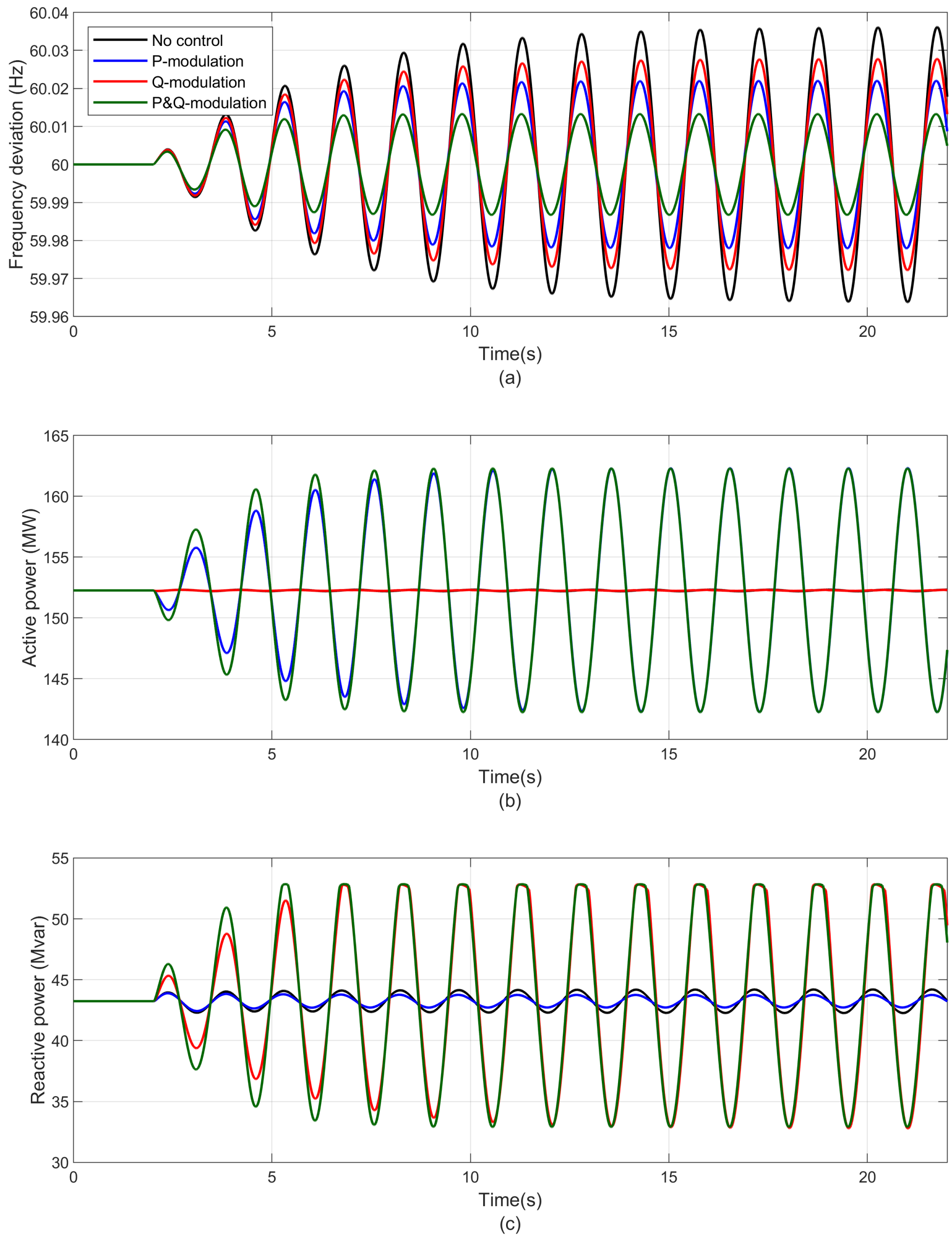

Figure 7.13: Forced source at Area 4 Zone 19 (a) Frequency deviation improvement at Area 4 Zone 19 (b) Actuator active power at Area 4 Zone 19 (c) Actuator reactive power at Area 4 Zone 19

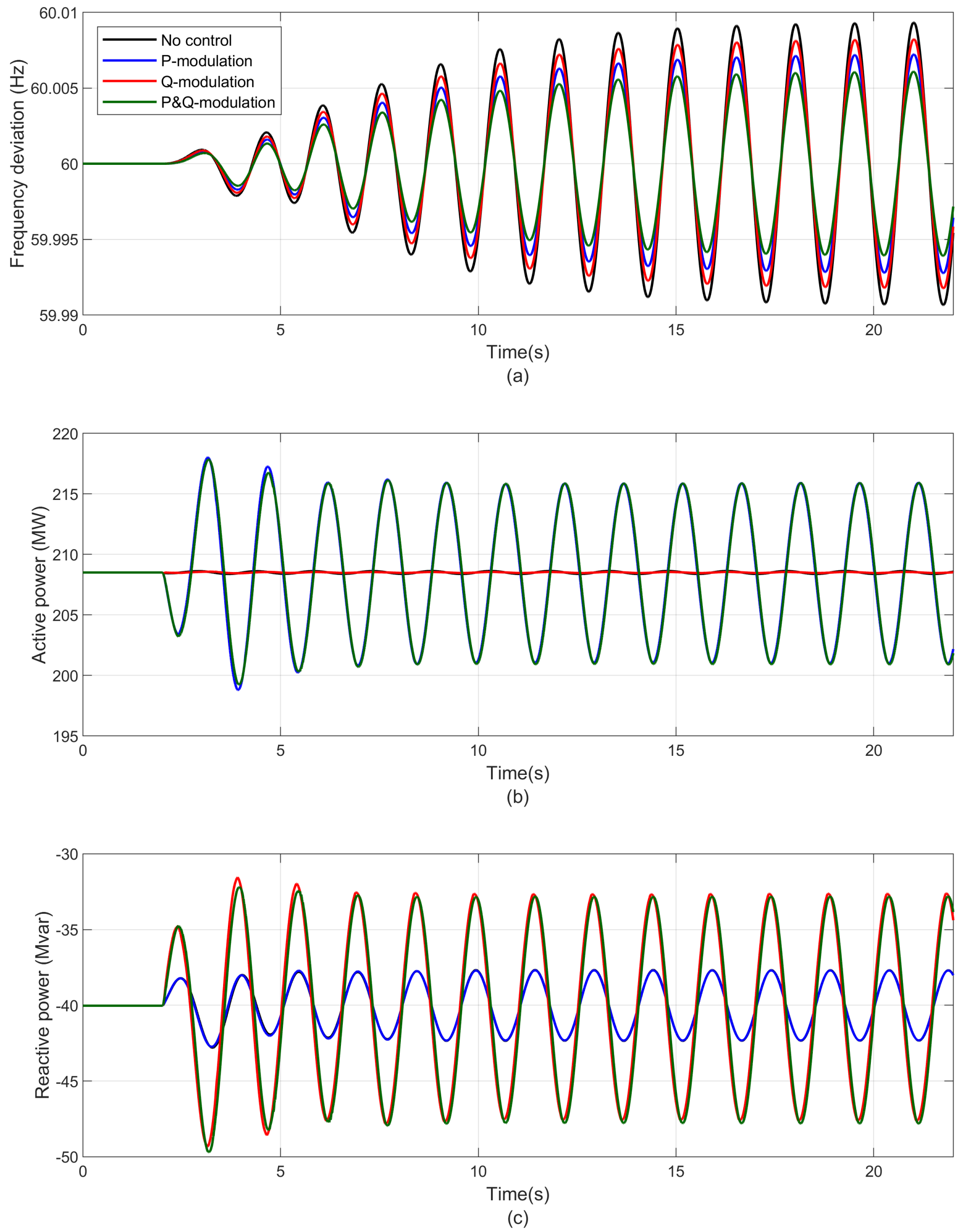

Figure 7.14: Forced source at Area 1 Zone 9 (a) Frequency deviation improvement at Area 4 Zone 19 (b) Actuator active power at Area 1 Zone 9 (c) Actuator reactive power at Area 1 Zone 9

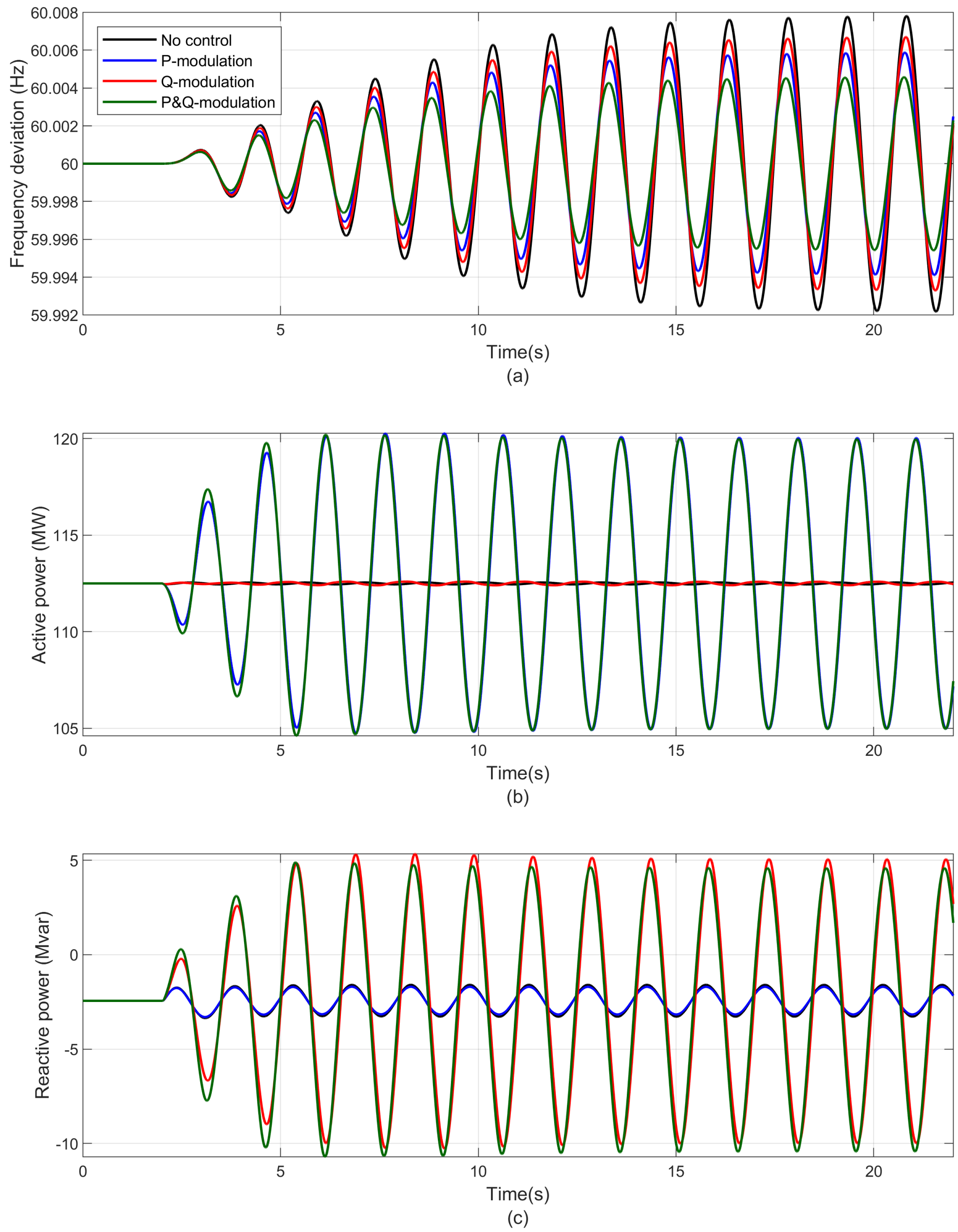

Figure 7.15: Forced source at Area 2 Zone 11 (a) Frequency deviation improvement at Area 4 Zone 19 (b) Actuator active power at Area 2 Zone 11 (c) Actuator reactive power at Area 2 Zone 11

Table 7.8: Summary of the forced oscillation damping control performance when forced disturbance through active power of the load.

Case #	Forced Source Area/Zone	No Control Frequency Deviation (mHz)	P Modulation of Actuator		Q Modulation of Actuator		P&Q Modulation of Actuator	
			Peak to Peak					
			Actuator Output (MW)	Freq.Dev (mHz)	Actuator Output (MVar)	Freq.Dev (mHz)	Actuator Output (MW)+(MVar)	Freq.Dev (mHz)
1	Area 1 Zone 9	163.13	20	134.96	20	144.74	20+20	115.72
2	Area 4 Zone 19	33.80	15	29.55	15	31.00	15+15	26.86
3	Area 2 Zone 11	31.13	15	27.26	15	28.66	15+15	24.62

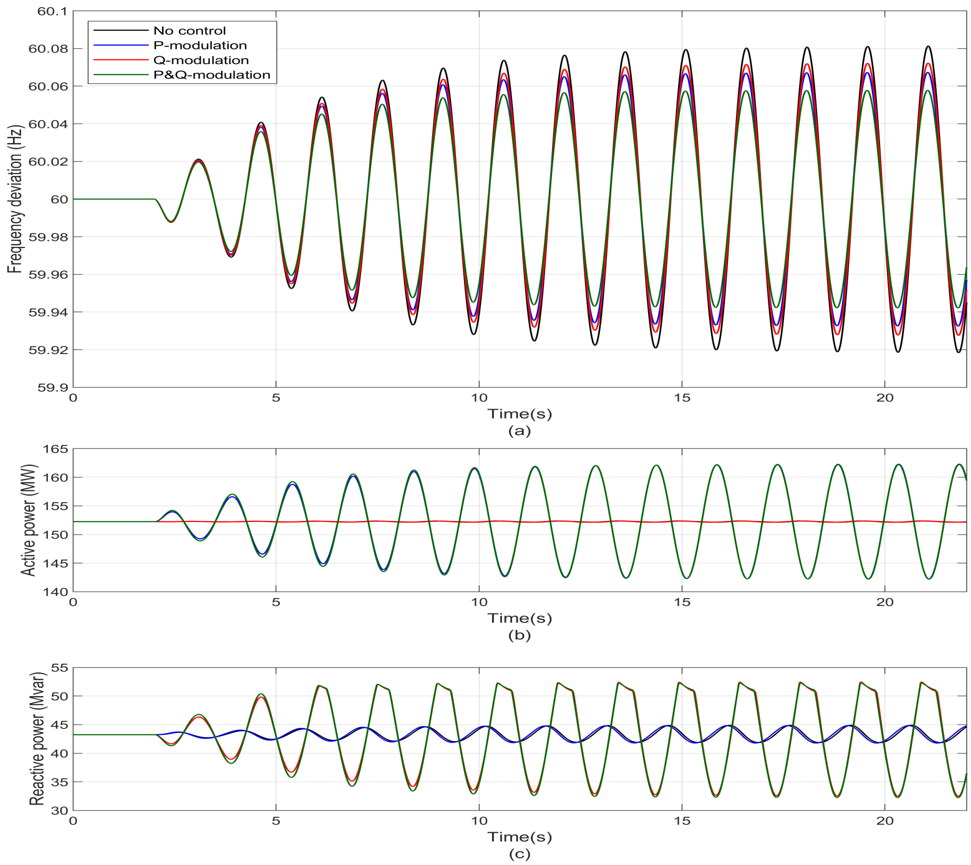

Figure 7.16: Forced source at Area 4 Zone 19 (a) Frequency deviation improvement at Area 4 Zone 19 (b) Actuator active power at Area 4 Zone 19 (c) Actuator reactive power at Area 4 Zone 19

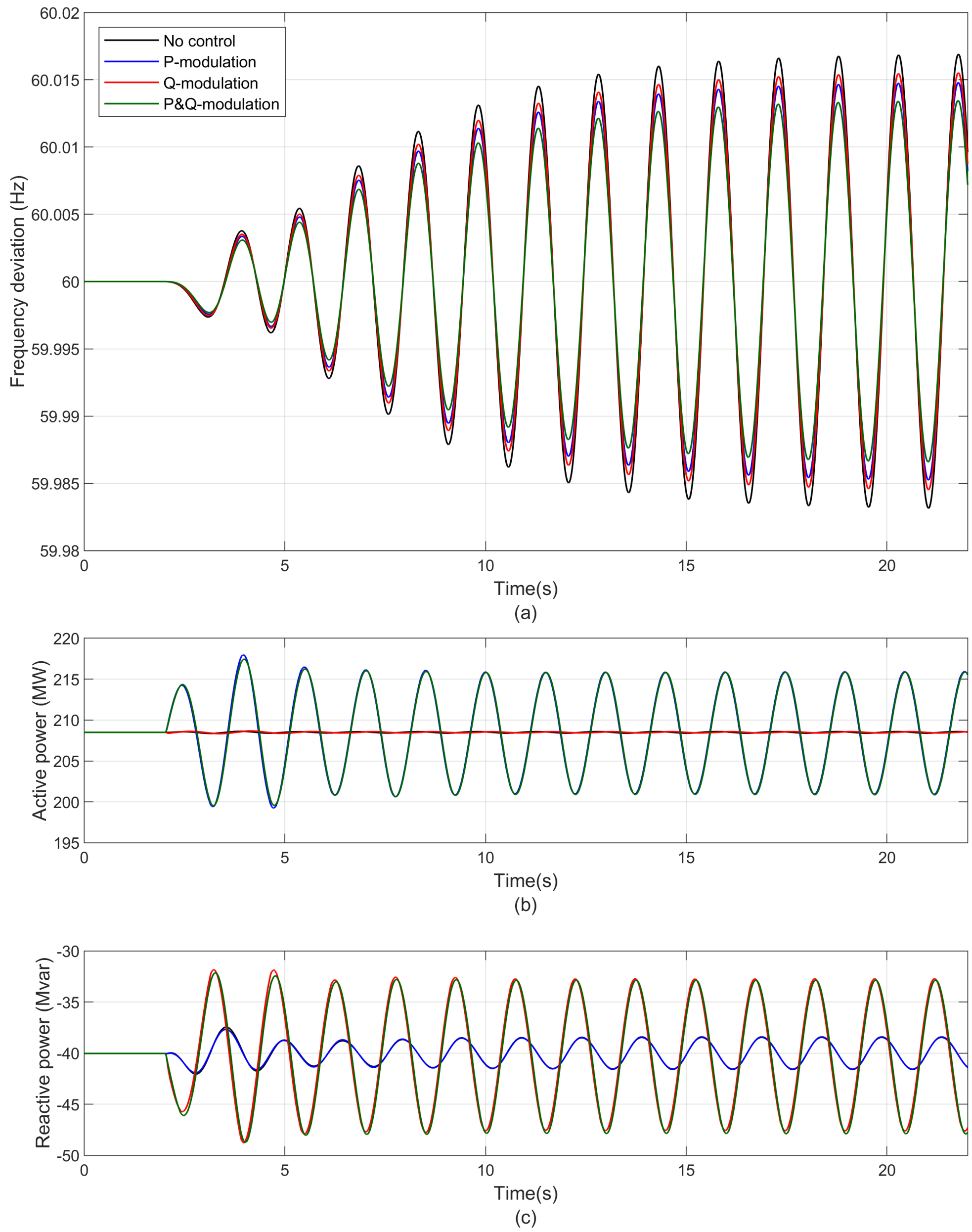

Figure 7.17: Forced source at Area 1 Zone 9 (a) Frequency deviation improvement at Area 4 Zone 19 (b) Actuator active power at Area 1 Zone 9 (c) Actuator reactive power at Area 1 Zone 9

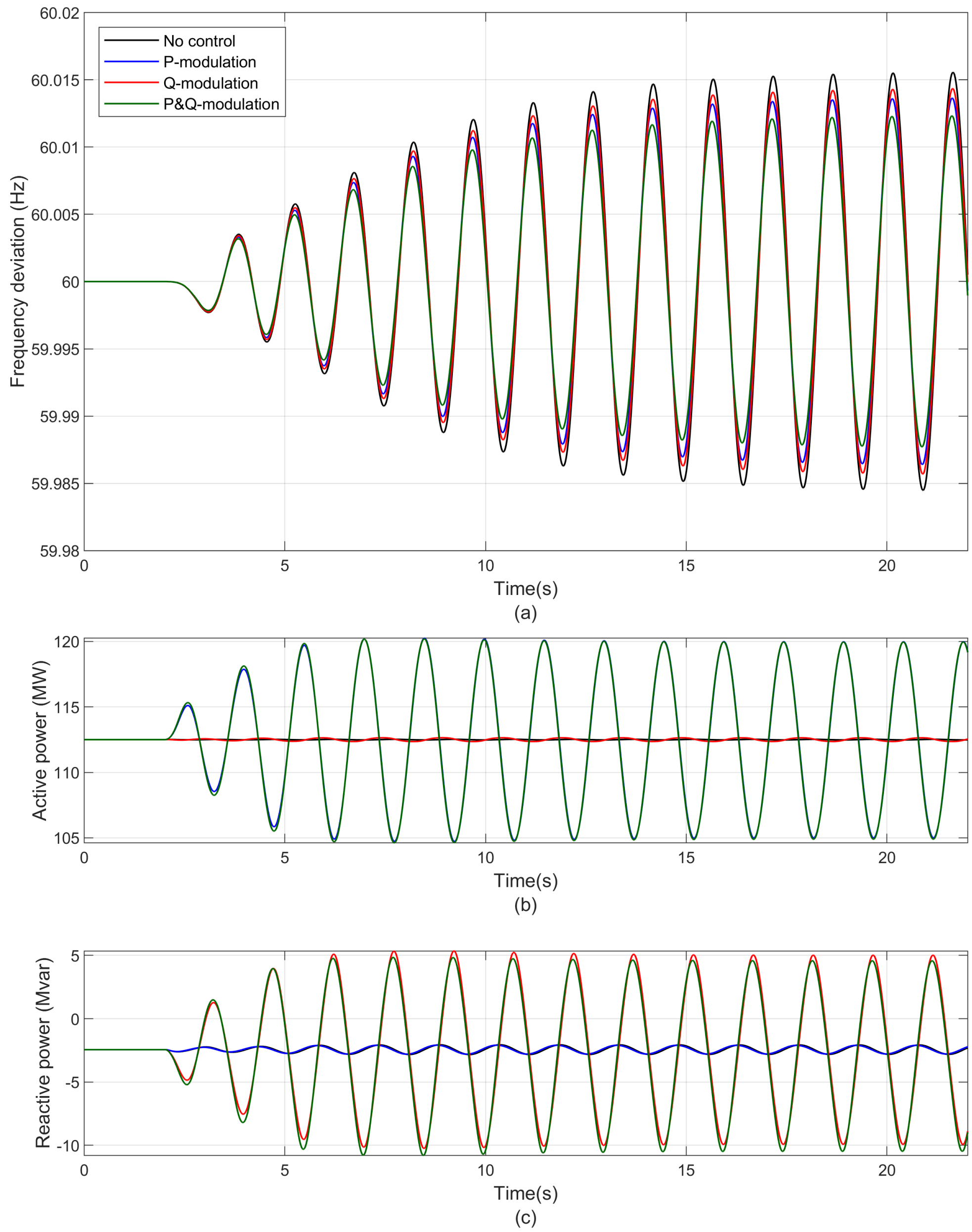

Figure 7.18: Forced source at Area 2 Zone 11 (a) Frequency deviation improvement at Area 4 Zone 19 (b) Actuator active power at Area 2 Zone 11 (c) Actuator reactive power at Area 2 Zone 11

7.6 Grid Vulnerability Analysis - Active and Reactive Forced Disturbance through Load

In this section, the forced oscillation is excited through both the active and reactive power disturbance of the load. In sections 7.2 and 7.3, the forced oscillation is excited through the active and reactive power disturbance of the load, respectively. In addition, the peak-to-peak forced oscillation energies were 100 MW and 100 Mar, respectively, which are equivalent to 100 MVA. To compare the results of this section with those of sections 7.2 and 7.3, the apparent power energy of forced oscillation will be set to 100 MVA. Three cases are tested at the resonance when the forced oscillation frequency coincides with the dominant mode of 0.67 Hz. The peak-to-peak active and reactive forced oscillation energies of the three cases are 70.7 MW and -70.7 Mvar, 85 MW and -52.67 Mvar, and 52.67 MW and -85 Mvar, which are equivalent to 100 MVA.

In sections 7.2 and 7.3, the most severe frequency deviation was observed at Area 4 Zone 19 when the forced source was located at Area 4 Zone 19. Figure 7.19 illustrates the bus frequency deviation at Area 4 Zone 19 when the forced source located at Area 4 Zone 19 is either excited by active power disturbance of the load or reactive power disturbance of the load. Moreover, the peak-to-peak oscillation energies are 70.7 MW, 70.7 Mvar, and -70.7 Mvar. When the forced oscillation energy is either 70.7 MW or -70.7 Mvar, the bus frequency deviation at the beginning of the event will decrease. In contracts, when the forced oscillation energy is 70.7 Mvar, the bus frequency deviation at the beginning of the event will increase. Therefore, when the forced source is at Area 4 Zone 19, and forced oscillation disturbance is excited through both active and reactive power of the load, there would be two scenarios for the frequency deviation at Area 4 Zone 19 as follows:

- If both the reactive and active power oscillation energy is positive or negative, they act against each other, and the frequency deviation caused by the forced oscillation will be partially damped, as seen in Figure 7.20 (red).

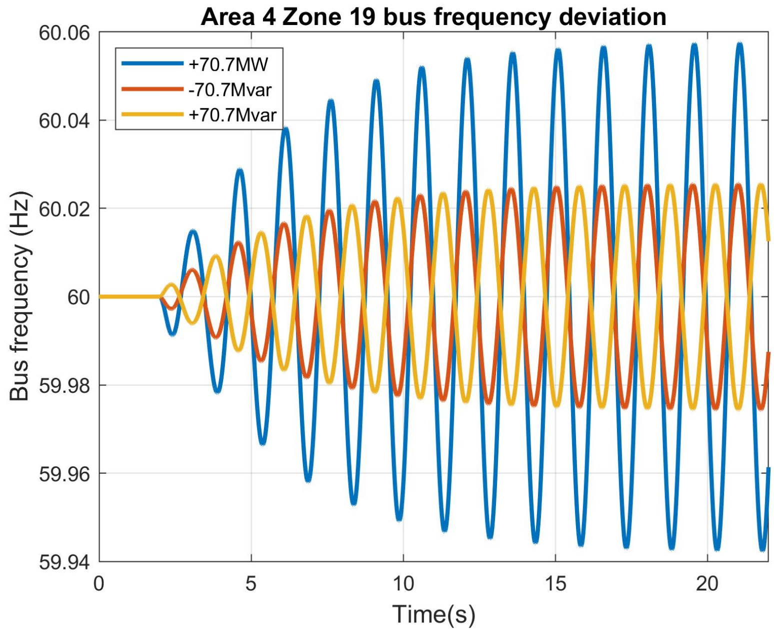

Figure 7.19: Bus frequency deviation at Area 4 Zone 19 when the forced source located at Area 4 Zone 19 is either excited by active or reactive power disturbance of the load

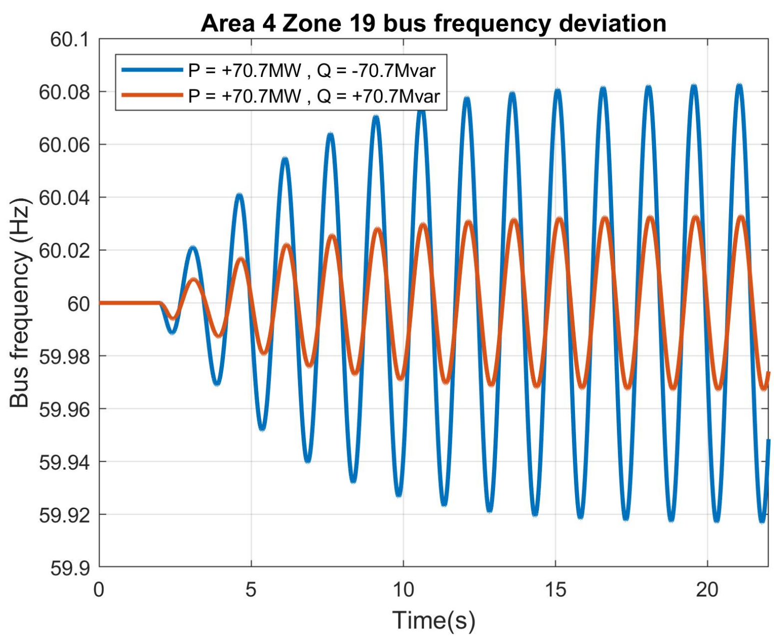

Figure 7.20: Bus frequency deviation at Area 4 Zone 19 when the forced source located at Area 4 Zone 19 is excited by both active and reactive power disturbance of the load

- If both the reactive and active power oscillation energy have opposite signs, the frequency deviation caused by the forced oscillation event will propagate, as seen in Figure 7.20 (blue).

Figures 7.21 and 7.22 show the result from sections 7.2 and 7.3 of the location dimension scanning when the oscillation frequency is set at 0.67 Hz, and the forced oscillation energy is 100 MW and 100 Mar, respectively. The filled circles represent the zone's location of the forced source on the map, and the circle's color represents the value of the largest peak-to-peak bus frequency deviation in mHz caused by each forced source. It can be noted in Figures 7.21 and 7.22 that the largest peak-to-peak frequency deviations are 163.49 mHz and 72.49 mHz, respectively, and they occur when the forced source is at Area 4 Zone 19. Figures 7.23, 7.24, and 7.25 depict the location dimension scanning when the oscillation frequency is set at 0.67Hz, and the forced oscillation energy is (70.7 MW and -70.7 Mvar), (85 MW and -52.67 Mvar), and (52.67 MW and -85 Mvar), which are equivalent to 100 MVA. In the three figures, the forced source at Area 4 Zone 19 excites the largest peak-to-peak frequency deviation observed at Area 4 Zone 19 with a frequency deviation of 165.58 mHz, 176.21 mHz, and 146.85 mHz, respectively. Table 7.9 shows the largest peak-to-peak frequency deviation at different forced oscillation energies that are equivalent to 100 MVA, and the oscillation frequency is 0.67 Hz.

During a forced oscillation event, the frequency deviation at some locations in the system may be impacted by a forced disturbance through active power of the load more than reactive power of the load and vice versa. When the forced oscillation disturbance is through both active and reactive power of the load and if the frequency deviation of a location in the system is impacted more by active power disturbance than reactive power disturbance of the load, then increasing the active power forced oscillation energy would result in a more severe impact in that location than increasing the reactive power forced oscillation energy. This is true given that the frequency deviation caused by the active and reactive power disturbance deviate in the same direction as shown in the red and blue bus frequency signal in Figure 7.19. For example, from Table 7.9, when the forced source at Area 4 Zone 19, 100 MW forced disturbance causes a higher frequency deviation than 100 Mvar forced disturbance.

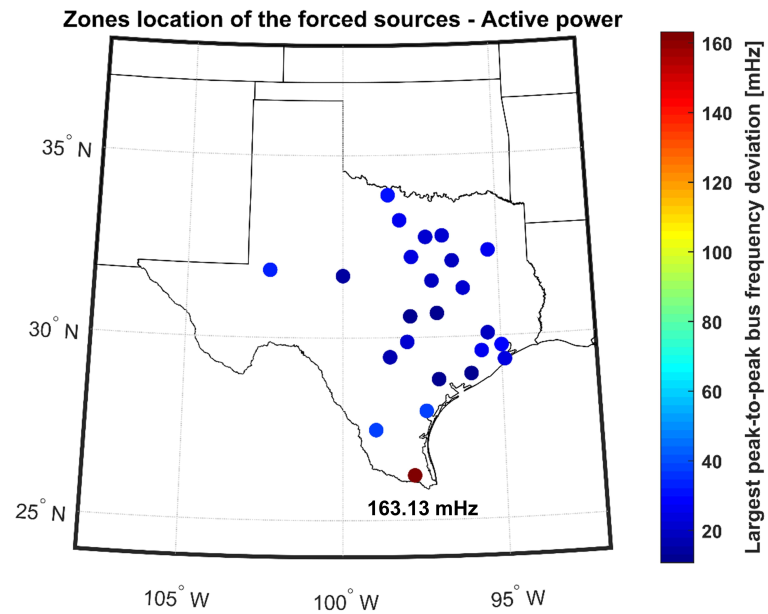

Figure 7.21: Bus frequency deviation at Area 4 Zone 19 when the forced source is excited by both active and reactive power disturbance of the load

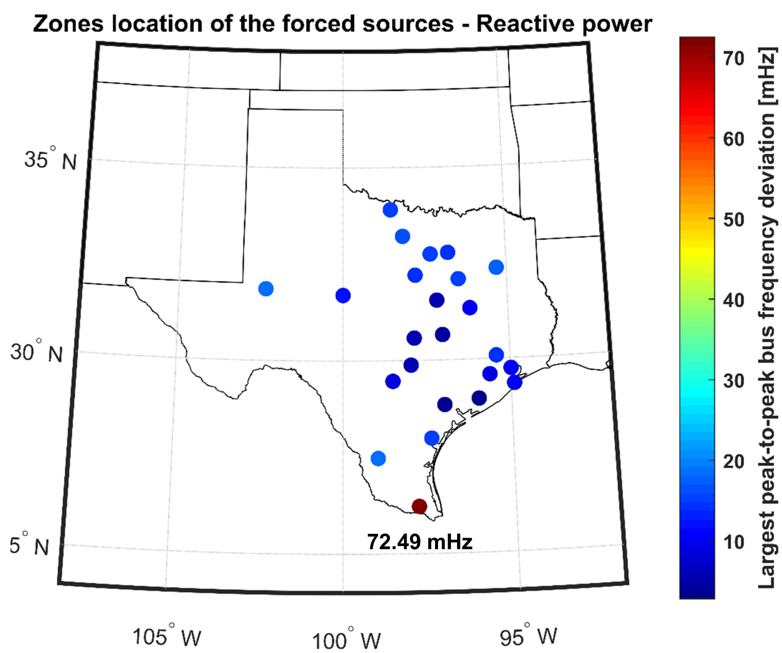

Figure 7.22: Bus frequency deviation at Area 4 Zone 19 when the forced source is excited by both active and reactive power disturbance of the load

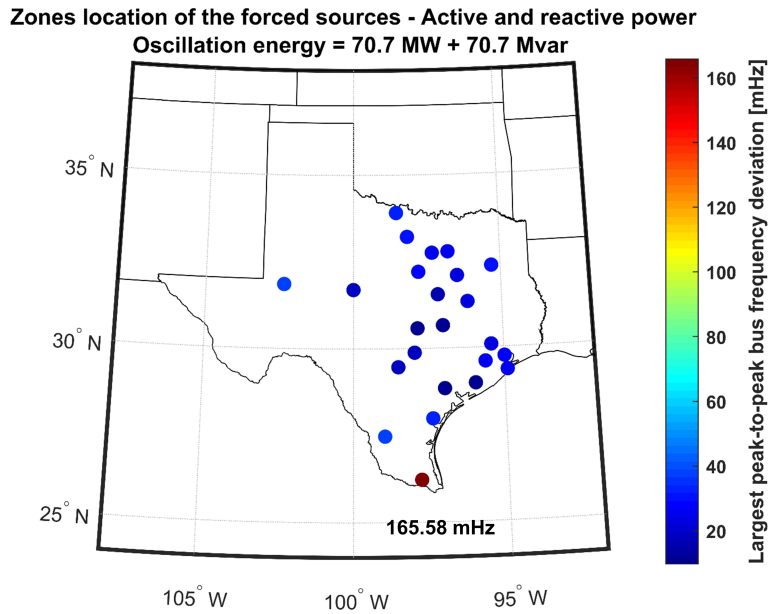

Figure 7.23: Bus frequency deviation at Area 4 Zone 19 when the forced source is excited by both active and reactive power disturbance of the load

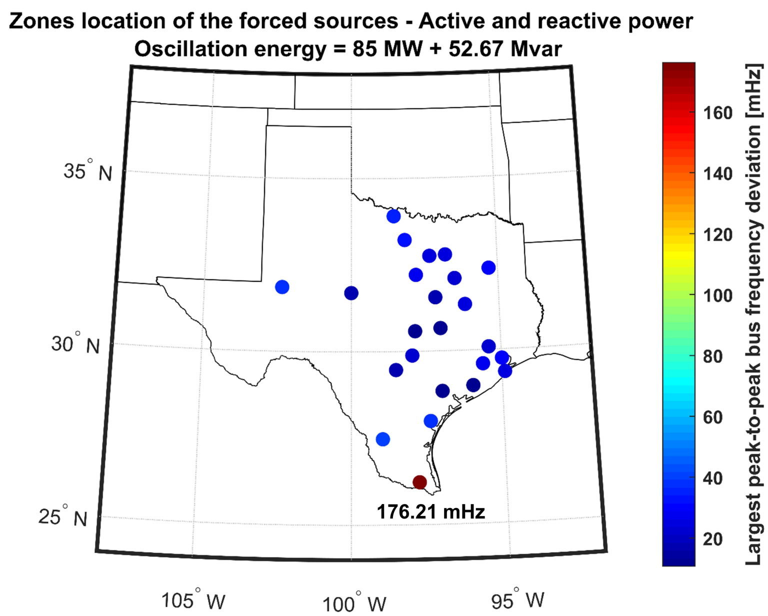

Figure 7.24: Bus frequency deviation at Area 4 Zone 19 when the forced source is excited by both active and reactive power disturbance of the load

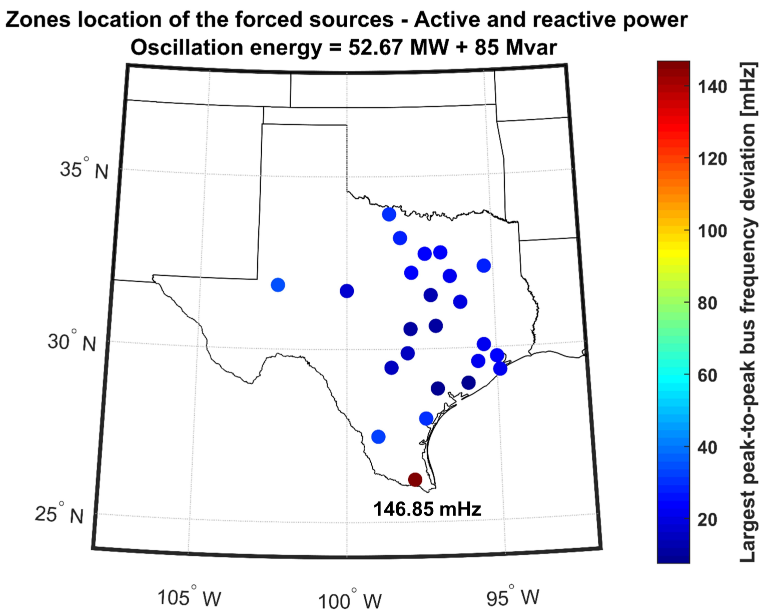

Figure 7.25: Bus frequency deviation at Area 4 Zone 19 when the forced source is excited by both active and reactive power disturbance of the load

Table 7.9: Summary of the forced oscillation damping control performance when forced disturbance through active power of the load.

Peak-to-peak forced oscillation energy	Forced Source Location	Area—Zone with Largest Bus Frequency Deviation	Peak-to-Peak Bus Frequency Deviation (mHz)
100 MW	Area 4 Zone 19	Area 4 Zone 19	163.13
100 Mvar	Area 4 Zone 19	Area 4 Zone 19	72.49
70.7 MW and 70.7 Mvar	Area 4 Zone 19	Area 4 Zone 19	165.58
85 MW and -52.67 Mvar	Area 4 Zone 19	Area 4 Zone 19	176.21
52.67 MW and -85 Mvar	Area 4 Zone 19	Area 4 Zone 19	146.85

Therefore, when the forced source is at Area 4 Zone 19 and the disturbance is through both active and reactive power disturbance of the load, increasing the active power disturbance causes a higher frequency deviation than increasing the reactive power disturbance. This can be observed when the forced oscillation energy is (85 MW and -52.67 Mvar) and (52.67 MW and -85 Mvar), where the former excites a higher frequency deviation than the latter when the forced source is at Area 4 Zone 19.

7.7 Summary

A two-dimensional scanning grid vulnerability analysis method is implemented to identify the critical areas/zones to forced oscillation in the synthetic Texas grid model. The result of the two-dimensional scanning method is assessed and compared when the forced disturbance through active and reactive power of the load. An effective actuator location is determined based on the two-dimensional scanning result to mitigate the forced oscillation in the most severe cases. The performance of the forced oscillation damping control through active and reactive modulation of the IBR is discussed and compared. A summary of the finding is listed below:

- The two-dimensional scanning result shows when the forced oscillation frequency is close to the system's dominant natural mode of 0.67 Hz, the largest peak-to-peak frequency deviation is observed. This observation is valid for both the active and reactive power forced disturbance through the load.

- When the forced oscillation source is located in a zone with a high participation factor to the natural oscillation mode, the amplitude of frequency deviation is amplified across the system and could significantly impact the system stability.

- In each of the 30 scenarios, the largest peak-to-peak frequency deviation caused by a forced source through the active power of the load is higher than the reactive power of the load.

- Forced oscillation damping control through both active and reactive power modulation of IBR is effective in mitigating the impact of force disturbance.
- Active power modulation of the IBR can reduce frequency deviation better than reactive power modulation of the IBR.
- The proposed forced oscillation damping control can reduce the frequency deviation at all the zones in the system in the synthetic Texas grid model when the actuator is close to the forced source.
- When active and reactive power modulation of IBR are combined, they can coordinate and provide a better damping performance.

Chapter 8

Impact of Increasing Renewable Penetration on Oscillation Frequency - Texas Case Study

8.1 Renewable Penetration Scenarios and modeling

In this chapter, the 2000-bus synthetic Texas power grid model is used for this study. The base case has an actual generation of 68747.86 MW, and around 13% of the actual generation comes from renewables. The dynamic models of the renewables in the base case are the generator/converter model (REGCAU2) and the electrical control model (REECCU1). The oscillation frequency and damping ratio are investigated under five renewable penetration levels of 13% (base case), 30%, 50%, 70%, and 82%. When increasing the renewable penetration in the Texas system, the renewable penetration level is increased in each area of the system by approximately the same percentage. Moreover, the synchronous generators that have low capacity are replaced first in each area. The nuclear and hydro generators have an actual capacity of 7262.9 MW and are not replaced by renewable. In this case study, the renewable generators above 13% (base case) are modeled by reducing the inertia constant of the generator to be replaced by renewable to 75% of the original value and removing the governer and PSS models. Moreover, the exciter model gain is reduced to a small value.

Figure 8.1 illustrates the 23-bus system. The 23-bus has 6 synchronous generators, and the exciter models for the generators are IEEET1, SCRX, and SEXS. The actual generation is 3258.6 MW. The penetration level in the system has increased to 30% and 49.4%. The system frequency response under generation trip when the renewables are modeled by the generator/converter model (REGCAU2) and the electrical control model (REECCU1) are compared when modeling the renewable by the following:

1- Reducing the synchronous generator inertia and removing the governer and PSS models.

2- Reducing the synchronous generator inertia, removing the governer and PSS, and reducing the regulator gain of exciter models to a small value.

3- Reducing the synchronous generator inertia and removing the governer, PSS, and exciter models.

It is to be noted that the REGCAU2 and REECCU1 renewable models have the same parameters as in the base case of the Texas system. In this study, generators at buses 3011 and 101 are replaced by renewable in the 31% penetration level, and generators at buses 3011, 101, and 211 are replaced by renewable in the 49% penetration level. In addition, the generator at bus 3018 with an actual generation of 100 MW is the tripped generator. Figures 8.2 and 8.3 illustrate bus 151 frequency response due to a 100 MW generation trip when the renewable penetration levels are 31% and 49%, respectively. It can be seen that under generation trip when representing the renewable by reducing the synchronous generator inertia, removing the governer and PSS, and reducing the regulator gain of exciter models to a small value (green), it has the closest response as when representing the renewable by grid following model (REGCAU2 and REECCU1) (black). Table 8.1 shows the exciter models in the 23-bus system and the original gains, and the value of the reduced gains for the generators that are to be replaced by renewable. Table 8.2 shows the exciter models in the 2000-bus synthetic Texas model and the symbol of the gains, and the new reduced values for the generators that are to be replaced by renewable.

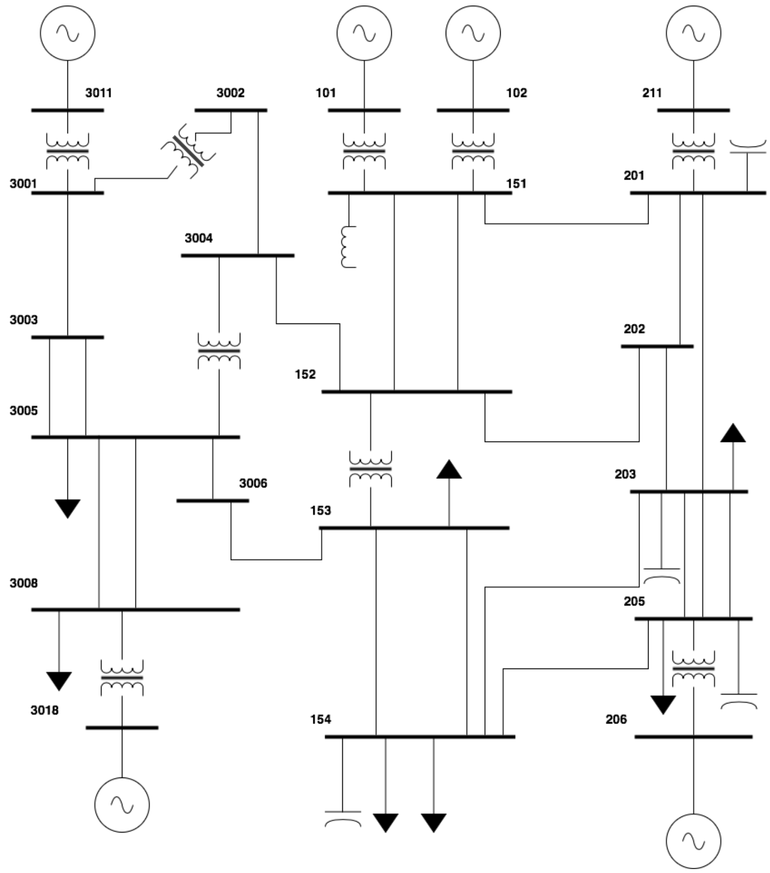

Figure 8.1: 23-bus power system.

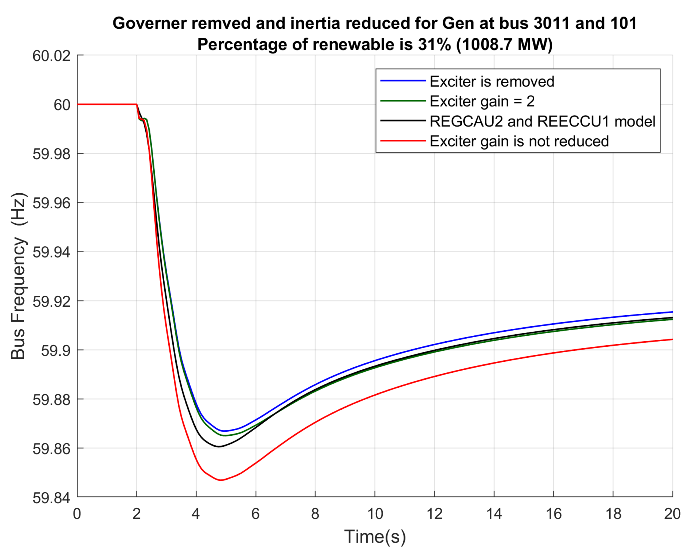

Figure 8.2: Bus 151 frequency response due to a 100 MW generation trip with a renewable penetration level of 31% .

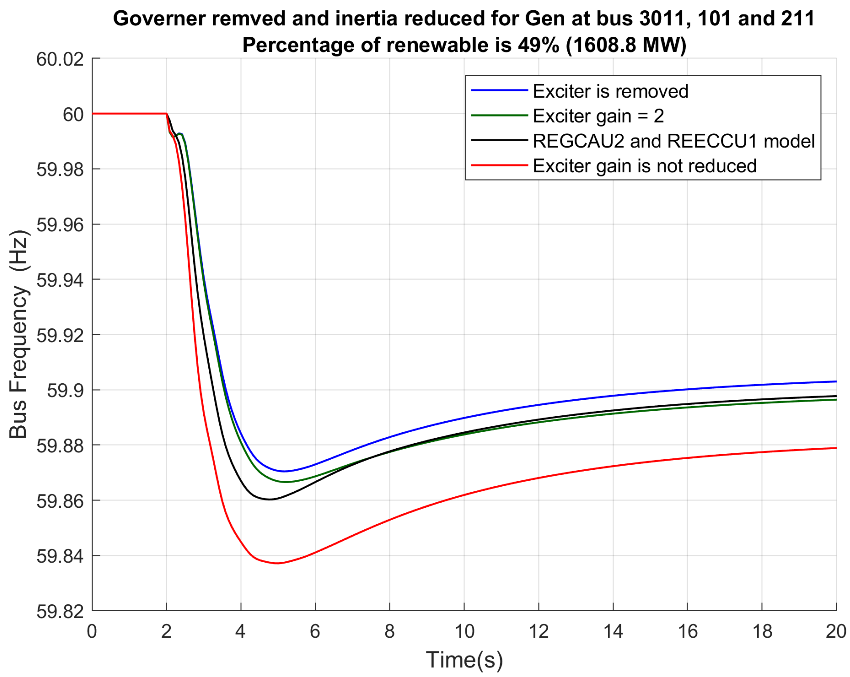

Figure 8.3: Bus 151 frequency response due to a 100 MW generation trip with a renewable penetration level of 49% .

Table 8.1: Exciter models in the 2000-bus synthetic Texas model, the symbol of the gains, and the value of the reduced gain for the generators that are to be replaced by renewable.

Generator bus number	Exciter model	Gain	Original Value	Reduced Value
101	IEEET1	KA	400	2
211	SCRX	K	200	2
3011	SEXS	K	100	2

Table 8.2: Exciter models in the 23-bus system and the original gains, and the value of the reduced gain for the generators that are to be replaced by renewable.

Exciter Model	**Variable**	**Value**
ESAC1A, ESAC6A, ESDC1A, EXAC1, EXAC2, IEEET1	KA	2
SCRX, SEX	K	2
ESDC2A	KA	0.2
EXPIC1	KA	0.01
ESST4B	KPR, KIR	0.1, 0

8.2 Impact of Increasing Renewable Penetration on Texas Oscillation Frequency

This section investigates the impact of increasing renewable penetration on oscillation frequency and damping ratio in the synthetic Texas power system. In this study, the oscillation is excited using a temporary three-phase fault applied at the line between bus 4040 and bus 4079. This disturbance can excite the dominant oscillation mode of 0.67 Hz in the synthetic Texas power system in the base case with 13% renewable penetration [120]. The renewable penetration levels are increased with the following percentages: 30%, 50%, 70%, and 82%. Table 8.3 shows the actual generation of renewables at each penetration level.

Figure 8.4 shows the frequency response of Area 4 Zone 19 when tripping the largest two generators in the synthetic Texas system. The two tripped generators are nuclear generators located at Area 7 (Coast) with an actual generation of 2590 MW. It is to be noted under the two nuclear generation trip, the scenario with 82% renewable penetration is the maximum renewable penetration level that the system can reach and still be stable. Table 8.4 shows the frequency nadir for all penetration scenarios when tripping the largest two generators in the synthetic Texas system.

In the PSS/e simulation, in the base case of the Texas synthetic power system, the dominant oscillation mode of 0.67 Hz can be observed during a temporary three-phase fault between the line at bus 4040 and bus 4079. The frequency of a high voltage bus at Area 4 Zone 19 is observed during the temporary three-phase fault applied at the line between bus 4040 and bus 4079 under each renewable penetration level. Figure 8.5 depicts the bus frequency response at Area 4 Zone 19 during the disturbance under each renewable penetration level. Table 8.5 shows the Prony analysis of bus frequency in Figure 8.5 under each renewable penetration scenario. Figure 8.6 illustrates the oscillation frequency and damping ratio trend as the renewable penetration level increases. It can be noted in the synthetic Texas power system, the oscillation frequency increases as the renewable penetration increases, whereas the damping ratio reduces as the renewable penetration reduces until the 70%

Table 8.3: Summary of the forced oscillation damping control performance when forced disturbance through active power of the load.

Scenario	Percentage of renewable penetration (%)	Renewable actual generation (MW)
1	13 (base case)	8962.38
2	30	20618.01
3	50	34363.35
4	70	48108.69
5	82	56373.25

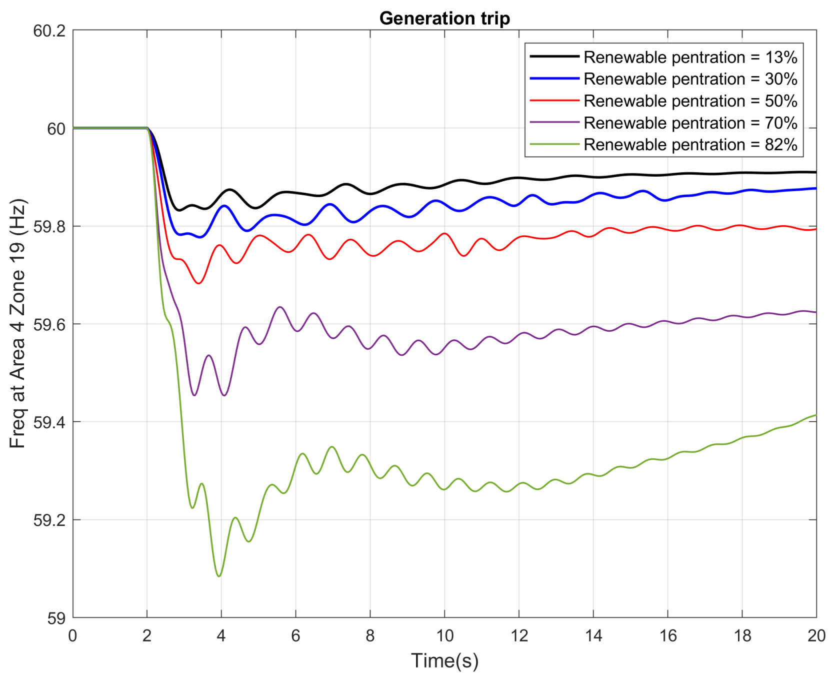

Figure 8.4: Bus frequency response of Area 4 Zone 19 when tripping the largest two generators in the synthetic Texas system.

Table 8.4: frequency nadir for all penetration scenarios when tripping the largest two generators in the synthetic Texas system.

Scenario	Percentage of renewable penetration (%)	Frequency nadir (Hz)
1	13 (base case)	59.78
2	30	59.72
3	50	59.63
4	70	59.43
5	82	59.07

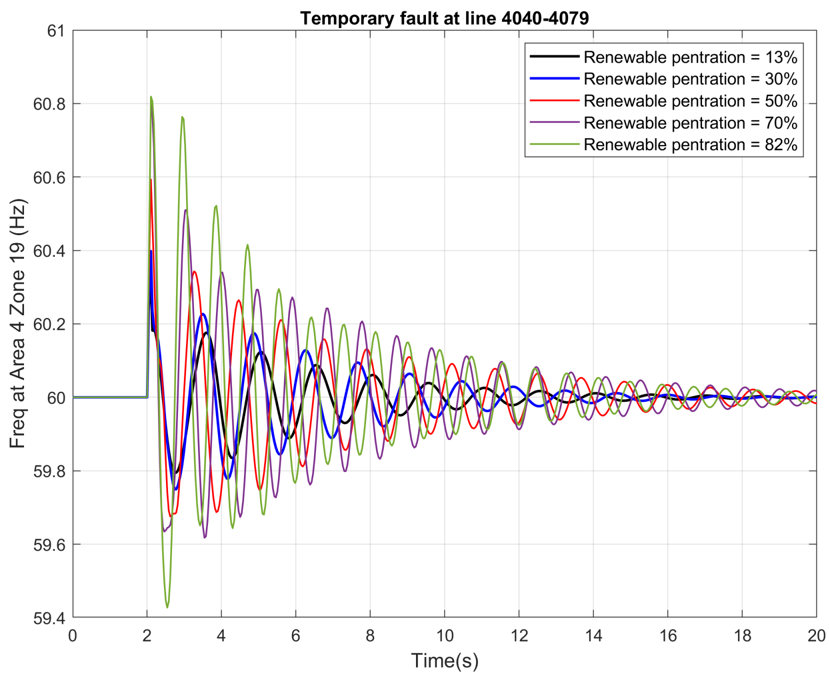

Figure 8.5: Bus frequency response of Area 4 Zone 19 under temporary three-phase fault at the line between bus 4040 and bus 4079 under different renewable penetration levels.

Table 8.5: Summary of the oscillation frequency and damping ratio under different renewable penetration levels.

Scenario	Percentage of renewable penetration (%)	Mode 1	
		Oscillation Freq (Hz)	Damping ration (%)
1	13 (base case)	0.67	6.38
2	30	0.747	5.52
3	50	0.867	3.23
4	70	1.07	2.82
5	82	1.169	2.86

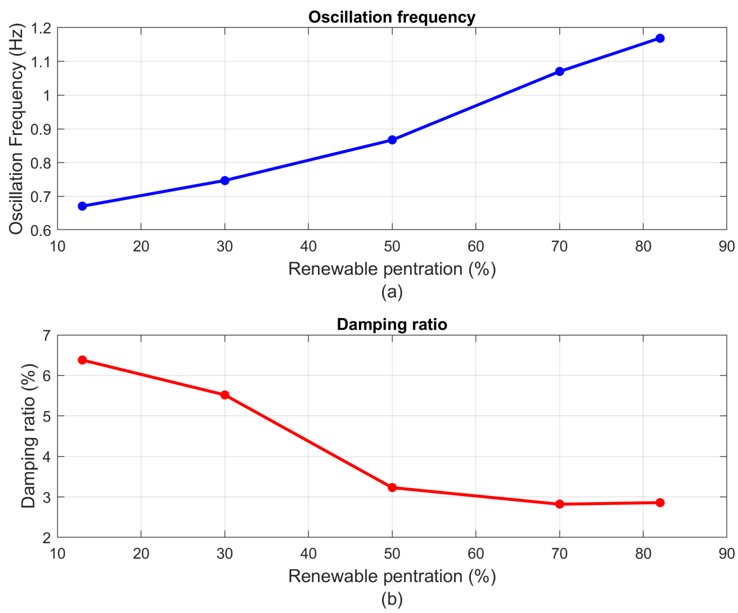

Figure 8.6: Oscillation frequency and damping ratio trend as the renewable penetration level increases.

penetration level and then slightly increases at the 82% penetration level. The damping ratio may be impacted by the synchronous generators being replaced by renewable because some generators may have more impact on the oscillation than other generators. In this study, the generators on buses 4026 and 4082 in Area 4 were converted to renewables when the percentage of renewable penetration increased from 70% to 82%. Suppose these two generators are not replaced with renewable and instead replace other generators with approximately the same capacity in other areas in the Texas system. In that case, the damping ratio of 82% renewable penetration can be lower than 70% penetration. Thus, the relationship between the increased renewable penetration level and the damping ratio level is unclear. Figure 8.7 illustrates the bus frequency response at Area 4 Zone 19 during a temporary three-phase fault between the line at bus 4040 and bus 4079 when the renewable penetration level is 82% with and without converting the generators on buses 4026 and 4082 to renewables. Table 8.6 shows the oscillation frequency and damping ratio under two 82% renewable penetration scenarios.

8.3 Impact of POD Control on Damping Oscillation at High Renewable Penetration

The POD through active power modulation of IBR in Figure 8.8 is tested under the five renewable penetration levels. The IBR at bus 4153 is chosen as the actuator, and the controller's input is the frequency of a local high-voltage bus. The controller gain is set to -200, and the controller limit is set to 20% of the actuator's active power output. Tw is set to 10 and Q is set to 1, and the phase compensation is zero.

POD control performance at 13% renewable penetration level:
Figure 8.9 (a and b) illustrates the bus frequency in Area 4 Zone 19 with and without POD, as well as the actuator active power output at bus 4153, during a temporary three-phase line fault between buses 4040 and 4079. The damping ratio increases from 6.38% to 13.82%, and the oscillation frequency increases from 0.67 Hz to 0.702 Hz. The POD control can effectively suppress the oscillation.

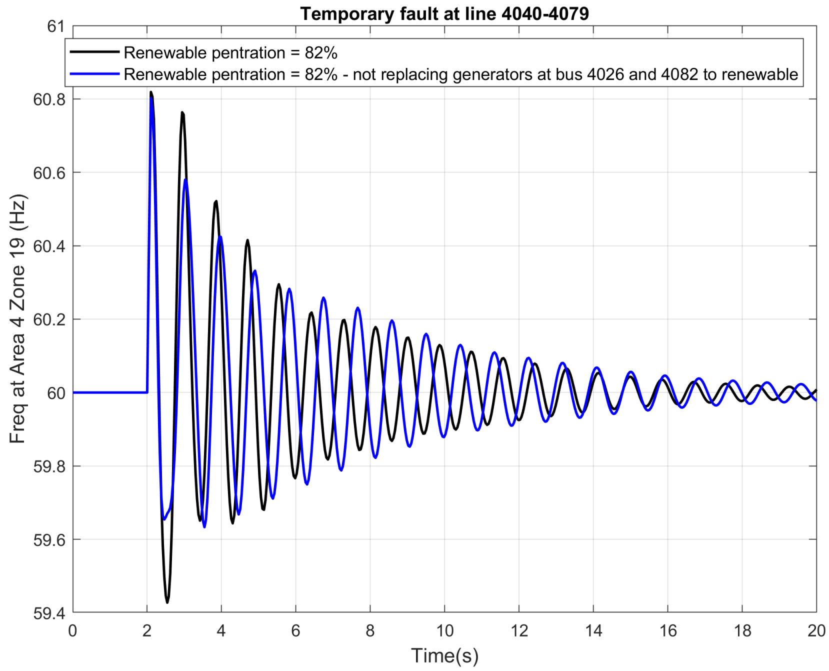

Figure 8.7: Bus frequency response of Area 4 Zone 19 under temporary three-phase fault at the line between bus 4040 and bus 4079 under two cases of 82% renewable penetration level.

Table 8.6: The oscillation frequency and damping ratio under two 82% renewable penetration scenarios.

Renewable penetration (%)	**Generator at bus 4026 and 4082**	**Oscillation Freq (Hz)**	**Damping (%)**
82	Replaced to renewable	1.169	2.86
82	Not replaced to renewable	1.088	2.52

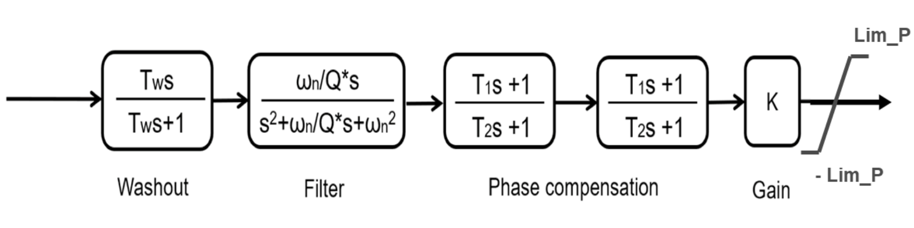

Figure 8.8: POD control structure.

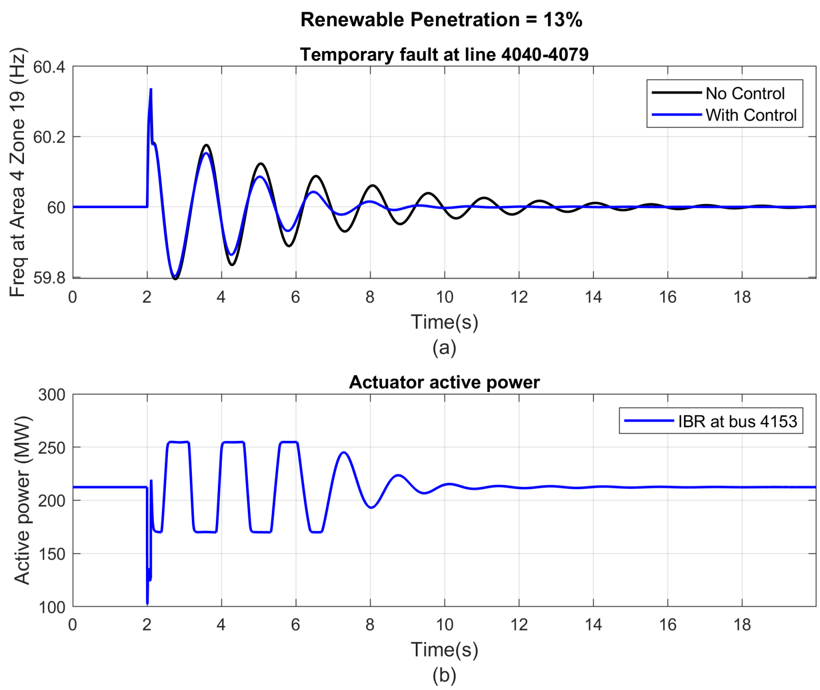

Figure 8.9: (a) Area 4 Zone 19 bus frequency with and without POD when the renewable penetration level is 13%. (b) Actuator active power output at bus 4153.

POD control performance at 30% renewable penetration level: Figure 8.10 (a and b) depicts the bus frequency in Area 4 Zone 19 with and without POD, as well as the actuator active power output at bus 4153 after a temporary three-phase line fault between buses 4040 and 4079. The damping ratio increases from 5.52% to 12.37%, and the oscillation frequency is around 0.747 Hz. The POD control can dampen oscillations effectively.

POD control performance at 50% renewable penetration level: Following a temporary three-phase line fault between buses 4040 and 4079, Figure 8.11 (a and b) demonstrates the bus frequency in Area 4 Zone 19 with and without POD as well as the actuator active power output at bus 4153. The damping ratio increases from 3.23% to 11.46%, and the oscillation frequency increases from 0.867 Hz to 0.887 Hz. As seen in Figure 8.11 (a), the oscillation can be dampened after implementing the damping control.

POD control performance at 70% renewable penetration level: Figure 8.12 (a and b) shows the bus frequency in Area 4 Zone 19 with and without POD, as well as the actuator active power output at bus 4153 after a temporary three-phase line fault between buses 4040 and 4079. The damping ratio increases from 2.82% to 10.31%, and the oscillation frequency increases from 1.07 Hz to 1.117 Hz. After employing the damping control, the oscillation can be suppressed, as shown in Figure 8.12 (a).

POD control performance at 82% renewable penetration level: Following a temporary three-phase line fault between buses 4040 and 4079, Figure 8.13 (a and b) demonstrates the bus frequency in Area 4 Zone 19 with and without POD as well as the actuator active power output at bus 4153. The damping ratio increases from 2.86% to 10.41%, and the oscillation frequency increases from 1.169 Hz to 1.197 Hz. The POD control can effectively suppress the oscillation.

Table 8.7 illustrates a summary of the oscillation frequency and damping ratio calculated using Prony analysis at each renewable penetration scenario after implementing the local POD control.

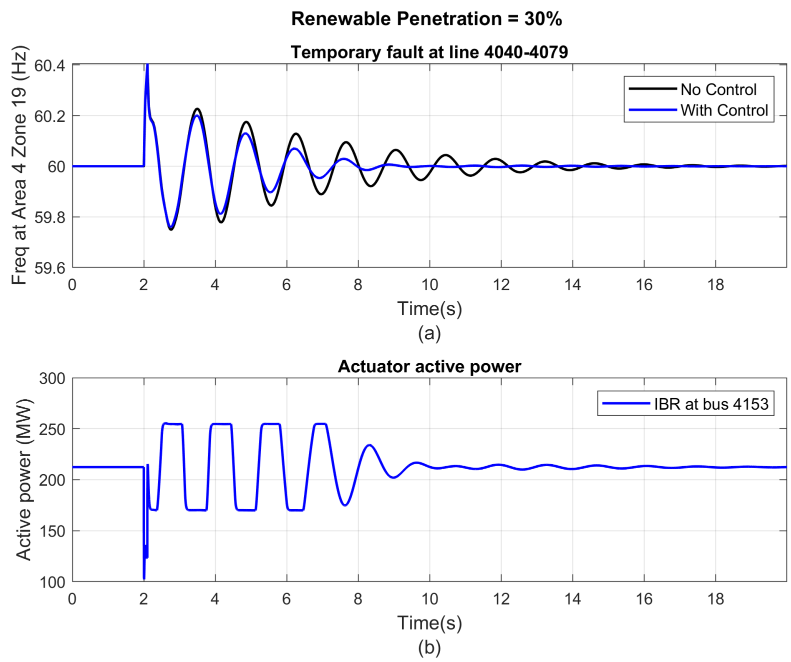

Figure 8.10: (a) Area 4 Zone 19 bus frequency with and without POD when the renewable penetration level is 30%. (b) Actuator active power output at bus 4153.

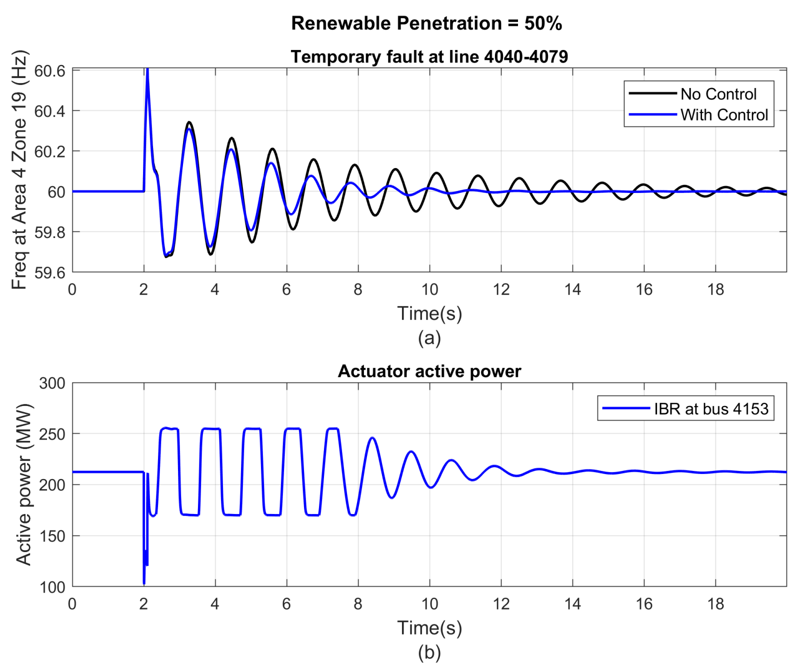

Figure 8.11: (a) Area 4 Zone 19 bus frequency with and without POD when the renewable penetration level is 50%. (b) Actuator active power output at bus 4153.

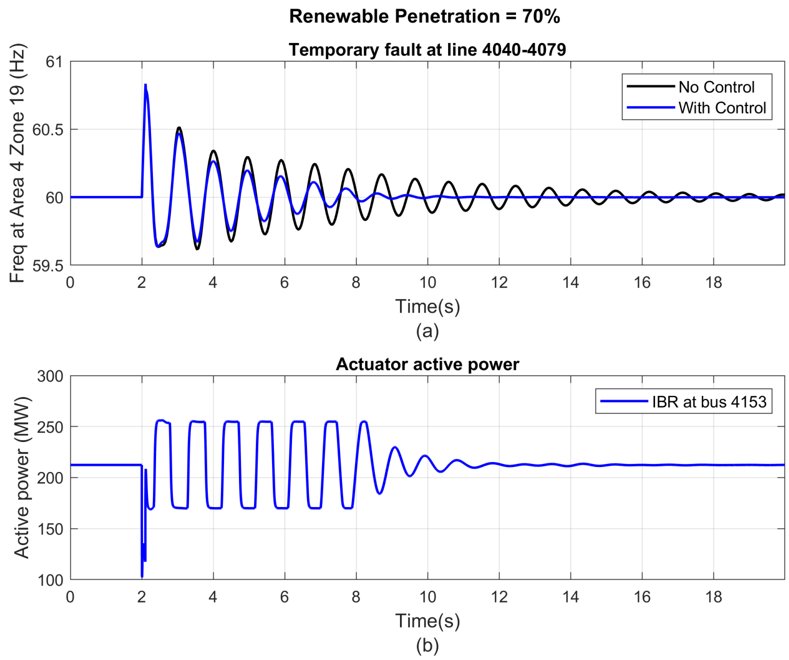

Figure 8.12: (a) Area 4 Zone 19 bus frequency with and without POD when the renewable penetration level is 70%. (b) Actuator active power output at bus 4153.

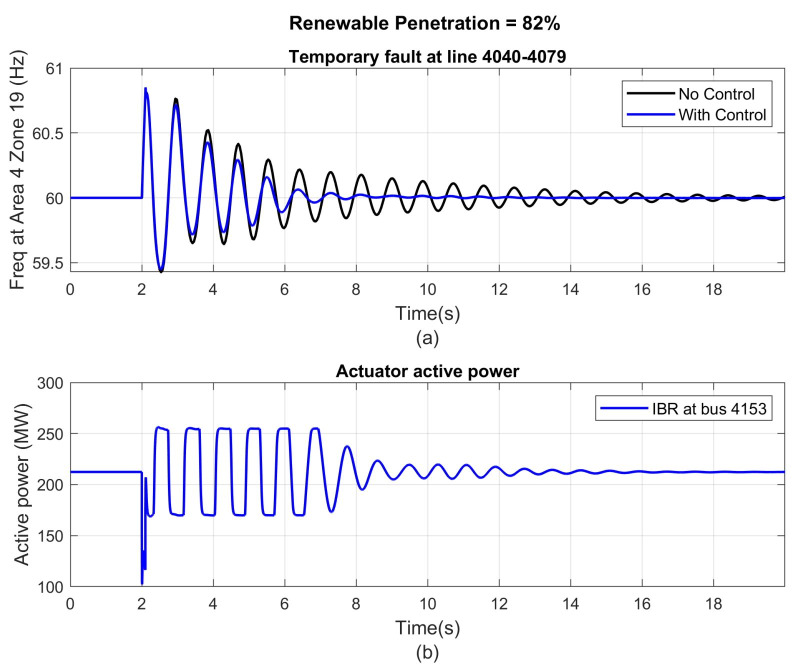

Figure 8.13: (a) Area 4 Zone 19 bus frequency with and without POD when the renewable penetration level is 82%. (b) Actuator active power output at bus 4153.

Table 8.7: Summary of the oscillation frequency and damping ratio with POD control under different renewable penetration levels.

Scenario	Percentage of renewable penetration (%)	Mode 1	
		Oscillation Freq (Hz)	Damping ratio (%)
1	13 (base case)	0.702	13.82
2	30	0.746	12.37
3	50	0.887	11.46
4	70	1.117	10.31
5	89	1.197	10.41

8.4 Summary

The impact of increasing renewable penetration on oscillation frequency and damping ratio was investigated using the 2000-bus synthetic Texas power grid. The oscillation frequency was observed at Area 4 Zone 19 under a temporary three-phase fault applied at the line between bus 4040 and bus 4079. The renewable generators above the base case of 13% were represented by reducing the synchronous generator inertia by 75%, removing the governer and PSS, and reducing the gain of exciter models to a small value. It was observed that as the renewable penetration increases in the synthetic Texas power grid, the oscillation frequency increases. On the other hand, the damping ratio reduces until the system reaches a 70% renewable penetration level and slightly increases at the 82% renewable penetration level. Therefore, the correlation is unclear between the impact of increased renewable penetration and the damping ratio level in the synthetic Texas power grid. The POD control with a local measurement was tested under different renewable penetration levels. It was observed that POD control can effectively dampen the oscillation under high renewable penetration levels.

Chapter 9

Conclusion and Future Work

In general, the dissertation investigated the impact of wide-area POD control to dampen low-frequency oscillation. In addition, the identification of critical areas and frequency to force oscillation events was investigated using the proposed forced oscillation grid vulnerability analysis and mitigation method. The POD control with local measurement was applied to mitigate the forced oscillation. The impact of high renewable penetration on the synthetic Texas system's oscillation frequency and damping ratio was studied. The dissertation's conclusions and summary include the following:

- The wide-area POD controller through active power modulation of VSC-HVDC was utilized to dampen the low-frequency oscillation in the UK grid. The developed POD controller was implemented on a general-purpose hardware platform CompactRIO and tested on a HIL test setup with actual PMU devices and a communication network impairment simulator. Realistic operating conditions are considered in the HIL tests, including measurement error/noise, occasional/consecutive data package losses, constant/random time delays, and multiple backups PMUs. The results show that the POD controller can suppress the targeted oscillation mode.

- A forced oscillation grid vulnerability Analysis and mitigation method were used to identify the critical areas and frequency to forced oscillation based on a two-dimensional frequency and location scanning approach. The critical areas/zones can be effective locations to deploy forced oscillation damping control. In this dissertation, a forced disturbance was investigated by injecting a sinusoidal wave to the governor model's active power set point and modulating the added load's active and reactive power. The forced oscillation grid vulnerability method was tested and validated using the 2000-bus synthetic Texas power grid model.

- Forced oscillation event with forced oscillation frequency at or close to the dominant natural mode can excite the most severe peak-to-peak frequency deviation in the entire Texas system. In addition, when the forced source is located in an Area with a high participation factor to the dominant natural mode, the frequency deviation amplitude is amplified throughout the system and could significantly impact the system stability.

- In each of the studied 30 scenarios, when the oscillation frequency ranges from 0.1 Hz to 1.5 Hz with a step size of 0.05 Hz, including the 0.67 Hz oscillation frequency, the largest peak-to-peak frequency deviation caused by forced oscillation through active power disturbance of the load is larger than reactive power disturbance of the load.

- Forced oscillation controller through active power modulation of IBR with local measurement effectively reduced the frequency deviation caused by forced oscillation. In the most severe forced oscillation case, the forced oscillation controller can reduce all the zones' frequency deviation in the synthetic Texas power grid below the governor Deadband of ± 36 mH when the forced oscillation controller is located close to the forced source.

- Active power modulation of IBR can reduce the frequency deviation more than reactive power modulation of IBR when forced oscillation disturbance is through active or reactive power of the load. Damping performance will improve further when modulating both the active and reactive power of the IBR.

- The impact of high renewable penetration on the oscillation frequency and daping ratio in the synthetic Texas power grid was investigated. The renewable above the base case was modeled by reducing the inertia of the synchronous generator by 75%, reducing the exciter gain, and removing the governor and PSS model. The oscillation frequency was excited by a temporary line fault at Area 4, and it was observed using the bus frequency at Area 4 Zone 19. The result shows that the oscillation frequency increases as the renewable increases. However, there was no clear trend between the damping ratio and the increase in the renewable penetration level. POD with local measures effectively damped the oscillation at different renewable penetration levels.

Future work will include forced oscillation damping controller performance validation through Hardware-in-the-loop (HIL) test. In addition, a methodology to calculate an effective droop gain of the damping controller will also be investigated. Furthermore, the impact of forced oscillation in the system as the renewable penetration level increases will be investigated.

Bibliography

[1] Atika Qazi, Fayaz Hussain, Nasrudin ABD. Rahim, Glenn Hardaker, Daniyal Alghazzawi, Khaled Shaban, and Khalid Haruna. Towards sustainable energy: A systematic review of renewable energy sources, technologies, and public opinions. *IEEE Access*, 7:63837–63851, 2019. 1

[2] Qingxin Shi, Hantao Cui, Fangxing Li, Yilu Liu, Wenyun Ju, and Yonghui Sun. A hybrid dynamic demand control strategy for power system frequency regulation. *CSEE Journal of Power and Energy Systems*, 3(2):176–185, 2017. 1

[3] Changgang Li, Yue Wu, Yanli Sun, Hengxu Zhang, Yutian Liu, Yilu Liu, and Vladimir Terzija. Continuous under-frequency load shedding scheme for power system adaptive frequency control. *IEEE Transactions on Power Systems*, 35(2):950–961, 2020. 1

[4] Najda Vadakkeveettil Mohamed, Gopakumar Pathirikkat, and Sunitha Rajan. Modelling of inter-area angular dynamics and proactive defence strategy in deregulated power grids with large-scale integration of renewable energy sources. *IET generation, transmission & distribution*, 14(15):2940–2950, 2020. 1

[5] North American Electric Reliability Corporation (NERC). Integrating inverterbased resources into low short circuit strength systems, 2017. 1

[6] Mohd Zuhaib, Mohd Rihan, and Mohd Tayyab Saeed. A novel method for locating the source of sustained oscillation in power system using synchrophasors data. *Protection and control of modern power systems*, 5(1):1–12, 2020. 1, 7

[7] Hua Ye, Yutian Liu, Peng Zhang, and Zhengchun Du. Analysis and detection of forced oscillation in power system. *IEEE Transactions on Power Systems*, 32(2):1149–1160, 2017. 1, 7

[8] Chi Su, Weihao Hu, Zhe Chen, and Yanting Hu. Mitigation of power system oscillation caused by wind power fluctuation. *IET renewable power generation*, 7(6):639–651, 2013. 1, 7

[9] Yi Zhao, Yuqing Dong, Lin Zhu, Kaiqi Sun, Khaled Alshuaibi, Chengwen Zhang, Yilu Liu, Brian Graham, Evangelos Farantatos, Benjamin Marshall, Md Rahman, Oluwole Adeuyi, Simon Marshall, and Ian L. Cowan. Coordinated control of natural and sub-synchronous oscillations via hvdc links in great britain power system. In *2022 IEEE/PES Transmission and Distribution Conference and Exposition (TD)*, pages 1–5, 2022. 1, 2, 19, 20, 22, 31

[10] Bikash Pal. *Robust control in power systems*. Power electronics and power systems. Springer, New York, 2005. 1

[11] Yong Li, Christian Rehtanz, Sven Ruberg, Longfu Luo, and Yijia Cao. Wide-area robust coordination approach of hvdc and facts controllers for damping multiple interarea oscillations. *IEEE Transactions on Power Delivery*, 27(3):1096–1105, 2012. 2, 13

[12] Alexander Fuchs, Markus Imhof, Turhan Demiray, and Manfred Morari. Stabilization of large power systems using vsc–hvdc and model predictive control. *IEEE Transactions on Power Delivery*, 29(1):480–488, 2014. 2

[13] Chengwen Zhang, Yi Zhao, Lin Zhu, Yilu Liu, Evangelos Farantatos, Mahendra Patel, Hossein Hooshyar, Cosimo Pisani, Roberto Zaottini, and Giorgio Giannuzzi. Implementation and hardware-in-the-loop testing of a wide-area damping controller based on measurement-driven models. In *2021 IEEE Power Energy Society General Meeting (PESGM)*, pages 1–5, 2021. 2

[14] Samuel C. Chevalier, Petr Vorobev, and Konstantin Turitsyn. Using effective generator impedance for forced oscillation source location. *IEEE Transactions on Power Systems*, 33(6):6264–6277, 2018. 2

[15] Khaled Alshuaibi, Yi Zhao, Lin Zhu, Evangelos Farantatos, Deepak Ramasubramanian, Wenpeng Yu, and Yilu Liu. Forced oscillation grid vulnerability analysis and mitigation using inverter-based resources: Texas grid case study. *Energies*, 15(8), 2022. 2, 3, 7, 55, 68

[16] Felipe Wilches-Bernal, Brian J. Pierre, David A. Schoenwald, Ryan T. Elliott, Raymond H. Byrne, Jason C. Neely, and Daniel J. Trudnowski. Forced oscillations in the western interconnection with the pacific dc intertie wide area damping controller. In *2020 IEEE Power Energy Society Innovative Smart Grid Technologies Conference (ISGT)*, pages 1–5, 2020. 2

[17] S. Arash Nezam Sarmadi, Vaithianathan Venkatasubramanian, and Armando Salazar. Analysis of november 29, 2005 western american oscillation event. *IEEE Transactions on Power Systems*, 31(6):5210–5211, 2016. 2

[18] Ping Jiang, Zikai Fan, Shuang Feng, Xi Wu, Hui Cai, and Zhenjian Xie. Mitigation of power system forced oscillations based on unified power flow controller. *Journal of Modern Power Systems and Clean Energy*, 7(1):99–112, 2019. 2

[19] P. Kundur, J. Paserba, V. Ajjarapu, G. Andersson, A. Bose, C. Canizares, N. Hatziargyriou, D. Hill, A. Stankovic, C. Taylor, T. Van Cutsem, and V. Vittal. Definition and classification of power system stability ieee/cigre joint task force on stability terms and definitions. *IEEE Transactions on Power Systems*, 19(3):1387–1401, 2004. 6

[20] Debasish. Mondal. *Power System Small Signal Stability Analysis and Control.* Elsevier Science & Technology, San Diego, 2014. 6

[21] Leonard L. Grigsby. *Power System Stability and Control.* CRC Press LLC, Baton Rouge, 3rd ed. edition, 2012. 6

[22] M. Maheswari, N. Suthanthira Vanitha, and N. Loganathan. *Wide-Area Measurement Systems and Phasor Measurement Units*, pages 105–126. Springer International Publishing, Cham, 2021. 6

[23] P. (Prabha) Kundur. *Power system stability and control.* The EPRI power system engineering series. McGraw-Hill, New York, 1994. 6

[24] K Prasertwong, N Mithulananthan, and D Thakur. Understanding low-frequency oscillation in power systems. *International journal of electrical engineering & education*, 47(3):248–262, 2010. 6

[25] Kwan-Shik Shim, Seon-Ju Ahn, and Joon-Ho Choi. Synchronization of low-frequency oscillation in power systems. *Energies (Basel)*, 10(4):558–, 2017. 6

[26] José Luis Rodríguez-Amenedo and Santiago Arnaltes Gómez. Damping low-frequency oscillations in power systems using grid-forming converters. *IEEE Access*, 9:158984–158997, 2021. 6, 13

[27] Jaime Quintero, Vijay Vittal, Gerald T. Heydt, and Hui Zhang. The impact of increased penetration of converter control-based generators on power system modes of oscillation. *IEEE Transactions on Power Systems*, 29(5):2248–2256, 2014. 6

[28] Nilesh Modi, Tapan K. Saha, and N. Mithulananthan. Effect of wind farms with doubly fed induction generators on small-signal stability — a case study on australian equivalent system. In *2011 IEEE PES Innovative Smart Grid Technologies*, pages 1–7, 2011. 6

[29] Yong Liu, Joe R. Gracia, Thomas J. King, and Yilu Liu. Frequency regulation and oscillation damping contributions of variable-speed wind generators in the u.s. eastern interconnection (ei). *IEEE Transactions on Sustainable Energy*, 6(3):951–958, 2015. 6

[30] Shutang You, Gefei Kou, Yong Liu, Xuemeng Zhang, Yi Cui, Micah J. Till, Wenxuan Yao, and Yilu Liu. Impact of high pv penetration on the inter-area oscillations in the u.s. eastern interconnection. *IEEE Access*, 5:4361–4369, 2017. 7, 13

[31] Lida Yazdani and Mohammad Reza Aghamohammadi. Damping inter-area oscillation by generation rescheduling based on wide-area measurement information. *International journal of electrical power & energy systems*, 67:138–151, 2015. 7, 13

[32] Jegatheeswaran Thambirajah, Nina F. Thornhill, and Bikash C. Pal. A multivariate approach towards interarea oscillation damping estimation under ambient conditions via independent component analysis and random decrement. *IEEE Transactions on Power Systems*, 26(1):315–322, 2011. 7

[33] Mohamed Fayez, Mohamed Mandor, Mohamed El-Hadidy, and Fahmy Bendary. Stabilization of inter-area oscillations in two-area test system via centralized interval type-2 fuzzy-based dynamic brake control. *Journal of Electrical Systems and Information Technology*, 8(1):1–19, 2021. 7

[34] Guoping Liu and Vaithianathan Venkatasubramanian. Oscillation monitoring from ambient pmu measurements by frequency domain decomposition. In *2008 IEEE International Symposium on Circuits and Systems (ISCAS)*, pages 2821–2824, 2008. 7

[35] Hussain M. Behbehani, Janusz Bialek, and Zbigniew Lubosny. Enhancement of power system stability using fuzzy logic based supervisory power system stabilizer. In *2008 IEEE 2nd International Power and Energy Conference*, pages 479–484, 2008. 7

[36] Argyrios C. Zolotas, Balarko Chaudhuri, Imad M. Jaimoukha, and Petr Korba. A study on lqg/ltr control for damping inter-area oscillations in power systems. *IEEE Transactions on Control Systems Technology*, 15(1):151–160, 2007. 7

[37] North American Electric Reliability Corporation (NERC). Reliability guideline: Forced oscillation monitoring and mitigation, 2017. 7

[38] Mohammadreza GHORBANIPARVAR. Survey on forced oscillations in power system. *Journal of modern power systems and clean energy*, 5(5):671–682, 2017. 7

[39] North American SynchroPhasor Initiative (NASPI). Power system oscillatory behaviors: Sources, characteristics, and analyses, 2017. 7

[40] Md. Arif Khan and John W. Pierre. Detection of periodic forced oscillations in power systems using multitaper approach. *IEEE Transactions on Power Systems*, 34(2):1086–1094, 2019. 7

[41] Jiaxing Lei, H. T. Shi, Ping Jiang, Yi Tang, and Shuang Feng. An accurate forced oscillation location and participation assessment method for dfig wind turbine. *IEEE Access*, 7:130505–130514, 2019. 7

[42] Tossaporn Surinkaew, Kianoush Emami, Rakibuzzaman Shah, Syed Islam, and N. Mithulananthan. Forced oscillation in power systems with converter controlled-based resources–a survey with case studies. *IEEE Access*, 9:150911–150924, 2021. 7

[43] Pablo Gill Estevez, Pablo Marchi, Cecilia Galarza, and Marcelo Elizondo. Non-stationary power system forced oscillation analysis using synchrosqueezing transform. *IEEE Transactions on Power Systems*, 36(2):1583–1593, 2021. 7

[44] North American Electric Reliability Corporation (NERC). Eastern interconnection oscillation disturbance january 11, 2019 forced oscillation event, 2019. 7

[45] S. Arash Nezam Sarmadi and Vaithianathan Venkatasubramanian. Inter-area resonance in power systems from forced oscillations. *IEEE Transactions on Power Systems*, 31(1):378–386, 2016. 7

[46] Yuan Zhi and Vaithianathan Venkatasubramanian. Interaction of forced oscillation with multiple system modes. *IEEE Transactions on Power Systems*, 36(1):518–520, 2021. 7

[47] Samuel Chevalier, Petr Vorobev, and Konstantin Turitsyn. A bayesian approach to forced oscillation source location given uncertain generator parameters. *IEEE Transactions on Power Systems*, 34(2):1641–1649, 2019. 7

[48] Shuang Feng, Binqing Zheng, Ping Jiang, and Jiaxing Lei. A two-level forced oscillations source location method based on phasor and energy analysis. *IEEE Access*, 6:44318–44327, 2018. 7

[49] Yi Zhao, Lin Zhu, Huangqin Xiao, Yilu Liu, Evangelos Farantatos, Mahendra Patel, Atena Darvishi, and Bruce Fardanesh. An adaptive wide-area damping controller via facts for the new york state grid using a measurement-driven model. In *2019 IEEE Power Energy Society General Meeting (PESGM)*, pages 1–5, 2019. 8

[50] Yongli Zhu, Chengxi Liu, Bin Wang, and Kai Sun. Damping control for a target oscillation mode using battery energy storage. *Journal of Modern Power Systems and Clean Energy*, 6(4):833–845, 2018. 8

[51] Mahdi Saadatmand, Gevork B. Gharehpetian, Ali Moghassemi, Josep M. Guerrero, Pierluigi Siano, and Hassan Haes Alhelou. Damping of low-frequency oscillations in power systems by large-scale pv farms: A comprehensive review of control methods. *IEEE Access*, 9:72183–72206, 2021. 8

[52] Shuang Feng, Xi Wu, Ping Jiang, Le Xie, and Jiaxing Lei. Mitigation of power system forced oscillations: An e-statcom approach. *IEEE Access*, 6:31599–31608, 2018. 8

[53] Tossaporn Surinkaew, Rakibuzzaman Shah, Mithulananthan Nadarajah, and S.M Muyeen. Forced oscillation damping controller for an interconnected power system. *IET generation, transmission & distribution*, 14(2):339–347, 2020. 8

[54] Yanhui Xu, Wei Bai, Shimeng Zhao, Junfeng Zhang, and Yanjun Zhao. Mitigation of forced oscillations using vsc-hvdc supplementary damping control. *Electric power systems research*, 184:106333–, 2020. 8

[55] Lin Zhu, Wenpeng Yu, Zhihao Jiang, Chengwen Zhang, Yi Zhao, Jiaojiao Dong, Weikang Wang, Yilu Liu, Evangelos Farantatos, Deepak Ramasubramanian, Andrew Arana, and Ryan Quint. A comprehensive method to mitigate forced oscillations in large interconnected power grids. *IEEE Access*, 9:22503–22515, 2021. 8

[56] Benjamin R.T. Cotts, Jay R. Prigmore, and Kevin L. Graf. 6 - hvdc transmission for renewable energy integration. In Brian W. D'Andrade, editor, *The Power Grid*, pages 171–196. Academic Press, 2017. 8

[57] Erika Pierri, Ole Binder, Nasser G.A. Hemdan, and Michael Kurrat. Challenges and opportunities for a european hvdc grid. *Renewable and Sustainable Energy Reviews*, 70:427–456, 2017. 8, 9

[58] Zhenying Pei, Peng Liu, Aijun Zhang, and Yaping Zhou. An overview on vsc-hvdc power transmission systems. *International Journal of Control and Automation*, 9:33–44, 05 2016. 8

[59] Yan Li, Hongzhi Liu, Xiaojie Fan, and Xinshou Tian. Engineering practices for the integration of large-scale renewable energy vsc-hvdc systems. *Global Energy Interconnection*, 3(2):149–157, 2020. 8

[60] R. Preece and J.V. Milanović. Comparison of dynamic performance of meshed networks with different types of hvdc lines. In *9th IET International Conference on AC and DC Power Transmission (ACDC 2010)*, pages 1–5, 2010. 8

[61] Neville R. Watson and Jeremy D. Watson. An overview of hvdc technology. *Energies (Basel)*, 13(17):4342–, 2020. 8

[62] Imdadullah, Syed Muhammad Amrr, M. S. Jamil Asghar, Imtiaz Ashraf, and Mohammad Meraj. A comprehensive review of power flow controllers in interconnected power system networks. *IEEE Access*, 8:18036–18063, 2020. 8

[63] Feng Wang, Lina Bertling, Tuan Le, Anders Mannikoff, and Anders Bergman. An overview introduction of vsc-hvdc: State-of-art and potential applications in electric power systems. 2011. 8

[64] Jiuping Pan, Reynaldo Nuqui, Kailash Srivastava, Tomas Jonsson, Per Holmberg, and Ying-Jiang Hafner. Ac grid with embedded vsc-hvdc for secure and efficient power delivery. In *2008 IEEE Energy 2030 Conference*, pages 1–6, 2008. 8

[65] Nikolas Flourentzou, Vassilios G. Agelidis, and Georgios D. Demetriades. Vsc-based hvdc power transmission systems: An overview. *IEEE Transactions on Power Electronics*, 24(3):592–602, 2009. 9, 11

[66] Oluwole Daniel Adeuyi; Abdullah Emhemed; Simon Gill; Benjamin Marshall and Simon Marshall. Maximising hvdc support for gb black start and system restoration, 2019. 9

[67] Mircea Eremia, Chen-Ching Liu, and A. Edris. *Advanced Solutions in Power Systems: HVDC, FACTS, and AI Techniques*. 01 2016. 9

[68] Georgios Stamatiou. Converter interactions in vsc-based hvdc systems, 2015. 9

[69] Ramesh E Ramesh e and Shri Harsha J. Voltage source converter based hvdc transmission. *IJESIT*, 1:97–106, 09 2012. 9

[70] ABB. Hvdc light, it's time to connect. 9

[71] Giddani Kalcon, Grain P. Adam, Olimpo Anaya-Lara, Graeme Burt, and K.L. Lo. Analytical efficiency evaluation of two and three level vsc-hvdc transmission links. *International Journal of Electrical Power Energy Systems*, 44(1):1–6, 2013. 10

[72] Arun G. Phadke and Tianshu Bi. Phasor measurement units, wams, and their applications in protection and control of power systems. *Journal of Modern Power Systems and Clean Energy*, 6(4):619–629, 2018. 11

[73] P. Zhang. Phasor measurement unit (pmu) implementation and applications, 2017. 11

[74] Jiecheng Zhao, Jin Tan, Ling Wu, Lingwei Zhan, Wenxuan Yao, and Yilu Liu. Impact of the measurement errors on synchrophasor-based wams applications. *IEEE Access*, 7:143960–143972, 2019. 11

[75] Ilias Zenelis and Xiaozhe Wang. Wide-area damping control for interarea oscillations in power grids based on pmu measurements. *IEEE Control Systems Letters*, 2(4):719–724, 2018. 11

[76] Ilias Zenelis, Xiaozhe Wang, and Innocent Kamwa. Online pmu-based wide-area damping control for multiple inter-area modes. *IEEE Transactions on Smart Grid*, 11(6):5451–5461, 2020. 11

[77] A. I. Konara and U. D. Annakkage. Robust power system stabilizer design using eigenstructure assignment. *IEEE Transactions on Power Systems*, 31(3):1845–1853, 2016. 13

[78] A.R. Fereidouni, B. Vahidi, T. Hoseini Mehr, and M. Tahmasbi. Improvement of low frequency oscillation damping by allocation and design of power system stabilizers in the multi-machine power system. *International Journal of Electrical Power & Energy Systems*, 52:207–220, 2013. 13

[79] Murilo E. C. Bento, Daniel Dotta, Roman Kuiava, and Rodrigo A. Ramos. A procedure to design fault-tolerant wide-area damping controllers. *IEEE Access*, 6:23383–23405, 2018. 13

[80] Haifeng. Wang. *Analysis and Damping Control of Power System Low-frequency Oscillations*. Power Electronics and Power Systems. Springer US, Boston, MA, 2016. 13

[81] Ming Yang, Wu Cao, Tingjun Lin, Jianfeng Zhao, and Wei Li. Low frequency damping control for power electronics-based ac grid using inverters with built-in pss. *Energies (Basel)*, 14(9):2435–, 2021. 13

[82] A. N. Hussain, F. A. Malek, M. A. Humayun, and M. A. Rashid. Power system oscillations damping by optimal coordinated design between multiple damping stabilizers based on statcom device. In *2012 IEEE Conference on Sustainable Utilization and Development in Engineering and Technology (STUDENT)*, pages 18–23, 2012. 13

[83] Matthew Weiss, Backer N. Abu-Jaradeh, Aranya Chakrabortty, Arash Jamehbozorg, Farrokh Habibi-Ashrafi, and Armando Salazar. A wide-area svc controller design for inter-area oscillation damping in wecc based on a structured dynamic equivalent model. *Electric Power Systems Research*, 133:1–11, 2016. 13

[84] N. Mithulananthan, C.A. Canizares, J. Reeve, and G.J. Rogers. Comparison of pss, svc, and statcom controllers for damping power system oscillations. *IEEE Transactions on Power Systems*, 18(2):786–792, 2003. 13

[85] Yu Shen, Wei Yao, Jinyu Wen, and Haibo He. Adaptive wide-area power oscillation damper design for photovoltaic plant considering delay compensation. *IET generation, transmission & distribution*, 11(18):4511–4519, 2017. 13

[86] Xianchao Sui, Yufei Tang, Haibo He, and Jinyu Wen. Energy-storage-based low-frequency oscillation damping control using particle swarm optimization and heuristic dynamic programming. *IEEE Transactions on Power Systems*, 29(5):2539–2548, 2014. 13

[87] M.W. Mustafa and Nuraddeen Magaji. Design of power oscillation damping controller for svc device. In *2008 IEEE 2nd International Power and Energy Conference*, pages 1329–1332, 2008. 13

[88] Yu Shen, Wei Yao, Jinyu Wen, Haibo He, and Weibiao Chen. Adaptive supplementary damping control of vsc-hvdc for interarea oscillation using grhdp. *IEEE Transactions on Power Systems*, 33(2):1777–1789, 2018. 13

[89] Ismael Abdulrahman, Rabie Belkacemi, and Ghadir Radman. Power oscillations damping using wide-area-based solar plant considering adaptive time-delay compensation. *Energy Systems*, 05 2021. 13

[90] Mohamed Ramadan Younis and Reza Iravani. Wide-area damping control for inter-area oscillations: A comprehensive review. In *2013 IEEE Electrical Power Energy Conference*, pages 1–6, 2013. 14

[91] Rtds simulator overview. https://www.rtds.com/wp-content/uploads/2020/11/RTDS-Simulator-Overview.pdf. Accessed: 2022-01-15. 14

[92] F.S. Al-Ismail, Mohammed Abido, and Mohamed Hassan. Rtds implementation of statcom based stabilizer for power system stability enhancement. pages 1431–1437, 07 2013. 14

[93] A. Srivastava and Noel Schulz. Applications of real time digital simulator in power system education and research. *ASEE Annual Conference and Exposition, Conference Proceedings*, 01 2009. 14

[94] R. Kuffel, J. Giesbrecht, T. Maguire, R.P. Wierckx, and P. McLaren. Rtds-a fully digital power system simulator operating in real time. In *Proceedings 1995 International Conference on Energy Management and Power Delivery EMPD '95*, volume 2, pages 498–503 vol.2, 1995. 14

[95] Paul Forsyth and Rick Kuffel. Utility applications of a rtds® simulator. In *2007 International Power Engineering Conference (IPEC 2007)*, pages 112–117, 2007. 14

[96] Tsat-rtds interface - the development of a hybrid simulation tool. http://site.ieee.org/pes-itst/files/2017/06/2017-Panel-1.pdf. Accessed: 2022-01-15. 14, 15

[97] Tsat transient security assessment tools. https://www.dsatools.com/wp-content/uploads/2017/07/TSAT.pdf. Accessed: 2022-01-15. 15

[98] Tri brochure. https://www.dsatools.com/wp-content/uploads/2020/01/TRI_brochure.pdf. Accessed: 2022-01-15. 15, 23

[99] Modelling large systems alternatives for network equivalents. https://knowledge.rtds.com/hc/en-us/article_attachments/360044408514/Modelling_Large_Systems_-_Alternatives_for_Network_Equivalents.pdf. Accessed: 2022-01-15. 15, 23, 27

[100] Ibrahim Altarjami, Lin Zhu, Dongbin Lu, Xianda Deng, Yilu Liu, Evangelos Farantatos, Deepak Ramasubramanian, Mahendra Patel, Muhammad Ijaz, Ahmed H. Al-Mubarak, and Salem O. Bashraheel. Impact of wide-area oscillation damping control using measurement-driven approach on system separation - saudi grid case study. In *2020 IEEE/PES Transmission and Distribution Conference and Exposition (TD)*, pages 1–5, 2020. 19

[101] Yuqing Dong, Yi Zhao, Khaled Alshuaibi, Chengwen Zhang, Yilu Liu, Lin Zhu, Evangelos Farantatos, Kaiqi Sun, Benjamin Marshall, Md Rahman, Oluwole Adeuyi, Simon Marshall, and Ian L. Cowan. Adaptive power oscillation damping control via vsc-hvdc for the great britain power grid. In *2023 IEEE Power Energy Society Innovative Smart Grid Technologies Conference (ISGT)*, pages 1–5, 2023. 19, 22, 31

[102] Xiaoqing Yang and A. Feliachi. Stabilization of inter-area oscillation modes through excitation systems. *IEEE Transactions on Power Systems*, 9(1):494–502, 1994. 20

[103] José Luis Domínguez-García, Carlos E. Ugalde-Loo, Fernando Bianchi, and Oriol Gomis-Bellmunt. Input–output signal selection for damping of power system oscillations using wind power plants. *International Journal of Electrical Power Energy Systems*, 58:75–84, 2014. 20

[104] Junbo Zhang, C. Y. Chung, and Yingduo Han. A novel modal decomposition control and its application to pss design for damping interarea oscillations in power systems. *IEEE Transactions on Power Systems*, 27(4):2015–2025, 2012. 20

[105] Yi Zhao, Chao Lu, Yongjun Liu, and Yingduo Han. Residue and identification based wide-area damping controller design in large-scale power system. In *2012 IEEE PES Innovative Smart Grid Technologies (ISGT)*, pages 1–7, 2012. 20

[106] Lin Zhu, Yi Zhao, Yilu Liu, Evangelos Farantatos, Mahendra Patel, Papiya Dattaray, Deepak Ramasubramanian, Luigi Michi, Enrico Carlini, Giorgio Giannuzzi, and Roberto Zaottini. Oscillation damping controller design using ringdown measurements for the italian power grid. In *2019 IEEE Milan PowerTech*, pages 1–6, 2019. 22

[107] Conghuan Yang, Ying Xue, Xiao-Ping Zhang, Yi Zhang, and Yuan Chen. Real-time fpga-rtds co-simulator for power systems. *IEEE Access*, 6:44917–44926, 2018. 23

[108] Jiyoung Song, Kyeon Hur, Jeehoon Lee, Hyunjae Lee, Jaegul Lee, Solyoung Jung, Jeonghoon Shin, and Heejin Kim. Hardware-in-the-loop simulation using real-time hybrid-simulator for dynamic performance test of power electronics equipment in large power system. *Energies*, 13(15), 2020. 23

[109] Rtds manual. 25, 27

[110] Harsha Ravindra, M. Omar Faruque, M. Steurer, Mike Andrus, and Md Kamrul Hasan Pulok. Conversion of pss®e models into rscad models: Lessons learned. In *IECON 2014 - 40th Annual Conference of the IEEE Industrial Electronics Society*, pages 3743–3749, 2014. 25

[111] Kati Sidwall and Paul Forsyth. Advancements in real-time simulation for the validation of grid modernization technologies. *Energies*, 13(16), 2020. 27

[112] National instruments - 9035. https://www.ni.com/en-us/support/model.crio-9035.html. Accessed: 2022-01-15. 41

[113] M.S. Almas, L. Vanfretti, and M. Baudette. Babelfish—tools for ieee c37.118.2-compliant real-time synchrophasor data mediation. *SoftwareX*, 6:209–216, 2017. 41

[114] National instruments - 9467. https://www.ni.com/en-us/support/model.ni-9467.htmll. Accessed: 2022-01-15. 43

[115] Ibrahim Abdullah Altarjami. Wide area damping control to improve transient stability and hardware-in-the-loop (hil) implementation. 45

[116] Buxin She, Yuqing Dong, and Yilu Liu. Time delay of wide area damping control in urban power grid: Model-based analysis and data-driven compensation. *Frontiers in energy research*, 10, 2022. 48

[117] Siemens. Model library, psse34. 63, 66, 67

[118] Generic solar photovoltaic system dynamic model specification; prepared by western electricity coordinating council (wecc) renewable energy modeling task force: Salt lake city, ut, usa, september 2012. https://www.wecc.org/_layouts/15/WopiFrame.aspx?sourcedoc=/Reliability/WECC%20Solar%20PV%20Dynamic%20Model%20Specification%20-%20September%202012.pdf&action=default&DefaultItemOpen=1. Accessed: 2022-01-15. 65

[119] Activsg2000: 2000-bus synthetic grid on footprint of texas. https://electricgrids.engr.tamu.edu/electric-grid-test-cases/activsg2000/. Accessed: 2022-01-15. 68

[120] Yi Zhao, Khaled Mohammed Alshuaibi, Xinlan Jia, Chengwen Zhang, Yilu Liu, Deepak Ramasubramanian, Lin Zhu, and Evangelos Farantatos. Comparison of wide-area and local power oscillation damping control through inverter-based resources. In *2023 IEEE Power Energy Society Innovative Smart Grid Technologies Conference (ISGT)*, pages 1–5, 2023. 69, 70, 125

Vita

Khaled Alshuaibi received B.S. in Electrical Engineering from the King Saud University, Saudi Arabia, in 2011. He received his M.S. in Electrical Engineering from Illinois Institute of Technology, Chicago, IL, USA, in 2016. He is pursuing Ph.D. in Electrical Engineering at the University of Tennessee, Knoxville, TN, USA. His research interests include power system stability and control, and renewable energy integration.